UNIVERSITY
OF TASMANIA

Conditionally and Acutely Ablating *Kif3a* from Oligodendrocyte Progenitor Cells Impairs Primary Cilum Assembly and Cell Function

Megan Elizabeth O'Rourke

Submitted in fulfilment of the requirement for the
Degree of Doctor of Philosophy

Menzies Institute for Medical Research
University of Tasmania
16th February 2018

Copyright statement

Statement of authority of access

Statement of co-authorship

All of the work included in this thesis was carried out by Megan O'Rourke, with the exception of Figure 4.5, which was created by Dr Kimberley Pittman.

Publications

Part of the work presented in this thesis has been published or submitted for publication as follows:

1) O'Rourke M, Gasperini R, Young KM (2014). Adult myelination: wrapping up neuronal plasticity. *Neural Regen Res*. 9(13):1261-4.

2) O'Rourke M, Cullen CL, Auderset L, Pitman KA, Achatz D, Gasperini R, and Young KM (2016). Evaluating Tissue-Specific Recombination in a Pdgfrα-CreER^{T2} Transgenic Mouse Line. *PloS One* 11(9), e0162858.

Summary

The primary cilium is a cellular organelle that can regulate the behaviour of many mitotic progenitor cells, and even some post mitotic cell types. Oligodendrocyte progenitor cells (OPCs) express genes associated with primary cilia assembly, disassembly and signalling. However, whether OPCs have primary cilia assembled on their surface and are functionally influenced by signalling at this organelle is unknown. In this thesis, I show that OPCs are ciliated, both *in vitro* and *in vivo*, while mature oligodendrocytes are not. Furthermore, OPCs disassemble and reassemble their primary cilia as they progress through the cell cycle, and this organelle is a critical regulator of OPC proliferation and oligodendrogenesis in adulthood.

In order to examine the importance of the primary cilium for OPC function, the *kinesin family member 3a (Kif3a)* gene, critical for cilium assembly, was deleted from OPCs *in vitro*. *Kif3a*-deletion significantly reduced the number of OPCs with assembled primary cilia on their surface and decreased OPC proliferation (Chapter 3). As *Pdgfrα-CreER*^{T2} transgenic mice target DNA recombination to OPCs, without significantly affecting PDGFRα^{+} cells in other tissues and organs (including the kidney, spleen, liver, intestine, heart, gastrocnemius, sciatic nerve, pituitary gland and adrenal gland) (Chapter 4), these mice were selected to conditionally delete *Kif3a* from OPCs, to examine the importance of this organelle *in vivo* (Chapter 5). Consistent with the *in vitro* findings, *Kif3a*-deletion from OPCs reduced the number of OPCs that had assembled primary cilia on their surface in the corpus callosum (CC) and reduced proliferation by ~30% in the CC and ~50% in the motor cortex. While Kif3a-deleation had no effect on OPC density, it halved the number of new oligodendrocytes produced in both the CC and the motor cortex. As the reduced proliferation rate of *Kif3a*-deleted OPCs does not account for the substantial decrease in new oligodendrocyte number, these data indicate that the primary cilium also promotes oligodendrocyte differentiation and / or new oligodendrocyte survival in the brain.

Genetically ablating OPCs, disrupting OPC function and preventing oligodendrogenesis can have behavioural consequences ranging from increased anxiety and depressive behaviours to reduced motor performance and impaired motor learning. However, when oligodendrogenesis was reduced in the CC and motor cortex over a 6-week period, by the conditional deletion of *Kif3a* from OPCs *in vivo*, no such behavioural phenotype was observed. These data indicate that deleting *Kif3a* from OPCs in the adult central nervous system (CNS), which does not remove OPCs from the brain, and only moderately reduces oligodendrogenesis, is not sufficient, at least in the short-term, to have overt behavioural

consequences. However, these experiments also pose interesting questions about the function of OPCs, and whether oligodendrogenesis is their only role in the mature CNS.

Overall this research demonstrates that primary cilia are present on the surface of OPCs but absent from mature, myelinating oligodendrocytes and that preventing cilium assembly reduces both OPC proliferation and oligodendrogenesis. I also determined that preventing cilium assembly and reducing oligodendrogenesis did not affect normal CNS function by 7 weeks post gene-deletion.

Acknowledgements

I'd like to start by acknowledging my supervisory team, Dr Kaylene Young, Dr Carlie Cullen and Dr Rob Gasperini. I'm incredibly lucky to have had supervisors with such a diverse range of areas of expertise and I would like to thank you all for your support. First and foremost thank you to Dr Kaylene Young for agreeing to take me on as the first PhD student in the Young lab. Thanks for all your support and guidance. It's been a wonderful opportunity and I've learned so much. Thanks also to Dr Rob Gasperini, particularly for your technical support in the lab and helping troubleshoot my *in vitro* experiments. Special thanks to Dr Carlie Cullen, my behaviour guru, thanks for teaching me your craft. Those late nights in the behaviour room were one of the highlights of the last few years. I am so incredibly honoured to have been your first PhD student, thank you for your constant support, both in and out of the lab, I honestly don't know if I could have done it without you.

Thank you to the remaining members of the Young lab (the glial mutant ninja turtles), past and present. Thanks for the Friday morning coffee, celebration drinks, commiseration drinks and weekend lab sessions. Thanks for coming along for the ride. I'm going to miss you all.

Thanks also to the animal services staff, particularly Peta for her patience when teaching me animal handling and Lynda and Keri for everything you do for all the Young Lab colonies off-site, I know it's not a small job and I'm very grateful. I would also like to thank Dr Terry Pinfold for all his help with the Astrios cell sorter. Thank you to the Menzies Institute for Medical Research, for my scholarship funding for the duration of my PhD.

To my PhD companions, Macarena Pavez, Amanda Patchett, Rachel Atkinson and Dean Picone, there is nobody else I would rather have experienced this rollercoaster ride alongside. It's been wonderful watching each of you go through the submission process and I can't believe my turn has finally come. I'm going to miss seeing you guys around every day. Special thanks to Rachel for always being in the right place at the right time and always having a free shoulder to cry on and a box of tissues in hand. I owe you roughly a billion chocolate frogs.

To all my friends and family, thank you for your support and your patience over the last four years. I'm sorry I've been so absent, particularly over the last few months, but I promise I'll make up for it (and then some). To my mum and dad, thank you for everything you have done for me. Thanks for your never-ending support and for always encouraging me to do my best, for always allowing me to ask endless questions and encouraging me to learn. I'm so lucky to have had such supportive parents and wonderful role models. I love you both

and I am so grateful to have you in my life. To my sister Lauren. I love you. Thanks for always having a collection of funny pictures and podcast recommendations at the ready, it helps more than you realise. Finally, to my wonderful girlfriend Tash, I know it hasn't been easy dating me for the last four years, but I'm so damn grateful that you've stuck it out and put up with all the late nights and tears. It's been pretty wonderful building a life with you and I can't wait to see what our post PhD life together entails. Thank you for always being understanding and patient and kind. Thanks for your eternal optimism and for believing in me and my capabilities even when I'm struggling. I love you. Also Misty. Thanks for bringing him into my life because I love him too.

Last but definitely not least, thanks to me. Because look at this awesome thing you have achieved. It was hard, but you persevered and I'm so bloody proud of you. I can't wait to see what you do next, it's going to be great. You go girl!

Abbreviations

ALS	Amyotrophic lateral sclerosis
ANOVA	Analysis of variance
AP	Alkaline phosphatase
APC	Adenomatous polyposis coli
Arl13b	ADP-ribosylation factor-like protein 13b
BAC	Bacterial artificial chromosome
β-Arr	β-Arrestin
BBS	Bardet-Biedl syndrome
BrdU	Bromodeocyuridine
BSA	Bovine serum albumin
BMP	Bone morphogenic protein
CAR	CXCL12-abundant reticular cells
CC	Corpus callosum
CW	Clockwise
CCW	Counter clockwise
CNS	Central nervous system
cpd	Cycles per degree
Cre	Cre recombinase
DEPC	Diethyl pyrocarbonate
DIC	Differential interference contrast
DIG	Digoxigenin
DIV	Days in vitro
DMEM	Dulbecco’s modified eagle medium
DNA	Deoxyribonucleic acid
DTI	Diffusion tensor imaging
DTT	Dithiothreitol
Dvl	Disheveled
E	Embryonic day
EAE	Experimental autoimmune encephalomyelitis
EBSS	Earle’s balanced salt solution

EdU	5-Ethynyl-2’-deoxyuridine
FAP	Fibroadipogenic precursor
FCS	Fetal calf serum
FGF	Fibroblast growth factor
FGFR	Fibroblast growth factor receptor
Fz	Frizzled
gDNA	Genomic DNA
GFAP	Glial fibrillary acidic protein
GFP	Green fluorescent protein
GSK3β	Glycogen synthase 3β
HDAC6	Histone deacetylase 6
HEK	Human embryonic kidney
Hh	Hedgehog
HRP	Horseradish peroxidase
IFT	Intraflagellar transport
IFT81	Intraflagellar transport protein 81
IFT88	Intraflagellar transport protein 88
INPP5E	Inositol phosphate 5-phosphatase
i.p.	Intraperitoneal injection
Jbn	Jouberin
Kif3a	Kinesin family member 3a
LB	Luria broth
MABT	Maleic acid buffer-Tween-20
MBP	Myelin basic protein
MCS	Multiple cut site
MEF	Mouse embryonic fibroblast
MRI	Magnetic resonance imaging
mRNA	Messenger ribonucleic acid
MS	Multiple sclerosis
MYRF	Myelin regulatory factor
NG2	neural / glial antigen 2

OPC	Oligodendrocyte progenitor cell
ORPK	Oak Ridge polycystic kidney
P	Postnatal day
PαS	PDGFRα^{+} Sca1^{+}
PBS	Phosphate buffered saline
PCR	Polymerase chain reaction
PDGF	Platelet derived growth factor
PDGFRα	Platelet derived growth factor receptor α
PDL	Poly-D-lysine
PFA	Paraformaldehyde
PI	Propidium iodide
PLP	Proteolipid protein
pMN	Motor neuron progenitor zone
PTCHD	Patched
PTCHD2	Patched 2
PtdIns(4)P	Phosphatidylinositol 4-phosphate
PVDF	polyvinylidene fluoride
RIPA	Radioimmunoprecipitation assay
RNA	Ribonucleic acid
SDS	Sodium dodecyl sulfate
Shh	Sonic hedgehog
SMO	Smoothened
SNTN	Sentan
Std dev	Standard deviation
SUFU	Suppressor of fused
SVZ	Subventricular zone
TBS-T	Tris buffered saline-tween
Tx	Tamoxifen
Wnt	Wingless / integrated
YFP	Yellow fluorescent protein

Table of contents

Chapter 1: Literature review

1.1 The nervous system

The nervous system coordinates both voluntary and involuntary actions, such as deliberate movements and reflexive responses (Gibson and Ma, 2011). They contain neurons, which extend axons to connect to distal target cells and form networks that carry information, in the form of action potentials, around the body. The nervous system can be broken down into three major divisions, the central nervous system (CNS), the peripheral nervous system and the enteric (gastrointestinal) nervous system (Frantz, 2012). The CNS, which is the focus on in this thesis, is made up of the spinal cord, the optic nerve and the brain, while the peripheral nervous system comprises neurons and ganglia outside of the CNS, and conduct action potentials between the CNS and peripheral tissues and organs (Catala and Kubis, 2013).

The CNS contain multiple cell types in addition to neurons, including vascular cells and supporting cells called glia. The three major CNS glial cell types are astrocytes, oligodendrocytes and microglia. Astrocytes perform many critical functions within the CNS, they provide nutrients to axons (Müller et al., 2014; Tang et al., 2014) and maintain the extracellular ion balance (Walz, 2000). By contrast, microglia are phagocytic cells often referred to as the immune cells of the CNS, as they prune synapses (Paolicelli et al., 2011) and clear myelin debris (Skripuletz et al., 2013; Zhu et al., 2016). Oligodendrocytes, which are the topic of this thesis, are the myelinating (insulating) cells of the CNS (Baumann and Pham-Dinh, 2001). They extend multiple processes to ensheath and add myelin to multiple axon segments. This close association between oligodendrocytes and axons, enables rapid information transfer, but also allows oligodendrocytes to provide critical trophic support to axons (Dougherty et al., 2000; Du and Dreyfus, 2002; Wilkins et al., 2003; Bradl and Lassmann, 2010), making them critical for healthy CNS function. Ongoing myelination is important for the maintenance of a healthy CNS. Errors in myelination have been implicated in impaired motor function (Liao et al., 2014; Schneider et al., 2016) as well as depression (Regenold et al., 2007; Williams et al., 2015) and anxiety (Birey et al., 2015). Changes in myelin are also associated with learning and memory acquisition (Zhang et al., 2012; McKenzie et al., 2014; Kim et al., 2015).

1.2 Developmental myelination

During CNS development, oligodendrocyte progenitor cells (OPCs) are born from stem cells located within the ventricular zone of the embryonic brain and spinal cord (reviewed in Richardson et al., 2006; 2011). The majority of spinal cord OPCs are derived from $OLIG2^+$ stem cells in the motor neuron progenitor (pMN) domain, and these OPCs migrate, proliferate and differentiate to give rise to ~85% of the mature oligodendrocytes present in the adult spinal cord (Zhou et al., 2001). OPCs derived from more dorsal spinal cord stem cell domains produce the smaller number of mature oligodendrocytes for the adult spinal cord (Cai et al., 2005; Fogarty et al., 2005; Vallstedt et al., 2005), that preferentially myelinate the corticospinal and rubrospinal tracts, despite these regions being inhabited by ventrally-derived OPCs earlier in development (Tripathi et al., 2011).

In the developing brain, OPCs similarly arise from stem cells in distinct dorsal and ventral stem cell zones, including those in the neuroepithelium of the medial ganglionic eminence, the anterior entopeduncular region (Kessaris et al., 2006), the lateral ganglionic eminence and the cortex (Kessaris et al., 2006). OPCs express a number of proteins that can be used to distinguish them from other cell types in the CNS, including oligodendrocytes (**Fig. 1.1**). For example, neural / glial antigen 2 (NG2), a chondroitin sulphate proteoglycan, is expressed by other cell types outside the CNS, including vascular mural cells, cells of mesenchymal lineages and stem cells in the skin (Levine et al., 1986; Trotter et al., 2010), but within the CNS it is exclusively expressed by OPCs and pericytes. Pericytes are contractile cells located in the walls of blood vessels, and while they express NG2, they do not readily bind the anti-NG2 antibody in fixed tissue, such that NG2 is a specific immunohistochemical marker of OPCs (Mishra et al., 2014). Platelet derived growth factor receptor alpha (PDGFRα) is a transmembrane receptor that is activated by binding of its ligand, platelet derived growth factor (PDGF)-A. In the CNS, PDGFRα is exclusively expressed by OPCs, and when activated, can promote their proliferation (van Heyningen et al., 2001), migration (Baroti et al., 2016) and survival (Watzlawik et al., 2013). The use of these proteins as markers to identify OPCs, has led to OPCs being referred to as NG2-glia or $PDGFR\alpha^+$ cells in the literature.

Once generated, all OPCs proliferate (Clarke et al., 2012). They are capable of both symmetric and asymmetric cell division, resulting in two identical OPCs or one OPC and one cell destined to differentiate into a mature, myelinating oligodendrocyte, respectively (Sugiarto et al., 2011; Zhu et al., 2011; Hill et al., 2014). As OPCs differentiate into oligodendrocytes, they undergo a drastic change in morphology, extending many processes to contact axons and commence myelination (Kukley et al., 2010), and these changes are

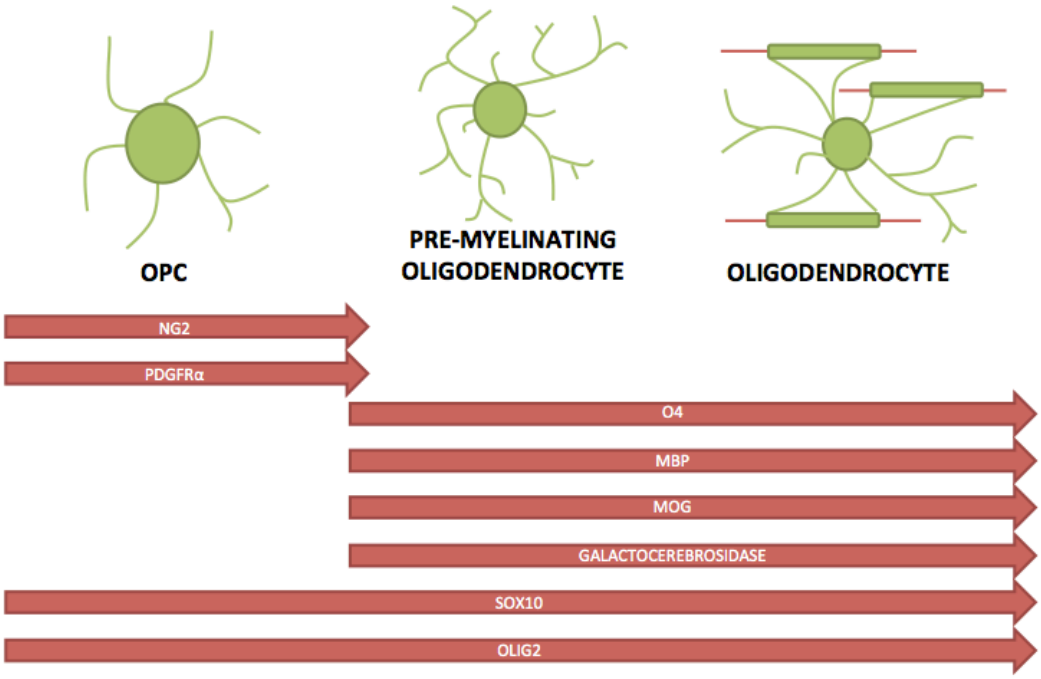

Figure 1.1: Schematic of OPC differentiation

OPCs are identified by their expression of the NG2 proteoglycan and the mitogenic receptor PDGFRα. These proteins are downregulated early in OPC differentiation into premyelinating oligodendrocytes. Pre-myelinating and myelinating oligodendrocytes express MBP, MOG and galactacerebrosidase. SOX10 and OLIG2 are expressed throughout the lineage.

associated with altered gene expression within the cell. OPCs rapidly down-regulate the expression of proteins associated with their progenitor cell function, including NG2 and PDGFRα, and begin to express myelin-associated proteins. While myelin is a double layer of plasma membrane that is ~70% lipids, it is also ~30% protein - as myelin associated proteins are embedded in the membrane to anchor the many lipid bilayers together for stability. The most abundant of these proteins include proteolipid protein (PLP), myelin oligodendrocyte glycoprotein, 2', 3'-cyclic nucleotide 3'-phosphodiesterase, myelin associated glycoprotein and myelin basic protein (MBP) (Dubois-Dalcq et al., 1986) (Nishiyama et al., 2009) (**Fig. 1.1**) – many of which are used as markers to identify oligodendrocytes in the CNS.

While OPCs and oligodendendrocytes have distinct gene expression profiles, reflecting their immature and mature functions respectively, they also share genes common to the oligodendrocyte lineage. Two proteins commonly used to identify all cells of the oligodendrocyte lineage, are the transcription factors SOX10 and OLIG2 (Nishiyama et al., 2009) (**Fig. 1.1**). SOX10 is a member of the SOX family of transcription factors, and while it is expressed by OPCs and oligodendrocytes in the CNS, it is also expressed by Schwann cells, the myelinating glia of the peripheral nervous system (Wegner, 2001). Similarly, in the embryonic CNS, OLIG2 is expressed by stem cells in the OLIG2 domain of the developing spinal cord (Liu and Rao, 2004), as well as OPCs throughout the CNS (Ortega et al., 2013). However by adulthood, OLIG2 expression is restricted to cells of the oligodendrocyte lineage and it has not been reported to be expressed outside of the CNS (Rowitch et al., 2002).

During development, neurons extend axons towards their target cells, but the axons also grow in girth (Cajal et al., 1995; Raper and Mason, 2010). Axon myelination typically starts when axon diameter reaches ~0.2μm (Waxman and Bennett, 1972; Voyvodic, 1989). When an oligodendrocyte process contacts an axon it triggers polarisation of the plasma membrane, which itself triggers the initial stages of myelination (Simons and Trotter, 2007). As myelination starts, the oligodendrocyte process begins to wind itself around the axon. The tip of this process, known as the leading edge, continues to wrap itself around the axon pushing underneath the previously deposited layers (Snaidero et al., 2014, reviewed by Hughes and Appel, 2016). As the leading edge wraps around the axon it squeezes the cytoplasmic material out of the oligodendrocyte process, leaving the axon surrounded by layers of 'empty' cell membrane. As this is occurring, the myelin membrane extends laterally, spreading out wider towards the nodal regions so that it covers a greater area of axon.

Each myelin segment added to an axon is an internode. Each oligodendrocyte is capable of simultaneously laying down internodes on multiple different axons, and each myelinated axon has a series of internodes laid down by multiple oligodendrocytes along its length. The number of myelin internodes on an axon, and their length can vary, depending on the location of the neuron and its role (Bechler et al., 2015). As myelin is a highly insulating substance, it increases the resistance and decreases the capacitance of the axon, at the site of the internode. Internodes are interspersed by unmyelinated gaps called nodes of Ranvier. Each node is 0.5-1μm in length and contains a high concentration of voltage-gated sodium channels (Purves, 2012). When a neuron is depolarized to threshold, these channels open and allow sodium ions to enter the axon, generating the action potential. When travelling along a myelinated axon, the action potential is regenerated at each node of Ranvier, in a process called saltatory conduction, that allows the action potential to jump from node to node. In this way, an action potential travels along an unmyelinated axon at speeds between 0.5 and 10m/s, but along a myelinated axon can reach 150m/s (Purves, 2012). As myelin it critical to achieving increased conduction speeds, it is critical to vertebrate CNS function.

In humans, myelin development can be measured using a number of neuroradiological techniques such as T1 and T2 weighted magnetic resonance imaging (MRI) as well as fluid-attenuated inversion recovery, diffusion-weighted imaging, diffusion-tensor imaging (DTI) and proton MR spectroscopy (Barkovich, 2000; Guleria and Kelly, 2014). Myelination is first observed in the dorsal brainstem prior to birth at about 26-30 weeks of gestation. After birth, in the first couple of months of life, myelination spreads to the middle cerebellar peduncle and posterior limb of the internal capsule (Barkovich and Raybaud, 2012). This continues into the anterior limb of the internal capsule and the corpus callosum (CC) before 6 months of age, and the occipital white matter develops before the age of 1 year. Frontal white matter is the final region to develop, with the deep frontal white matter developing by 16 months of age and the subcortical frontal white matter developing by 24 months or 2 years of age (Barkovich and Raybaud, 2012). At this point the myelination pattern is structurally similar to that of an adult human (Guleria and Kelly, 2014), however myelination continues throughout childhood and “complete” myelination is not achieved until 25-30 years of age (Fields, 2008). Furthermore, continued myelin deposition has been observed beyond 30 years of age in response to learning new tasks (Scholz et al., 2009).

In the mouse, the vast majority of myelination occurs in the early postnatal period. It starts in the ventral spinal cord at embryonic day (E)17, and continues in the rostral to caudal direction. In the dorsal spinal cord, myelination starts at the cervical enlargement and continues in both the rostral and caudal directions (Foran and Peterson, 1992). In the brain,

the deep regions of the cerebellum are the first to be myelinated, before myelin spreads towards the pial surface. Myelination of the optic nerve starts proximal to the retina at postnatal day (P)7 and continues rapidly towards the optic chiasm, with dense myelination evident along the retinal end of the optic nerve by P8 (Foran and Peterson, 1992). While few myelinating oligodendrocytes are present in the optic chiasm at P7 itself, the rate of myelination is slow, with complete myelination achieved at P23. The rate of myelination along the optic nerve also slows towards the optic chiasm, at P11 the optic nerve is 4μm long, and fully myelinated, with the exception of a less than 0.5μm section immediately next to the optic chiasm. The entire optic nerve, from the retina to the optic chiasm, is not uniformly myelinated until P15 (Foran and Peterson, 1992). However, myelination stops abruptly approximately 200μm from the eye. Myelin deposition continues throughout life in the mouse CNS, even in the fully myelinated optic nerve (Young et al., 2013).

1.3 Oligodendrogenesis in the mature CNS

OPCs were first identified when Raff et al. (1983) found a novel neural precursor cell type in the P6 rat optic nerve. This cell was capable of differentiating into two different cell types depending on the culture medium used. Culture medium containing fetal calf serum (FCS) would stimulate growth into a type 2 astrocyte, but serum-free culture medium would result in oligodendrogenesis. The new cell type was called an O2A progenitor cell due to its ability to differentiate into either an oligodendrocyte or a type 2 astrocyte. O2A progenitors cultured from the rat optic nerve express PDGFRα, and respond to PDGF by proliferating, but lose their PDGFRα expression and PDGF responsiveness once they begin to differentiate (Hart et al., 1989). Pringle et al. (1992) found that O2A progenitors in the developing rat brain and optic nerve at E16 also expressed PDGFRα and that this PDGFRα expression in the CNS was exclusive to these cells, with neurons, mature oligodendrocytes and other glial cells all lacking PDGFRα expression. By tracing O2A progenitors from early postnatal development through to six months of age they were able to observe their migration throughout the developing CNS and into adulthood, where a small population of PDGFRα$^+$ O2A progenitors were found to persist, evenly distributed throughout the brain (Pringle et al., 1992, Dawson et al., 2000). The true identity and purpose of these cells was not identified until a number of years later.

1.3.1 Oligodendrogenesis occurs throughout the mature rodent CNS

Rivers et al. (2008) generated *Pdgfrα-CreER^{T2}::Rosa26-YFP* transgenic mice to label and track the fate of the PDGFRα$^+$ cells in the adult brain. *Pdgfrα-CreER^{T2}::Rosa26-YFP* mice received tamoxifen (Tx) at P45 or P180, inducing yellow fluorescent protein (YFP)

expression in approximately half of the PDGFRα$^+$ cells (Rivers et al., 2008). The proportion of YFP$^+$ cells that expressed PDGFRα decreased overtime, suggesting that these cells were differentiating. By dye-filling the YFP$^+$ cells and performing immunohistochemistry, many of the YFP$^+$ PDGFRα-negative cells in the cortex and CC were shown to have the distinct morphology of pre-myelinating and myelinating oligodendrocytes, and their cell bodies were positive for the oligodendrocyte proteins CNPase and MBP (Rivers et al., 2008). These experiments demonstrated that the PDGFRα$^+$ NG2$^+$ cells, present in the adult mouse brain, were indeed OPCs.

Using an alternative lineage-tracing approach, Dimou et al (2008) crossed *Olig2-CreER^{T2}* mice with the *lacZ/EGFP* or *Rosa26-YFP* cre-sensitive reporter mice, and administered Tx to the offspring at ~P75. Tx administration fluorescently labelled a subset of OLIG2$^+$ cells in the cerebral cortex – the vast majority of which co-labelled with NG2, and only a small fraction were CC1$^+$ oligodendrocytes (Dimou et al., 2008). However, at P75+65, the proportion of reporter$^+$ cells that were NG2$^+$ OPCs had dropped to ~19% in the white matter, and the proportion of reporter$^+$ cells that were CC1$^+$ oligodendrocytes had increased to about 82% (Dimou et al., 2008). Many studies have subsequently shown that OPCs can generate new oligodendrocytes in the brain, spinal cord and optic nerve of mice (Nishiyama et al., 2009; Kang et al., 2010; De Biase et al., 2011; Clarke et al., 2012; Young et al., 2013; Auderset et al., 2016).

1.3.2 Oligodendrogenesis occurs in the adult human brain

In humans, it is difficult to examine changes in myelination that occur at a cellular level. However, OPCs have been shown to reside and proliferate in the healthy adult human brain and in response to multiple sclerosis (MS) lesions (Dawson et al., 2000). However, nuclear weapons testing in 1955, which released C^{14} atoms into the atmosphere, has made it possible to "birth date" cells in any carbon-based life form. Using accelerator mass spectrometry, Yeung et al. (2014) used C^{14} levels to determine the age of myelin and oligodendrocyte nuclei within the CC of post-mortem tissue, collected from people aged between 0.2 and 92 years of age. In people of all ages, myelin was observed to have a C^{14} concentration, corresponding to the levels observed near their time of death (Yeung et al., 2014). This suggests that myelin is only ever a few years old and that it is continuously renewed. However, the C^{14} concentration in the oligodendrocyte nuclear extract was similar to the atmospheric C^{14} levels present in the first few years of life, suggesting that most oligodendrocytes were born early in life and survived long-term. However, individuals born before the nuclear testing, also had C^{14} concentrations higher than the atmospheric C^{14} levels prior to the nuclear testing, suggesting that some oligodendrocytes are born later in

life. It was suggested that ~0.32% of oligodendrocytes are new each year (Yeung et al., 2014), and given the very large number of oligodendrocytes present in the human brain, this still represents significant oligodendrocyte generation. However, these findings also indicate that this rate of oligodendrogenesis is unlikely to account for the rapid changes in myelination observed in response to learning in humans (Bengtsson et al., 2005; Scholz et al., 2009), and suggest that humans may have a different mechanism to modify myelin to the one demonstrated in rodents.

1.4 What is the purpose of ongoing myelination in adulthood?

The exact role that adult-born oligodendrocytes and new myelin play in regulating CNS function is unknown, but this novel from of neural plasticity has the potential to modify circuit function and influence behaviour, or alternatively, could play a maintenance role, replacing oligodendrocytes and myelin that are lost over the lifespan.

A number of human studies have shown that myelination in the adult human brain can change in response to learning and training. Bengtsson et al. (2005) utilised DTI to compare the pattern of brain myelination in people who had studied piano with those who had not, and found that extensive piano practice induced changes to white matter tracts such as the CC and internal capsule, that correlated with the hours of practice, but not with age. Similarly, adults who undertake four weeks of juggling training have increased fractional anisotropy of the white matter underlying the right anterior intraparietal sulcus, suggesting new myelin was added to the brain region activated by the task i.e. involved in hand-eye-coordination (Scholz et al., 2009).

To determine whether motor learning not only increased myelination, but required the generation of new oligodendrocytes, McKenzie et al. (2014) selectively ablated *myelin regulatory factor* (*Myrf*) from adult OPCs, using *Pdgfrα-CreER*^{T2} :: *Myrf* $^{fl/fl}$ transgenic mice. In the absence of the transcription factor MYRF, OPCs are unable to mature into oligodendrocytes and begin myelination (McKenzie et al., 2014). Control and *Myrf*-deleted mice were placed on a complex running wheel, with an irregular rung pattern, so that they had to undergo motor learning to adjust their running style and gait to account for the missing rungs (McKenzie et al., 2014). The daily average and maximum running speeds were lower in the *Myrf*-deleted mice, relative to controls. However, there was no significant difference in the time spent on the wheel, suggesting the lower speeds were not the result of decreased motivation. Furthermore, there was no difference in their performance on a rotorod, suggesting that they were not motor impaired (McKenzie et al., 2014). High speed video showed that the gait of the *Myrf*-deleted mice was less rhythmic than that of the

controls. When retested one month later, the difference between the two genotypes remained (McKenzie et al., 2014). These data suggest that learning a complex motor task requires oligodendrogenesiss (McKenzie et al., 2014).

As many CNS axons are unmyelinated, even in adulthood, it is possible, that the myelin addition that occurs in response to learning is *de novo* myelination – the addition of myelin to previously unmyelinated axons (**Fig. 1.2**). The possibility that previously unmyelinated axons can become myelinated throughout life, is also supported by a transmission electron microscopy study, showing that in the CC and cingulate bundle of the mature primate brain, the number of unmyelinated axons decreases with increasing age (Bowley et al., 2010; Wang and Young, 2014). However, *de novo* myelination has not been experimentally demonstrated – likely due to the lack of genetic markers available to distinguish unmyelinated, partially myelinated and myelinated axons.

It is also possible that newborn oligodendrocytes replace those lost across the lifespan, as they do, for example, following injury (Lucchinetti et al., 1999; Tripathi et al., 2010; Zawadzka et al., 2010; Kang et al., 2013) (**Fig. 1.3**). Demyelination, which is the loss of or damage to the protective myelin sheath surrounding an axon, can be caused by inflammation, viral infection, hypoxia, metabolic dysfunction, or physical injury, such as focal compression (Love, 2006). Myelin loss, results in a reduced action potential conduction velocity, which in turn can result in reduced sensation, movement and cognition, as well as other symptoms depending on which neurons are affected (Karussis, 2014). Furthermore, demyelination can be associated with axon degeneration, and the accrual of permanent disability. The most prevalent demyelinating disease is MS, which affects 2-2.5 million people globally (Dua et al., 2008). MS is characterised by the presence of large, demyelinating lesions in the CNS. A number of genetic and environmental risk factors are associated with the susceptibility of this disease, in which the bodies' own T-cells target myelin self-antigens (Allegretta et al., 1990; Zhang et al., 1994), however, the event that triggers the immune cascade is unknown. A range of neurological symptom can be associated with MS, including physical, cognitive and occasionally psychiatric problems. The autonomic, visual, motor and sensory systems are most often affected, but the symptoms are highly dependent on the affected axons.

It is well established that remyelination i.e. the replacement of lost myelin sheaths, can occur in people with acute or early MS (Lucchinetti et al., 1999). During this process OPCs migrate to the lesion site and proliferate (Maki et al., 2013). They then differentiate into oligodendrocytes and lay down new myelin sheaths on the demyelinated axons. Remyelinated lesions can be seen as shadow plaques histologically (Lassmann, 1983), as the new myelin sheaths are thinner and shorter than those originally covering the axons

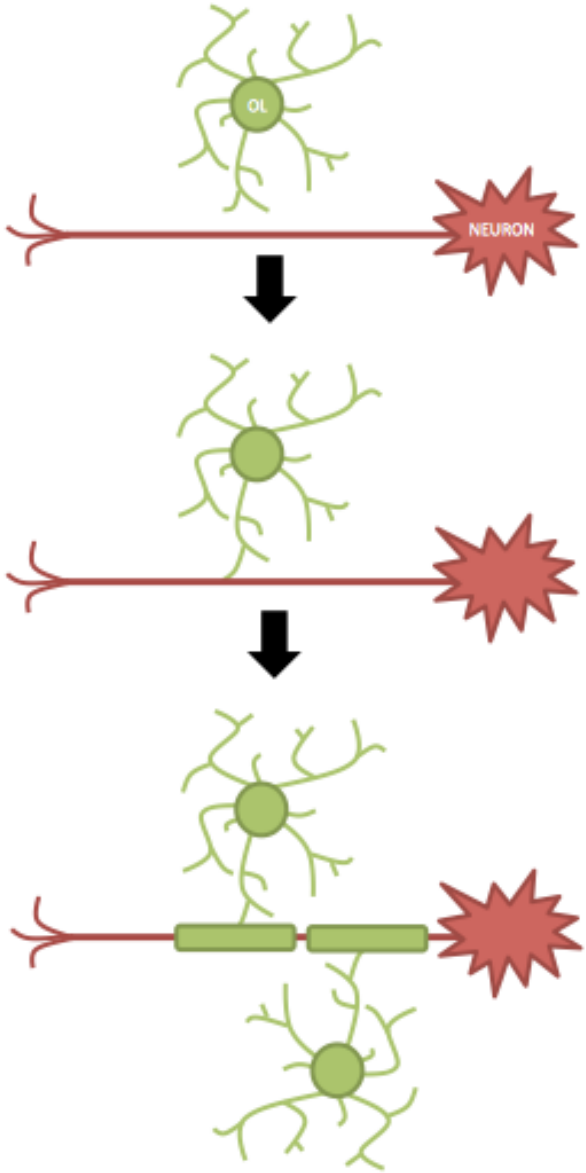

Figure 1.2: Schematic of de novo myelination

De novo myelination refers to the myelination of a previously unmyelinated axon. In adulthood, learning changes the firing pattern of neurons. It has been suggested that it could change the activity of previously unmyelinated axons (red), such tat a pre-myelinating oligodendrocyte (green) will contact the naked axon, and differentiate, elaborating a myelin sheath.

A: Oligodendrocyte turnover

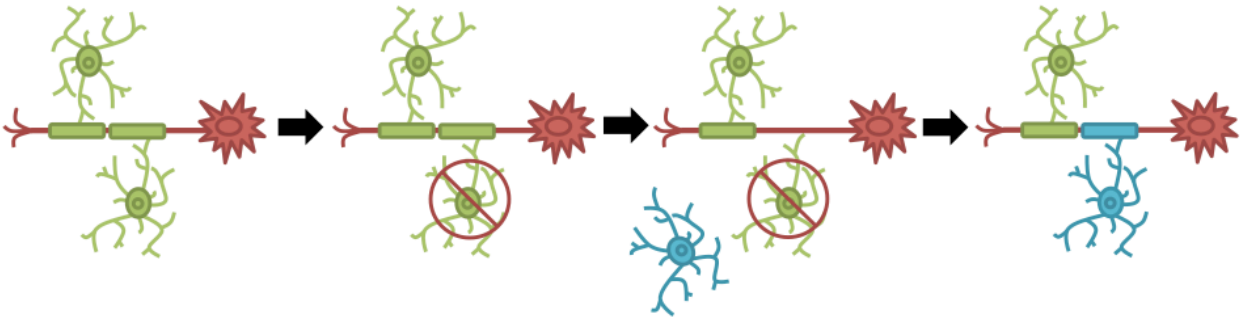

B: Myelin remodelling

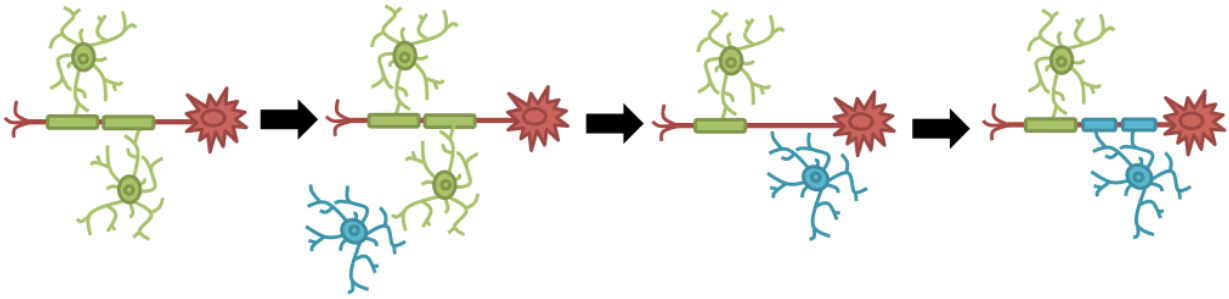

Figure 1.3: Schematic of oligodendrocyte turnover and myelin remodelling

(A) When a mature, myelinating oligodendrocyte (green) dies, an OPC or pre-myelinating oligodendrocyte (blue) can contact the demyelinated axon and differentiate to remyelinate the region. This occurs in response to injury and disease and could conceivably occur in healthy adulthood. (B) Oligodendrocytes generated from OPCs in adulthood (blue) are known to elaborate shorter sheaths than oligodendrocytes laid down in development (green). Therefore, it is possible, that in the absence of oligodendrocyte death, new short internodes are added to partially or fully myelinated axons (red), to change the pattern of myelination and fine-tune conduction velocity.

(Hanafy and Sloane, 2011, reviewed by Olsen and Akirav, 2015). In mice, OPCs also proliferate and generate new oligodendrocytes, in response to demyelinating injuries induced by: the induction of experimental autoimmune encephalomyelitis (EAE; Tripathi et al., (2010); the focal injection of lysolecithin or ethdium bromide (Zawadzka et al., (2010); and the expression of human genes producing pathology reminiscent of amyotrophic lateral sclerosis (Kang et al., 2013) and Alzheimer's disease (Behrendt et al., 2013). However, in the amyotrophic lateral sclerosis model, the newly generated pre-myelinating oligodendrocytes failed to mature into myelinating oligodendrocytes to repair the myelin damage (Kang et al., 2013).

As new oligodendrocytes can replace those that die in response to some demyelinating injuries, it has also been proposed that new oligodendrocytes could replace those that die in the normal, healthy CNS (**Fig. 1.3**). However, recent evidence suggests that oligodendrocyte loss in the healthy mouse CNS is minimal. Mature oligodendrocytes, present in the P60 mouse brain, labelled using *Opalin-iCreER^{T2} :: Rosa26YFP* mice, largely remain at P600 (Tripathi et al., 2017), suggesting that oligodendrocytes are remarkably long-lived. Oligodendrocyte loss was observed in some CNS regions, such as the optic nerve and spinal cord (Tripathi et al., 2017), but the magnitude of this loss was small, suggesting that the ~6.5% of optic nerve oligodendrocytes, added between 4 and 6 months of age (Young et al., 2013), are not simply required to replace those that are lost. However, as the internodes laid down by adult-born oligodendrocytes are shorter than those laid down in development (Young et al., 2013), their alternative purpose could be to modify the pattern of myelin to, for example, fine tune conduction velocity (O'Rourke et al., 2014) (**Fig. 1.3**).

1.5 Growth factors and morphogens that regulate oligodendrogenesis

While the early stages of axon contact are intrinsically regulated by the developing oligodendrocyte, myelination is subsequently influenced by extrinsic factors, such as the electrical activity of neurons (reviewed in Bechler and ffrench-Constant, 2014). Key growth factor and morphogen signalling pathways that regulate myelination include the platelet-derived growth factor (PDGF), hedgehog (Hh), wingless / integrated (Wnt), Notch and bone morphogenic protein (BMP) / Id pathways (Wine-Lee et al., 2004; Feigenson et al., 2009; Ruat et al., 2012).

1.5.1 PDGF is a critical regulator of oligodendrogenesis

PDGF-A and PDGF-B are growth factors that form homo- and hetero-dimers, and bind to and activate PDGFRα and PDGFRβ, to regulate cell growth and proliferation (reviewed in Shim et al., 2010). In development, OPCs traverse large distances to populate the CNS,

before proliferating and differentiating into mature, myelinating oligodendrocytes (Vora et al., 2011), and OPCs also migrate in the mature CNS, into demyelinating lesion sites to initiate remyelination (Boyd et al., 2013). PDGF treatment is known to increase OPC migration, with even transient exposure to PDGF-A driving migration for up to 72 hours (Milner et al., 1997). By increasing PDGF-A levels within a demyelinated lesion, it is also possible to induce OPC migration to the lesion site, increase OPC proliferation and enhance remyelination (Yao et al., 2017).

The importance of PDGF signalling in promoting OPC proliferation, is reflected by the phenotype of PDGF-A knockout mice, which have fewer PDGFRα^{+} OPCs in comparison to their wildtype littermates, and have reduced oligodendrocyte number and myelin production (Fruttiger et al., 1999). However, this phenotype is likely to be the result of multiple functions of PDGF signalling, which not only promotes OPC proliferation, but is also a pro-survival factor for OPCs *in vitro* and *in vivo*. The treatment of cultured OPCs with PDGF results in an increase in both OPC proliferation and oligodendrocyte number (Grinspan et al., 1993) and the over-expression of PDGF-A *in vivo*, results in an increased number of OPCs (Calver et al., 1998; van Heyningen et al., 2001). However, the effects of serum starvation, which induces cell death in both OPCs and newly born oligodendrocytes in culture, can be reversed by the addition of PDGF to the culture medium (Barres et al., 1992). Similarly, increased PDGF signalling in the developing optic nerve, results in a 90% decrease in newborn oligodendrocyte death and a doubling of oligodendrocyte number (Barres et al., 1992).

1.5.2 FGF signalling in oligodendrogenesis

The fibroblast growth factor (FGF) family of growth factors regulate a number of cellular processes including proliferation, differentiation and organogenesis (reviewed in Ornitz and Itoh, 2015). It has 22 members, which bind to one of four FGF receptors (FGFR)1-4. At least 18 FGFs are expressed in the brain, across different developmental stages and brain regions (Ford-Perriss et al., 2001), and they are produced by several CNS cell types, including neurons and astrocytes, which each produce multiple members of the FGF family, in particular FGF1 and FGF2. Cells of the oligodendrocyte lineage express FGF receptors (Bansal et al., 1996; Fortin et al., 2005), with FGFR1, the receptor for FGF1 and FGF2, being expressed throughout the lineage (Fortin et al., 2005), while FGFR2 is expressed more highly by oligodendrocytes, relative to OPCs (Fortin et al., 2005). While FGFR3 is reportedly expressed by OPCs (Fortin et al., 2005), adult OPCs are not labelled in *Fgfr3-CreER*^{T2} transgenic mice (Young et al., 2010).

The binding of FGF9 to FGFR2 on oligodendrocytes encourages differentiation, leading to increased process length (Fortin et al., 2005), while FGF2 is important for the initial generation of OPCs during CNS development (Furusho et al., 2011), but also binds to the lineage-wide receptor FGFR1, to stimulate OPC proliferation and inhibit differentiation (McKinnon et al., 1990; Bansal, 2002; Fortin et al., 2005). Interestingly, Furusho et al. (2012) found that knocking out *Fgfr1* and *Fgfr2* did not affect the initiation of myelination, but did affect the regulation of myelin sheath thickness. From the second postnatal week *Fgfr1*/*Fgfr2* null animals had thinner myelin sheathes, a phenotype which persisted throughout adulthood (Furusho et al., 2012). Consistent with *in vitro* reports (Fortin et al., 2005), *Fgfr1*/*Fgfr2* null animals were also found to have a reduced transcription of myelin associated genes (Furusho et al., 2012). However, *Fgfr1* or *Fgfr2* knockdown can ameliorate the effect of cuprizone-induced demyelination, with reduction of either gene resulting in increased remyelination and increased recovery of running velocities on the complex running wheel (Mierzwa et al., 2013), suggesting that FGF signalling is actually inhibitory for repair following demyelination. However, as a cuprizone-induced callosal lesion is remyelinated by resident OPCs as well as OPCs newly generated from subventricular zone (SVZ) neural stem cells (Xing et al., 2014), these data also suggest that FGFR1 and FGFR2 are not critical for SVZ-derived oligodendrogenesis in adulthood.

1.5.3 Wnt signalling regulates OPC differentiation and myelination in the CNS

The Wnt protein family are secreted lipoproteins. Wnt signalling can occur either through the canonical or non-canonical arms of the Wnt pathway. The canonical Wnt pathway is dependent upon β-catenin, while the two non-canonical arms of the pathway, the planar cell polarity pathway and the Wnt/calcium pathway, are both β-catenin independent (Veeman et al., 2003). In unstimulated cells, β-catenin is phosphorylated in a destruction complex with axin, adenomatous polyposis coli (APC) and glycogen synthase 3β (GSK3β) and marked for ubiquitination and subsequently proteolytic degradation (Stamos and Weis, 2013). The canonical arm is activated by the binding of Wnt to the frizzled (Fz) receptor or a receptor complex consisting of Fz and its co-receptor low-density lipoprotein receptor-related protein 5/6, which transmits the Wnt signal to dishevelled (Dvl) a protein directly downstream of Fz (He et al., 2004; Feigenson et al., 2009), which acts as a switch between the canonical and non-canonical pathways. When Wnt is bound to Fz, the canonical pathway is initiated, starting with the disruption of the GSK3β-axin-APC destruction complex by translocation to the plasma membrane along with a negative regulator of axin (Reichsman et al., 1996). The negative regulator becomes associated with axin, dephosphorylating it and destabilising the destruction complex (Reichsman et al., 1996). Activation of Dvl leads to inhibition of the GSK3β of the destruction complex and release of β-catenin, allowing for its accumulation

and localisation to the nucleus. Once in the nucleus, β-catenin can induce a cellular response by activating specific target genes (Clevers, 2006).

Wnt signalling regulates multiple stages of OPC development, including OPC specification from stem cells, OPC differentiation, myelination and remyelination (reviewed in Guo et al., 2015; Gaesser and Fyffe-Maricich, 2016). Wnt signalling is a crucial regulator of the specification of OPCs during development, but the exact response of OPCs to Wnt signalling differs depending on developmental stage. Activation of *β-catenin* in the pMN domain of the developing spinal cord inhibit the generation and migration of OPCs from this zone (Dai et al., 2014), while the inhibition of Wnt signalling after OPC generation impairs oligodendrogenesis (Dai et al., 2014). These data suggest that Wnt signalling inhibits OPC specification early in development, but is necessary for differentiation later in development. *In vitro* studies have shown that inhibition of Wnt signalling can result in an increase in OPC proliferation (Ye et al., 2010), a decrease in proliferation (Chew et al., 2011) or have no effect on proliferation at all (Feigenson et al., 2009). When viewed *in vivo* however, Wnt signaling had no effect on OPC proliferation (Fancy et al., 2009; Feigenson et al., 2009).

Although the evidence linking Wnt signaling with myelination is strong, the exact relationship between Wnt signalling and the regulation of myelination is contradictory, with inhibition of Wnt signalling resulting in both the inhibition and promotion of myelination, depending on the genetic manipulations used (reviewed in Gaesser and Fyffe-Maricich, 2016). Early studies showed that activating the Wnt signalling pathway inhibited oligodendrogenesis (Fancy et al., 2009; Feigenson et al., 2009) and that deleting agonists such as APC, lead to an increase in oligodendrocyte development, but ultimately hypomyelination (Lang et al., 2013). Deleting *β-catenin* from the oligodendrocyte lineage may also have differing effects depending on the developmental stage. Deleting *β-catenin* from OLIG1^{+} cells prior to E10.5 in the mouse, results in fewer oligodendrocytes (Dai et al., 2014), while deletion from OPCs and oligodendrocytes after E12.5 has no effect on oligodendrocyte number (Lang et al., 2013). Interestingly, deleting *β-catenin* from astrocyte progenitors using a *hGFAP-Cre* mouse line at E13.5 reduced oligodendrocyte number (Gan et al., 2014), indicating that Wnt signalling in the surrounding cells may be a more important regulator for driving oligodendrogenesis than intracellular Wnt signalling. These data suggest that Wnt signalling is important for the regulation of myelination, although whether it is a positive driver of oligodendrogenesis or an inhibitor is still up for debate.

1.5.4 Shh regulates myelination and remyelination in the CNS

Sonic hedgehog (Shh), along with Indian hedgehog and Desert hedgehog, is one of three members of the Hh family. Shh signalling is vital for organogenesis and tissue patterning

during vertebrate development (reviewed in Xavier et al., 2016) and influences the the proliferation of adult neural stem cells (Wechsler-Reya and Scott, 1999; Kenney and Rowitch, 2000; Palma et al., 2005), and cancer development (reviewed in Skoda et al., 2017).

In the developing spinal cord, gradients of growth factors, including Hh and Wnt, create distinct progenitor domains. As Shh is secreted ventrally from the floor plate (Tekki-Kessaris et al., 2001) and Wnt is secreted dorsally from the roof plate, two opposing gradients of signalling molecules are created. The Hh gradient results in the creation of five distinct domains that can be identified in the ventral half of the ventricular spinal cord, p3, pMN, p1, p2 and p0, and six in the dorsal spinal cord, dP6, dP5, dP4, dP3, dP2 and dP1 (**Fig. 1.4**). (Dessaud et al., 2008). The combination of homeodomain transcription factors that are expressed in each domain, determines the identity of the cells arising from it, with each domain producing one or more neuronal subtypes (Wine-Lee et al., 2004).

The majority of spinal cord OPCs are derived from the pMN domain and these OPCs give rise to around 85% of the mature oligodendrocytes in the adult spinal cord (Zhou et al., 2001). As the pMN is the second closest of the 11 domains to the source of Shh secretion, this exposes the domain to a high concentration of Shh. This is also true in zebrafish, where both Shh and Indian hedgehog have been shown to be important for OPC specification during embryonic development (Park et al., 2004; Chung et al., 2013). It has, however, been proposed that the two Hh pathways are performing individual, contrasting roles, with Indian hedgehog regulating neural progenitor proliferation and Shh driving proliferation, although both are necessary for the specification of OPCs from neural progenitors (Chung et al., 2013). This is true also for the specification of OPCs from postnatal stem cell niches in the brain, where Shh activates the Shh receptor smoothened (SMO), to increase OPC production (Tong et al., 2015).

In addition to driving oligodendrocyte specification, Shh addition to human embryonic forebrain-derived mixed glial cultures, increased OPC proliferation (Ortega et al., 2013). Similarly, OPC proliferation was enhanced in spinal cord explant cultures, derived from rats that had experienced a contusion injury and been treated with the Shh agonist Ag11.1, relative to mice treated with vehicle (Bambakidis et al., 2010). This proliferative response appears to require the multi-ligand receptor megalin (also known as LRP2), as blockade of this receptor prevents the Shh-mediated increase in OPC migration and proliferation (Ortega et al., 2012). Megalin can be found on the surface of CNS astrocytes, where it can endocytose or exocytose Shh in order to mediate the proliferative response of OPCs (Ortega et al., 2012). In addition to mediating proliferation, Shh can promote oligodendrocyte

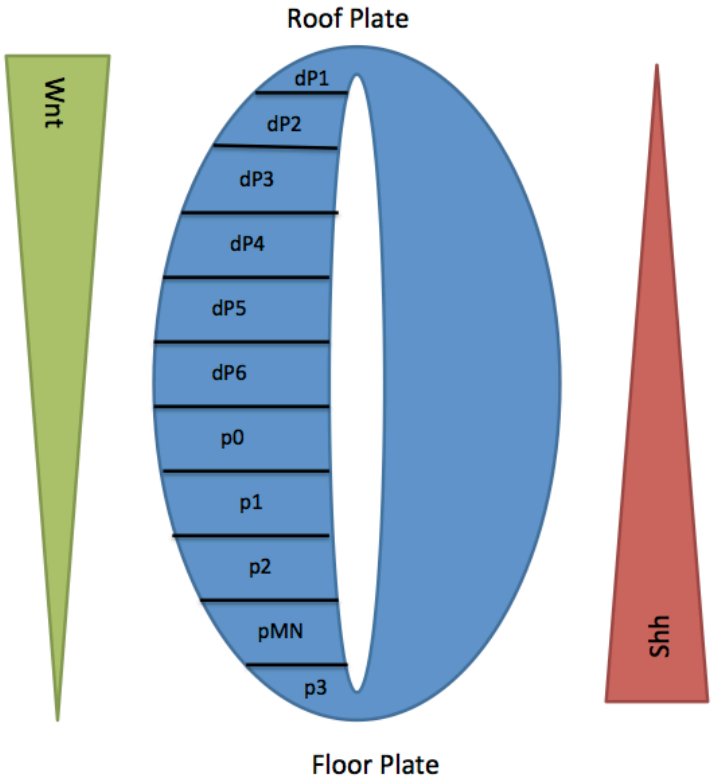

Figure 1.4: Shh and Wnt signalling gradients in the developing spinal cord

In the developing spinal cord, Shh is secreted from the floor plate and Wnt is secreted from the roof plate. This creates a gradient of signalling molecules, which stimulates the development of 11 distinct progenitor zones. 5 progenitor zones are ventrally located, p3, pMN, p2, p1 and p0 and 6 are dorsally located dP1- dP6. The pMN domain is a major site of OPC generation.

differentiation and myelination. For example, cortically-derived rat OPC cultures treated with Shh have a higher rate of oligodendrocyte differentiation when compared to untreated controls (Wu et al., 2012). Additionally, inhibition of Shh signalling using cyclopamine, an inhibitor of the Shh receptor SMO, results in decreased expression of myelin associated genes such as *MBP* and *myelin associated glycoprotein*, that can be rescued by activating SMO with the agonist SAG (Wang and Almazan, 2016).

Shh signalling is a strong driver of OPC proliferation, oligodendrogenesis and myelination in response to various models of demyelination, including: lysolecithin injection (Ferent et al., 2013); cuprizone-induced demyelination (Sanchez and Armstrong, 2018); traumatic brain injury in both the cortex and the CC (Mierzwa et al., 2014); spinal cord hemi-section (Thomas et al., 2014), and EAE (Zhang et al., 2015). OPCs react rapidly in response to demyelinating injury, increasing rates of proliferation and oligodendrogenesis (Levine, 1994; Hughes et al., 2013) and evidence suggests this relationship is due, at least partially, to Shh signalling.

Following a traumatic axonal injury, the OPC population in the mouse CC is increased in the SVZ and cortex of *Gli1-CreER^{T2} :: Rosa26-YFP* mice, where it is maintained until 6 weeks post-injury, but were unable to observe a change in the OPC population in the CC (Mierzwa et al., 2014). Increasing Shh signalling, by injecting the Shh pathway agonist SAG was found to further increase the OPC population in the SVZ of the *Gli1-CreRT^{T2}::R26YFP* mice after injury, although there was still no change in OPC numbers in the CC (Mierzwa et al., 2014). These data suggest that Shh is important for driving the increase in OPC proliferation in response to injury in the SVZ for up to six weeks in the SVZ, but may not be in the CC.

Lysolecithin injection into the CC of 6-8 week old *Plp-GFP* mice, produced a significant increase in OPC number and proliferation, alongside increased transcription of Shh by cells of the oligodendrocyte lineage (Ferent et al., 2013). Adenoviral over expression of Shh in the lesion site, further increased OPC proliferation, oligodendrogenesis and remyelination , while Shh inhibition was found to have the opposite effect (Ferent et al., 2013), suggesting that promoting Shh signalling could be therapeutically enhanced to treat demyelinating disease.

Fingolimod, an immunomodulatory drug that targets the sphingosine-1-phosphate receptor (Miron et al., 2008; 2010), and is commonly prescribed for MS, has been reported to influence Shh signalling. Following EAE induction in mice, Fingolimod treatment increases OPC proliferation, oligodendrogenesis and myelin gene expression, relative to saline treated controls (Zhang et al., 2015). Fingolimod treatment significantly increased the expression of Shh, its receptor SMO, and Gli1, and when Shh action was blocked by cyclopamine

administration, the effects of Fingolimod treatment on OPC behaviour and oligodendrogenesis were negated (Zhang et al., 2015). These data suggest that Shh signalling in the oligodendrocyte lineage drives OPC proliferation, oligodendrogenesis and myelination in the rodent CNS *in vivo,* and demonstrates that Shh signalling mediates the response of oligodendrocyte lineage cells to Fingolimod treatment in a model of demyelinating disease.

While there are many growth factor signalling pathways that influence oligodendrogenesis (reviewed in Waly et al., 2014), the Wnt, PDGF, FGF and Shh signalling pathways signal at or influence signalling at the primary cilium (Huangfu et al., 2003; Christensen et al., 2008; Lancaster et al., 2011; Zaghloul and Brugmann, 2011; Ruat et al., 2012). The primary cilium is an organelle that protrudes from the surface of many vertebrate cells.

1.6 The primary cilium

Vertebrate cilia are classified as motile and non-motile cilia (Satir and Christensen, 2007; Pedersen and Rosenbaum, 2008). Motile cilia are often present in clusters or bundles, found in wet, high mucous environments such as the respiratory epithelium (Enuka et al., 2012) or female reproductive tract (Enuka et al., 2012), and move in a synchronous manner, generating physical flow or movement (Lewin, 2007). The cytoskeleton of a motile cilium consists of nine microtubule doublets arranged in a ring called an axoneme, with a central pair of singlet microtubules - this is known as a 9+2 arrangement and all microtubules protrude from the basal body, a structure similar to the centrosome (Satir and Christensen, 2007).

Non-motile or primary cilia also have a cytoskeleton of nine microtubule doublets, but they lack the central pair of singlets that are required for cilliary movement, and instead have a 9+0 arrangement (Satir and Christensen, 2007). Primary cilia are also considerably smaller, being only 1-5μm in length. The mammalian primary cilium was first identified by KW Zimmermann (1898) as being assembled on a number of mammalian cells types and in several organisms, including human tissue. Zimmermann noted that in rabbit kidney tissue, every cell possessed a primary cilium (Zimmermann, 1898), and not only did the first transmission electron microscopy images of the primary cilium came from epithelial kidney cells, but the first reports defining the primary cilium as a sensory organelle, came from studies using tubule epithelial cells from the kidney, and the first evidence of ciliopathies began with studying polycystic kidney disease in a cilium knockdown Oak Ridge polycystic kidney (ORPK) mouse model (Bloodgood, 2009).

Despite its small size, the primary cilium is very important. Dysfunction of primary cilia or the associated proteins can lead to a large number of disorders termed ciliopathies. Ciliopathies produce clinically diverse symptoms, including errors in the left/right body axis, polydactyly, abnormal neural tube patterning and polycystic kidneys (Berbari et al., 2009). Genetically, ciliopathies can be less diverse, as different mutations in the same gene can produce distinctly different clinical symptoms, suggesting that the severity of the mutation can influence the clinical symptoms. Ciliopathy research is growing rapidly, as more diseases are being linked to defective ciliary function. While the function of many of genes identified as carrying mutations in confirmed ciliopathies are still unknown, others such as inositol polyphosphate-5-phosphatase E (Bielas et al., 2009) and intraflagellar transport protein 88 (IFT88) (McIntyre et al., 2012), are known to be responsible for ciliary signalling or the assembly and disassembly of primary cilia, respectively.

Cilia are assembled through an ordered pathway of distinct steps (Sorokin, 1968). Typically cilia formation begins following a cell division, when the cell is exiting the cell cycle, during the G_0 or G_1 (Ishikawa and Marshall, 2011). Assembly starts when the basal body differentiates from the centrosome as the cell exits the cell cycle. The basal body associates with membrane vesicles *en route* to the cell surface, and once the basal body is anchored to the cell membrane, the vesicles fuse to the plasma membrane establishing the ciliary membrane compartment (Sorokin, 1968). The basal body then nucleates α-tubulin and β-tubulin heterodimers, leading to outgrowth of the axonemal microtubules and creating a protrusion from the cell surface. In the transition zone, which is the region of the cilium distal of the basal body (Sánchez and Dynlacht, 2016), the outer doublets begin to form and continue exclusively at the distal end of the cilium (Rosenbaum and Child, 1967). As protein synthesis cannot occur inside the cilium, proteins are carried into the cilium by intraflagellar transport (IFT). Proteins are transported along the microtubule cytoskeleton to and from the cilia tip by IFT motor proteins in order to facilitate cilium elongation and assembly (Pedersen and Rosenbaum, 2008). The cilium remains highly dynamic, with new tubulin being laid down constantly and old tubulin being removed, in order to maintain the cilium at a constant length (Marshall and Rosenbaum, 2001).

As the cell re-enters the cell cycle after G_0 and prior to M phase, primary cilium disassembly occurs in two 'waves', with the first occurring during the G_1 phase and the second prior to mitosis (reviewed in Sánchez and Dynlacht, 2016). Although disassembly has been extensively studied, the process is not well understood. It has been proposed that disassembly is triggered by an interaction between the enzyme Aurora A, a centrosomal kinase, and histone deacetylase 6 (HDAC6), which in turn acts upon tubulin to collapse the primary cilium. However, as tubulin acetylation is not associated with microtubule

stabilisation, deacetylation would not be expected to weaken the microtubule cytoskeleton and collapse of the cilium (Palazzo et al., 2003). Additionally *HDAC6* knockout mice only have a weak phenotype as opposed to the severe disease phenotype and embryonic lethality that would be expected to be observed if cilia disassembly was not occurring (Zhang et al., 2008). In addition to regulating HDAC6, Aurora A has also been shown to activate inositol phosphate 5-phosphatase (INPP5E) (Plotnikova et al., 2015) which in turn produces phosphatidylinositol 4-phosphate (PtdIns(4)P). Accumulation of INPP5E and PtdIns(4)P has been observed in unciliated cells, but is absent in those with assembled primary cilia (Xu et al., 2016), indicating that INPP5E and PtdIns(4)P may be playing a role in the inhibition of ciliogenesis through an unknown mechanism.

In the assembly and maintenance of the cilium, axonemal subunits are transported from the cell body to the cilium tip via anterograde transport. Once the cargo has been delivered the IFT particles return to the cell body using retrograde transport systems. During cilia disassembly in the unicellular flagellate *Chlamydomonas,* an increased rate of cargo free IFT particles enter the primary cilium, suggesting the number of axoneme subunits being delivered to the cilium tip decreases. There is also an increase in the number of axoneme subunits being transported out of the cilium (Pan and Snell, 2005). However, in mammalian PTK1 cells, the entire axoneme is released into the cytoplasm before centriole length is decreased, reducing cilium length (Rieder et al., 1979), and suggesting that cilia disassembly can occur through IFT-independent mechanisms.

1.7 The role of primary cilia in nervous system development

An understanding of the proteins expressed by primary cilia and the genes involved in primary cilia assembly and disassembly has allowed researchers to study and disrupt the generation of primary cilia in a cell specific manner to reveal the critical role of this organelle in neural development.

1.7.1 Signalling at the primary cilium alters neural stem cell proliferation and differentiation in adulthood

While it is unknown whether the primary cilium is critical for oligodendrogenesis, signalling at the primary cilium is vital for the maturation and differentiation of a number of other stem and progenitor cell types in the CNS (Han et al., 2008; Carter et al., 2012). During embryonic tissue patterning, neurogenesis is reliant upon the same Shh gradient that influences OPC specification (see 1.5.4), with different neuronal subtypes generated from different stem cell domains. Inhibition of cilium assembly in the developing CNS result in developmental deformities in the brain (Gorivodsky et al., 2009; Goetz and Anderson, 2010). Shh signalling

at the primary cilium regulates neuroepithelial progenitor cell division, by inhibiting miR-219, which promotes the polarization and proliferation of these cells, during zebrafish development (Hudish et al., 2016). Additionally, the primary cilium is important for the development of retinal ganglion cells in the Zebrafish (Lepanto et al., 2016), and the ablation of ciliogenesis in these cells, reduces their proliferation, reduces neural retina volume and delays retinal development (Lepanto et al., 2016). Knockdown of miR-219 was also found to accelerate primary cilium growth (Hudish et al., 2016). These data indicate that signalling at the primary cilium is vital for the correct proliferative and neurogenic response of neural progenitors during CNS development.

Clium assembly is also a regulator of adult neural stem cell proliferation and neurogenesis in the subgranular zone of the dentate gyrus in mice (Han et al., 2008). *Kinesin family member 3A* (*Kif3a)* is a gene encoding a kinesin subunit, that is exclusively associated with primary cilia assembly. The conditional deletion of *Kif3a* from glial fibrillary acidic protein $(GFAP)^{+}$ cells, prevents neural stem cells from generating a primary cilium. Primary cilia were identified on stem cells in the dentate gyrus of P0 control mice, but those in the *Kif3a* deleted mice had stunted ciliogenesis, such that the primary cilia comprised only of a basal body and transition fibers under a short expansion membrane, without an axoneme (Han et al., 2008). Stem cell proliferation was reduced in the dentate gyrus of these mice, and the disorganized dentate gyrus was suggestive of a defect in postnatal granule neurogenesis (Han et al., 2008).

hGFAP-Cre::Kif3a$^{fl/fl}$ transgenic mice also had defective Hh signalling. Quantitiative polymerase chain reaction (PCR) and *in situ* hybridization indicated that expression of the Hh target gene *Gli1*, was reduced in the dentate gyrus of *hGFAP-Cre::Kif3a*$^{fl/fl}$ mice compared to controls (Han et al., 2008). Furthermore, β-galactosidase reporter activity confirmed that the Shh receptor Patched (Ptchd) was expressed by cells in the hippocampus of control mice, but absent from the hippocampus of *Kif3a* deleted mice (Han et al., 2008). These data indicate that the primary cilium and Hh signalling are vital for the proliferation of neural stem cells in the subgranular zone of the dentate gyrus, and consequently neurogenesis and the cellular organization of this brain region.

In order to examine the role of primary cilia in regulating adult neurogenesis, Tong et al. (2014) performed stereotaxic injections of Cre recombinase (Cre)-overexpressing adenovirus, into the ventral SVZ of *Kif3a*$^{fl/fl}$ *:: Z/EG* mice at P0, which simultaneous deletes the *Kif3a* gene, preventing cilium assembly, and expresses green fluorescent protein (GFP) in the recombined cells. This technique targeted a small population of radial glia in the ventral SVZ, allowing for normal development of the gross brain anatomy (Tong et al., 2014).

Reduced cilium assembly was not evident until P30 and as a result mice were given injections of bromodeoxyuridine (BrdU) from P40-P45 to label dividing cells. Mice were sacrificed at P60 and the number of recombined cells which lacked primary cilia, but had undergone cell division since P40 were quantified (Tong et al., 2014). Radial glia-derived ventral SVZ stem cells were less able to differentiate into deep granule neurons in the olfactory bulb of *Kif3a*$^{fl/fl}$*::Z/EG* when compared with control mice, suggesting that signalling at the primary cilium is important for differentiation in these cells.

1.7.2 Signalling at the primary cilium is important for neuronal function

Primary cilia are also on the surface of mature neurons. As neurons are not capable of proliferation or differentiation, it is likely that they perform a different role here, than on proliferative precursor cells, however what that is, remains unclear. In the developing neocortex, cilium assembly is initiated on neuronal cells during late fetal development, as the basal body can be observed docked to the cell surface (Arellano et al., 2012). However, elongation of the cilium cytoskeleton is not observed until P4 (Arellano et al., 2012). Primary cilia can be identified on the surface of excitatory pyramidal neurons and inhibitory interneurons, but preventing cilium assembly had no affect on neuronal migration, organisation or polarity (Arellano et al., 2012). By contrast, in adult-born hippocampal neurons, cilium assembly occurs as the migrating neurons reach their final destination (Kumamoto et al., 2012). In these neurons, cilia ablation severely affects dendritic refinement and synapse formation, suggesting that primary cilia are important for the connectivity of adult-born neurons (Kumamoto et al., 2012), although the exact signalling pathways affected remains unknown.

The activation of Shh signalling in rat hippocampal neurons initiates axon extension (Yao et al., 2015), suggesting that Shh may play a role at the primary cilia of mature neurons. However, axon elongation by ciliated and unciliated neurons suggested a cilia-independent mechanism of Shh signalling in neurons. By contrast, in the peripheral nervous system, Hh signalling at the primary cilium is heavily implicated in modulating the ciliary localisation of odorant receptors essential to the function of olfactory sensory neurons in drosophila (Sanchez et al., 2016). More specifically, inactivation of the Shh receptor Smo, which translocates to the cilium surface during Hh signalling, impairs the olfactory response of flies, while inactivation of the Shh receptor Ptchd, increased olfactory responsiveness, suggesting that Ptchd activation typically inhibits olfactory receptor binding (Sanchez et al., 2016), making the primary cilia critical for olfactory neuron function.

Communication is important for oligodendrocytes. While oligodendrocytes have been shown to communicate with neurons through the primary cilium, they are also capable of cilium

independent signalling pathways. For instance, oligodendrocytes have been shown to express receptors for neurotransmitters such as GABAA, which can be found on the cell surface (Hamilton et al., 2017).

1.7.3 Primary cilia promote Schwann cell progenitor proliferation

Shh signalling at the primary cilium is a critical regulator of myelination in the peripheral nervous system (Yoshimura and Takeda, 2012). In the peripheral nervous system, myelination is performed by Schwann cells, that myelinate a single segment of a single axon, by wrapping their entire cell body around the axon. When Schwann cell progenitors are co-cultured with dorsal root ganglion neurons, they differentiate into mature Schwann cells and myelinate the axons. Following Schwann cell differentiation, the number of cells in the cultures expressing molecular markers associated with assembled primary cilia decreases, and the primary cilia can no longer be detected on the cell surface (Yoshimura and Takeda, 2012). These data indicate that primary cilia are disassembled as Schwann cells differentiate, indicating that the mature myelinating cells, at least in the peripheral nervous system, are not subject to further regulation by this organelle.

Treating the co-cultures with desert hedgehog, but not Shh, significantly upregulated *Gli1* m messenger ribonucleic acid (mRNA) expression and increased the number of myelin segments per culture (Yoshimura and Takeda, 2012). This indicates that Hh signalling at the primary cilium can promote peripheral myelination by increasing the proliferation of Schwann cell precursors, resulting in a larger pool of cells that can differentiate and myelinate or accelerates Schwann cell differentiation.

1.8 The primary cilium as a regulator of CNS myelination

1.8.1 Could PDGF signalling at the primary cilium regulate CNS myelination?

In fibroblasts, PDGFRα signalling occurs at the primary cilium (Schneider et al., 2005). During the growth arrest phase, when cilia are assembled, PDGFRα expression is upregulated and localised to the primary cilium. However, in *Tg737*^{orpk} fibroblasts, that carry a mutation in the mouse homologue of *IFT88*, rendering them unable to assemble primary cilia, PDGFRα is no longer upregulated (Schneider et al., 2005). While this is a single study, it indicates that, under some circumstances, PDGFRα signalling, which is an important regulator of CNS myelination, can be localised to the primary cilium. Due to the extensive expression of PDGFRα throughout the cell body of OPCs, PDGFRα signalling is not solely localised to the primary cilium. However, if PDGFRα signalling also occurs at the primary cilium, it is unclear whether this would produce a distinct cellular response.

1.8.2 FGF signalling at the primary cilium regulating CNS myelination

While knockdown of *Fgfr1* or the *Fgf* in zebrafish reduces expression of IFT88, a protein essential for cilium assembly and ciliogenesis (Neugebauer et al., 2009), and results in primary cilia shortening, it is unclear whether these primary cilia alteration are associated with the dysregulates organ patterning and laterality that is also part of this phenotype (Hong and Dawid, 2009; Neugebauer et al., 2009; Yamauchi et al., 2009). However, these data identify FGF as regulating primary cilia parameters, and given the strong link that exists between FGF signalling and oligodendrogenesis and myelination (see section 1.5.2), it is possible that FGF exerts an influence on this lineage by modulation of the primary cilia structure.

1.8.3 Can Wnt signalling at the primary cilium regulate CNS myelination?

Evidence for Wnt signalling at the primary cilium has been mixed. Many studies have implicated canonical Wnt signalling at primary cilia, however primary cilia ablation has been shown to enhance the sensitivity of cells to Wnt signalling, suggesting that the primary cilium has an inhibitory effect upon Wnt signaling (Huang and Schier, 2009; Ocbina et al., 2009). Knockdown of *BBS1, BB4* and *MKKS*, three genes associated with Bardet-Beidl syndrome (BBS), results in primary cilia loss and a heightened response to Wnt in cultured cells (Gerdes et al., 2007), and the presence of a primary cilium reduced canonical Wnt signalling in mouse embryonic fibrobasts (MEFs) and embryonic stem cells (Corbit et al., 2008). Lancaster et al. (2011) found that MEFs, in which cilium retraction was induced, showed exaggerated Wnt activity relative to control cells. Similarly enhanced Wnt activity was observed in MEFs with a nonsense mutation in the *Dnchc2* gene, which lacked primary cilia development and dentate granule cells, expressing a recessive form *Kif3a*, preventing cilia assembly, displayed higher levels of β-catenin relative to wild type controls indicating increased canonical Wnt signalling (Kumamoto et al., 2012).

Furthermore, in MEFs lacking primary cilia, β-catenin and jouberin (Jbn) (a protein required for ciliogenesis) localised to the nucleus of the cell, while in ciliated MEFs β-catenin and Jbn were found to be localised to the basal body (Lancaster et al., 2011). These data suggest that the primary cilium mediates canonical Wnt signalling by compartmentalising β-catenin and Jbn. Activation of the Wnt signalling pathway by Wnt binding to the receptor Fz causes Jbn to interact with β-catenin. Jbn and β-catenin then translocate to the nucleus. In a ciliated cell, this translocation is inhibited by retrograde IFT, which restricts Jbn and β-catenin localisation to the primary cilium. In an unciliated cell the nuclear translocation of Jbn and β-catenin is uninhibited (Lancaster et al., 2011).

1.8.4 Evidence for Hh signalling at the primary cilium regulating CNS myelination

In vertebrate cell types, the Hh signalling pathway involves two trans-membrane proteins, the Hh receptor Ptchd and the transducer SMO, and the Gli family of transcription factors, Gli1-3 (Ruat et al., 2012). In the absence of the Hh ligand, Ptchd localises to the base of the cilium where it prevents Smo from binding to the cell membrane. The Gli transcription factors form a complex with kinesin family member seven, an anterograde kinesin motor involved in IFT, allowing them to be transported to the cilium tip. Suppressor of fused (SUFU) is located at the cilium tip where it promotes the truncation of Gli family members into their repressor forms known as GliR. GliR is transported back to the nucleus, using the IFT dynein motor, where it inhibits the transcription of the target genes (Ruiz i Altaba et al., 2007) (**Fig. 1.5**).

In the presence of Shh, the inhibition of Smo by Ptchd is relieved allowing Smo to interact with β-arrestin (β-Arr) and translocate into the cilium where it accumulates. The accumulation of Smo relieves the repression exerted on the Gli transcription factors by SUFU converting the Gli family transcription factors into their activator forms, known as GliA. Activated GliA translocates from the cilium tip to the nucleus to activate (or repress) the transcription of Hh target genes (Ruat et al., 2012) (**Fig. 1.5**).

The reliance of Shh signalling on the primary cilium and the importance of Shh signalling in OPCs, strongly implicates primary cilia in regulating CNS myelination. However, the importance of the primary cilium in regulating OPC and oligodendrocyte function has not been explored.

1.8.5 Signalling at the primary cilium regulates CNS myelination

While the importance of primary cilia for CNS myelination has not been investigated directly, disruption of the primary cilium has been shown to affect the development of $NG2^+$ $PDGFR\alpha^+$ cells in the periventricular zones of a $Bbs1^{M390R/M390R}$ mouse model of the human ciliopathy BBS (Carter et al., 2012). The M390R mutation of the *Bbs1* gene, affects the basal body of the primary cilium and results in abnormal cilia development and mice carrying this mutation develop ventriculomegaly between P0 and P3, and have twice as many apoptotic OPCs in the CC as control mice by P7 (Carter et al., 2012). Quantification of $BrdU^+$ $NG2^+$ $PDGFR\alpha^+$ cells in the SVZ, also showed that $Bbs1^{M390R/M390R}$ mice had approximately 50% fewer proliferating OPCs relative to wildtype controls.

The treatment of $Bbs1^{M390R/M390R}$ mice with lithium reduced the cross sectional area of the ventricles by ~50% relative to mice treated with sodium chloride, and doubled the number proliferating cells detected (Carter et al., 2012). Lithium treatment phosphorylates AKT and

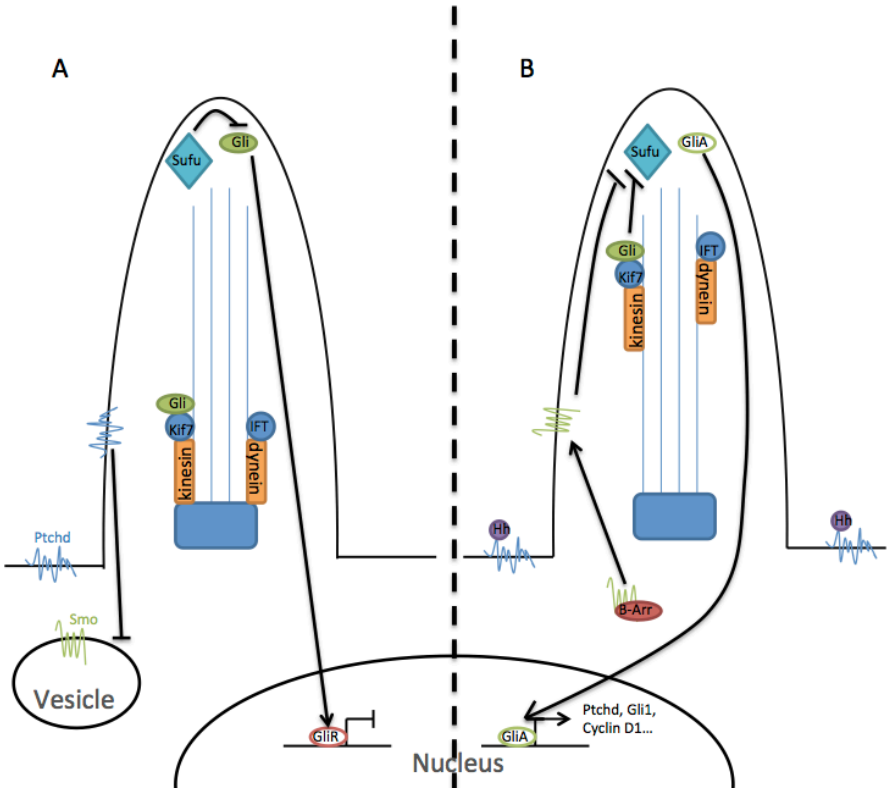

Figure 1.5: Hh signalling in the presence and absence of the hh ligand

(A) In the absence of the Hh ligand (purple), Ptchd localises to the base of the cilium where it prevents Smo insertion in the cell membrane. Gli transcription factors form a complex with Kif7, allowing them to be transported to the cilium tip. SUFU is located at the cilium tip where it promotes Gli truncation into the repressor form (GliR). GliR is transported to the nucleus, via the IFT dynein motor, where it inhibits the transcription of the target genes. (B) In the presence of the Shh ligand, inhibition of Smo by Ptchd is relieved, allowing Smo to interact with β-arrestin (β-Arr) and translocate into and accumulate in the cilium. The accumulation of Smo relieves the repression exerted on the Gli transcription factors by SUFU, allowing conversion of the Gli transcription factors into their activator form, GliA. GliA, bound to the Kif7 motor, are transported to the cilium tip where they accumulate. Activated GliA translocate from the cilium tip to the nucleus, where they activate transcription of Hh target genes. Adapted from Ruat et al. (2012).

GSK3β, key downstream effectors of, the PDGFRα signalling pathway. This effect would be consistent with the importance of PDGFRα signalling for cells of the oligodendrocyte lineage. However, lithium treatment, and the phosphorylation of GSK3β, would also affect a number of other signalling pathways, including some that have been shown to associate with the primary cilium such as Notch and Wnt (Espinosa et al., 2003). So while this study links OPC development and primary cilia, the signaling mechanism are unknown.

1.9 Hypotheses and aims

The presence of a primary cilium on oligodendrocyte lineage cells has never been directly investigated. Both gene and protein expression studies suggest that OPCs have the capacity to assemble primary cilia the only way to directly identify the role of the primary cilium in the oligodendrocyte lineage is through preventing primary cilium assembly or blocking pathways which are reliant upon the primary cilium. Signalling at the primary cilium, and regulation of the primary cilium, involves many of the signaling pathways that also instruct the behaviour of cells of oligodendrocyte lineage. PDGFRα is a key regulator of OPCs, particularly their survival and proliferation; FGF plays a vital role in the regulation of myelin thickness; Wnt regulates oligodendrocyte differentiation and myelination, and Shh is important for OPC specification and proliferation. Of these pathways, Shh signalling is most reliant upon the primary cilia in vertebrate cell types. However, due to the collective importance of these signaling pathways to for CNS myelination, I hypothesise that *primary cilia regulate OPC proliferation*. Furthermore, I hypothesise *that primary cilia are essential for oligodendrogenesis in the healthy CNS*. To test each of these hypotheses, I will achieve the experimental aims detailed below.

Hypothesis 1: That primary cilia regulate OPC proliferation

Aim 1: To determine whether OPCs assemble primary cilia in vitro and in vivo.
I will first determine whether OPCs express genes associated with primary cilium assembly and signalling by performing *in situ* hybridisation on mouse primary OPC cultures. Cilium assembly, by OPCs and oligodendrocytes, will be examined by performing immunocytochemistry and immunohistochemistry.

Aim 2: To determine whether primary cilia status is influenced by cell cycle entry
I will perform live imaging of cultured OPCs, with fluorescently-tagged primary cilia, to dynamically evaluate primary cilia assembly and disassembly over time, and in relation to cell cycle transition. To examine this *in vivo*, proliferating cells will be acutely labelled with EdU, and immunohistochemistry performed to identify OPCs currently or recently in s-phase of the cell cycle, and determine their primary cilia status.

Aim 3: To determine whether Kif3a (and cilia assembly) is critical for OPC proliferation

Primary OPC cultures from *Pdgfrα-histGFP::Kif3a*$^{fl/fl}$ mice will be treated with tat-Cre to delete Kif3a and prevent primary cilia assembly, before 5-ethynyl-2'-deoxyuridine (EdU) is added to the culture medium to identify proliferating cells. The number of EdU^+ OPCs will be quantified in control and *Kif3a*-deleted cultures.

Hypothesis 2: that primary cilia are essential for oligodendrogenesis in the healthy CNS

Aim 4: To induce DNA recombination selectively in adult OPCs

PDGFRα, which is often used to identify OPCs, is also expressed by a number of cell populations outside of the CNS – populations that may also rely on primary cilia for their correct function. To determine whether *Pdgfrα-CreER*^{T2} transgenic mice could be used to selectively target deoxyribonucleic acid (DNA) recombination in OPCs, adult *Pdgfrα-CreER*^{T2}*::Rosa26-YFP* transgenic will be given Tx and DNA recombination assessed in PDGFRα-expressing cells in a number of tissues and organs.

Aim 5: To assess the effect of conditional Kif3a-deletion on oligodendrogenesis

Pdgfrα-CreER^{T2}*::Rosa26-YFP::Kif3a*$^{fl/fl}$ mice will receive Tx in adulthood, to conditionally ablate cilia assembly by OPCs. The number of newborn oligodendrocytes added to the brain will be identified by immunohistochemistry and quantified over time in control and *Kif3a*-deleted mice.

Aim 6: To determine whether acutely reducing adult oligodendrogenesis affects motor coordination or visual acuity

I will compare the performance of *Pdgfrα-CreER*^{T2}*::Kif3a*$^{fl/fl}$ and control transgenic mice across a series of motor and visual acuity tests including gait analysis, grip strength testing and the optokinetic visual acuity test.

Aim 7: To determine whether acutely reducing adult oligodendrogenesis alters short-term memory, anxiety-like behaviours or depression

I will compare the performance of *Pdgfrα-CreER*^{T2}*::Kif3a*$^{fl/fl}$ and control transgenic mice in the T-maze and novel object recognition task, to examine short-term memory. Anxiety-like state will be tested using the elevated plus maze, the open field test and the marble bury test and depression will be tested using the forced swim test.

Chapter 2: Methods

2.1 Transgenic mice

Pdgfrα-CreER^{T2} (Kang et al., 2010), *Pdgfr-H2BGFPknock-in* mice (referred to as *Pdgfrα-histGFP)* (Hamilton et al., 2003) *Plp-CreER^{T2}* (Doerflinger et al., 2003) and *Rosa26-YFP* (Srinivas et al., 2001) transgenic mouse lines were obtained from Jackson Laboratories, *Kif3a$^{fl/fl}$* (Marszalek et al., 1999) mice were obtained from the University of California, Davis and the *Sox10-GFP* mouse line was a kind gift from Professor William D Richardson (UCL) and maintained on a C57Bl6 background. *Pdgfrα-CreER^{T2}*, *Pdgfrα-histGFP and Plp-CreER^{T2}* (Doerflinger et al., 2003) mouse lines were maintained as heterozygous lines, renewed by mating with C57Bl6 mice (also from Jackson Laboratories), while the *Kif3a$^{fl/fl}$* and *Rosa26-YFP* transgenic mice were maintained as homozygous lines. All offspring were weaned at P28, but housed with gender-matched littermates after weaning to ensure normal myelin development (Makinodan et al., 2012). Mice were housed in individually ventilated Optimice^{TM} cages (Animal Care Systems, USA), on a 12-hour light-dark cycle, with food and water available *ad libitum*. Male and female mice were used for this study and all experiments were approved by the University of Tasmania Animal Ethics Committee (13741 and 16151).

2.2 Genotyping

Pdgfrα-histGFP and *Sox10-GFP* neonates were genotyped by light to determine GFP expression. For all other genotyping ear biopsies were collected from transgenic mice at ~P20 and used to obtain genomic DNA as previously described (O'Rourke et al., 2016). Each biopsy was digested in 100mM Tris-HCl / 5mM EDTA / 200mM NaCl / 0.2% SDS / 0.48mg/ml proteinase K (ThermoFisher Scientific; AM2542) overnight at 55°C. The cellular and histone proteins were precipitated by exposure to 6M ammonium acetate (Sigma; A1542) and incubation on ice for 15 minutes (min). After centrifugation, the genomic DNA (gDNA) was precipitated from the supernatant with isopropyl alcohol (Sigma; I9516). The DNA pellet was washed in 70% Ethanol (Sigma; E7023), and resuspended in sterile MilliQ water. 50-100ng of gDNA was used as the template and a region of the gene of interest amplified by PCR, in a 25µL reaction, also containing 0.5µL of each primer (100nmol/mL; GeneWorks) and 12.5 µL GoTaq® green master mix (Promega, M7123) in MilliQ water.

To genotype mice expressing the *Rosa26-YFP* transgene we used three primers: Rosa26 wildtype 5' AAAGTC GCTCT GAGTT GTTAT; Rosa26 wildtype 3' GGAGC GGGAG AAATGG ATATG and Rosa26 YFP 5' GCGAA GAGTT TGTCC TCAACC and a PCR

program of: 94°C for 4'; 37 cycles of 94°C for 30", 60°C for 45", and 72°C for 60", followed by 72°C for 10 min. If present, the *Rosa26-YFP* PCR product is a 550bp fragment of the wildtype *Rosa26* gene and a 250bp product corresponding to the *Rosa26* gene locus containing the loxp-stop-loxp-YFP transgene.

Kif3a$^{fl/fl}$ transgenic mice were genotyped by PCR using three primers: Kif3a_1 5' AGG GCA GAC GGA AGG GTG G, Kif3a_2 5' TCT GTG AGT TTG TGA CCA GCC and Kif3a_3 5' TGG CAG GTC AAT GGA CGC AG under the following conditions: 94°C for 4', followed by 34 cycles of 94°C for 30", 62°C for 45", and 72°C for 60", and a final 10 min at 72°C. This PCR has the potential to produce two DNA products - one product of ~350bp corresponding to expression of the wildtype *Kif3a* gene and an ~130bp (Marszalek et al., 2000) larger product corresponding to expression of the *Kif3a*$^{fl/fl}$ allele.

The PCR designed to detect expression of the gene coding for Cre recombinase was used to genotype both *Pdgfrα-CreER*^{T2} and *Plp-CreER*^{T2} mouse lines, and produced a 500bp product in the presence of Cre and no product when Cre was absent. The Cre PCR was carried out using the following primers: Cre 5' CAGGTC TCAGG AGCTA TGTCC AATTT ACTGA CCGTA; Cre 3' GGTGTT ATAAG CAATC CCCAGAA under the following conditions: 94°C for 4', followed by 34 cycles of 94°C for 30", 62°C for 45", and 72°C for 60", and a final 10 min at 72°C.

2.3 Tx administration

Tx (Sigma, T5648-5G) was reconstituted to 40 mg/ml in corn oil and sonicated for ≥ 1 hour until dissolved. Mice received 300mg/kg Tx by oral gavage, administered daily for 4 consecutive days, from postnatal day 57 (P57). Mice were weighed and monitored daily. No side-effects of Tx administration were observed. Our dosing regimen provides the maximal amount of Tx that can be tolerated by young adult mice without observing adverse side-effects (Rivers et al., 2008). Mice did not lose ≥10% of their starting body weight. Examining the tissue from 3 days after the final Tx dose (P57+7) allows recombination to occur and the fluorescent reporter to be expressed.

2.4 Perfusion fixation

Mice were terminally anaesthetised with a 30mg/kg intraperitoneal (i.p.) injection of sodium pentobarbitone (Ilium, Troy Laboratories, NSW, Australia). Once unconscious, but prior to respiratory failure, the chest cavity was opened to expose the heart. A small incision was made in the right atrium of the heart and the perfusion needle inserted into the left ventricle. 4% paraformaldehyde (PFA) (w/v) (Sigma, P6148) in phosphate buffered saline (PBS) was

perfused through the vasculature at approx. 9ml/min. Following fixation, tissues of interest were dissected. Brains were sliced into 2mm thick coronal slices using a brain matrix, and immersion fixed for 90 min at room temperature. All other tissue was removed and immersion fixed for 90 min at room temperature. Tissue was cryopreserved in 20% sucrose (w/v) (Sigma, S0389) in PBS overnight at 4°C prior to embedding in optimal cutting temperature cryomatrix (Thermo Scientific, 6769006) and storage at -80°C.

2.5 Cell culture

2.5.1 Generating mixed glial cultures

The protocol for generating mixed glial cultures was based on the protocol previously published in Young et al. (2013). P0-P5 *Pdgfrα-histGFP* and *Pdgfrα-histGFP* x *Kif3a*$^{fl/fl}$ transgenic mouse pups were genotyped with blue light to confirm histGFP fluorescence and then decapitated, the brains removed and cortices isolated into Earle's balanced salt solution (EBSS, Invitrogen, 14155-063). Cortices were chopped into pieces of approximately 2mm were collected into 2mL EBSS and treated with 50µl 0.25% (w/v) trypsin (Sigma, T4799) in EBSS at 37°C for 15-20 min (Pringle et al., 1996). 50µl 5.25mg/ml DNAse1 (Sigma, 5025) in MilliQ was added followed by 2mL EBSS / 10% FCS (Invitrogen, 10099-141). Tissue pieces were allowed to settle before the medium was removed and replaced with 2mL of EBSS. The tube was tapped sharply to dissociate cells, and tissue pieces allowed to settle before the medium was transferred to a clean tube. This process was repeated, and tissue pieces remaining after the second transfer were gently triturated before being transferred. The pooled cell suspension was passed through a 40µm cell sieve (BD, 352340) and centrifuged for 5 min at 500rcf, before the supernatant was removed and the pellet gently resuspended in 16mL of complete OPC medium (Appendix 1) and plated in 3 wells of a 6 well plate. Each well was pre-treated with >30,000 MW poly-D-lysine hydrobromide (PDL, Sigma, P7405) (2.6.3 PDL pre-treatment). Cultures were incubated at 37°C and 5% CO_2 .

2.5.2 Purifying OPCs by fluorescence activated cell sorting

7 days *in vitro* (DIV) primary mixed glial cultures were rinsed twice in EBSS before 2ml of 50% EBSS / 50% TryplE (Thermofisher Life Technologies, 12604013) was applied to each well, and plates were incubated at 37°C and 5% CO_2 for 15-20 min, to allow the cells to dislodge from the plastic. 200µl FCS was added to each well to inactivate trypsin and the well contents were gently triturated before being pooled and centrifuged at 500g for 5 min. The supernatant was removed and the pellet resuspended in 3ml 50% EBSS / 50% FCS and passed through a 40µm cell sieve. ~50µl of the cell suspension was reserved (propidium iodide (PI) negative control for flow cytometry) and the remainder treated with PI

(Sigma, P4170), diluted in PBS to a final concentration of 0.02mg/ml. OPCs (GFP^+, PI negative cells) were purified from the glial cell suspension using a Beckman Coulter MoFlo Astrios cell sorter (Beckman Coulter, CA, USA) and collected into 2ml complete OPC media.

After sorting, the OPC suspension was centrifuged at 500g for 5 min, the supernatant removed and the pellet resuspended in 1mL of complete OPC medium. The number of viable OPCs was quantified using a haemocytometer (Sigma, z359629) and trypan blue (Sigma, T8154) exclusion. OPCs were plated onto PDL-coated 13mm #1 glass coverslips (Lomb, CSC131GP) in 24 well plates, at a density of 30,000 cells / well in 500µl of complete OPC medium for immunocytochemistry or protein lysate collection. Alternatively cells were plated on PDL-coated 35mm glass bottom culture dishes with a 14mm glass diameter (In Vitro Scientific, D35-14-1-N) at a density of 20,000 cells per dish in 2ml of complete OPC medium for live imaging. Cultures were incubated at 37°C and 5% CO_2.

2.5.3 PDL pre-treatment

Prior to plating mixed glial or sorted OPC cultures cell substrates (culture wells, coverslips and turning dishes) were pre-treated with 0.05mg/mL >30,000 MW poly-D-lysine hydrobromide (PDL)(Sigma, P7405) for a minimum of 1 hour. PDL was then removed and the substrate rinsed twice in sterile MilliQ before being left to dry completely inside a biosafety cabinet.

2.5.4 HEK293T cell culture

HEK293T cells were grown in Dulbecco's Modified Eagle Medium (DMEM; Invitrogen, 10566-016) containing 10% FCS and 1% penicillin / streptomycin (Invitrogen, 15140122) and incubated at 37°C and 5% CO_2. The medium was changed at least twice a week or more frequently if the phenol red pH indicator indicated that the medium was becoming acidic (yellow).

Cells were subcultured when they reached a confluence of 75-90% (approx. once per week). Cells were treated with 50% TryplE in EBSS until they dislodged from the bottom of the dish with light swirling. The medium was transferred into a centrifuge tube and centrifuged at 500g for 5 min. The supernatant was removed and the pellet resuspended in fresh medium. Approx. 1/10 of the resuspended cells were seeded into a fresh flask and topped up with fresh media.

2.5.5 Tat-Cre treatment of cultured cells

A solution of 1, 2 or 4 mg/ml tat-Cre (Excellgen, EG-1001) was made up in OPC complete medium and used to replace the existing culture medium of 8-10 DIV sorted OPC cultures or 10 DIV mixed glial cultures, plated onto 13mm glass coverslips in a 24 well plate. Wells contained 150µl of complete OPC media and were topped-up to 300µl with the tat-Cre-containing medium, to a final concentration of 0.5µM, 1µM or 2µM. Cultures were incubated at 37°C and 5% CO_2 for 90 min, before the medium was removed and replaced with 500µl complete OPC media, and incubated for a further 72h before being fixed, used for live imaging or harvested for Western blot analysis.

2.5.6 Fixation of cultured cells

Culture medium was gently removed and replaced with ice-cold 4% PFA and incubated on ice for 5 min, before being replaced with ice-cold methanol, and incubated for a further 5 min. Methanol was removed and 3 x PBS washes performed. Cells were stored in PBS at 4°C until required for immunocytochemistry

2.5.7 Transfection of cultured cells

HEK cells were transfected using an Effectene transfection kit (QIAGEN, 301425) according to manufacturer's instructions, using 0.3-2µg of plasmid DNA per transfection.

Cultured OPCs were transfected using a NeuroMag magnetofection kit (OZ Biosciences, MN50200) according to manufacturer's instructions, using 0.5-1µg of plasmid DNA and 0.5-1µl of NeuroMag solution per transfection. A medium change was performed 1-2 hours after transfection.

2.5.8 Preparation of cells for live imaging

1-2 hours prior to live imaging, the culture medium was replaced with live imaging medium (Appendix 1). The live imaging protocol is described in section 2.11.2.

2.6 EdU administration

2.6.1 *In vitro* administration of EdU

Stocks of 2.5mg/ml 5-ethynyl-2'-deoxyuridine (EdU; E10415) in EBSS were stored at -20°C. Culture medium was gently removed from 8-10 DIV OPC cultures or 10 DIV mixed glial cultures (13mm coverslips; 24 well plate) and replaced with complete OPC medium containing 2.5µg/ml EdU. Cultures were maintained at 37°C and 5% CO_2.

2.6.2 Oral administration of EdU

To perform long-term labelling of proliferating OPCs *in vivo*, EdU was administered to adult mice via the drinking water at a concentration of 0.2mg/ml as previously described (Clarke et al., 2012). EdU is light sensitive, and was administered via opaque water bottles (Optimice, C79135A) and replenished every 48 hours.

2.6.3 i.p injection of EdU

To acutely label a population of OPCs transitioning through s-phase of the cell cycle, adult mice received 3 x 20µl i.p injections of EdU (1mg/ml in PBS), at 2 hourly intervals, with the final injection being given 2 hours prior to perfusion fixation. This protocol labels OPCs entering s-phase over a 6 hour period.

2.7 Protein quantification by western blot

2.7.1 Collecting cells for protein lysates

Cultured cells were rinsed twice with ice-cold PBS. 75-100µl of radioimmunoprecipitation assay (RIPA) buffer (Appendix 1) was added to the first well and the cells scraped off. The RIPA buffer and cells were then transferred to the next well and this was repeated until the cells were collected from 4 wells of a 12 well plate. Cell lysates were centrifuged at 13,000rpm for 5 min and the supernatant transferred to a fresh tube. Lysates were stored at -80°C until use.

2.7.2 Bradford assay

Bovine serum albumin (BSA; Sigma A7030) was diluted in MilliQ to create 2, 1, 0.5, 0.25 and 0.125 mg/ml standards. 5µl of each standard, RIPA-only and each protein lysate was assayed in triplicate. 25µl of the reagent mix, containing 1ml of protein assay reagent A (BioRad, 500-113) and 20µl protein assay reagent S (BioRad, 500-115), and 200µl of protein assay reagent B (BioRad, 500-115), was added to each well, and incubated at ~21°C for 15 min, before being read on a spectramax plate reader (Molecular Devices). The protein concentration of each lysate was determined from the standard curve.

2.7.3 Western blotting

Western blots were performed using a Bolt® western blotting system with pre-cast gels (BIO-RAD, Hercules, CA). Samples were mixed with 4x sample buffer (Thermofisher/Invitrogen, B0007), 500mM dithiothereitol (DTT; Sigma, D0632) and MilliQ and incubated at 70°C. Samples were run on an 8-12% precast sodium dodecyl sulfate (SDS) gel (Life

Technologies, NW04125BOX) with 2-(N-morpholino)ethanesulfonic (MES) running buffer (Life Technologies, B0002) for 22 min at 200V.

After the SDS gel was run, proteins were transferred onto a polyvinylidene fluoride (PVDF) membrane (BioRad, 162-0177) using a Bolt® transfer cassette. Each side of the cassette was assembled with two sponges and two pieces of filter paper soaked in transfer buffer (Appendix 1) before the protein gel and transfer membrane were sandwiched between the two halves. Once the cassette was loaded it was placed into the chamber and covered with transfer buffer. The protein was transferred from the gel to the membrane at 20V, over a 60 min period.

Once transfer was complete the membrane was blocked in 5% milk/tris buffered saline-Tween20 (TBS-T) (Appendix 1) for 1 hour at room temperature. Membrane was then incubated with primary antibodies (Appendix 2: Table 3) in milk/TBS-T on an orbital mixer at 4°C, overnight. The antibody-containing solution was removed, and three 10 min TBS-T washes performed. Membrane were incubated with secondary antibodies (Appendix 2: Table 3) in milk/TBS-T on an orbital mixer at 4°C, overnight, before 3 x 10 min TBS-T washes were performed.

Detection substrates (Millipore, WBKLS0500) were combined in a 1:1 ratio and warmed to approx. 37°C. Membranes were placed face up on the imager with the detection substrate mix poured over the top and covered with a sheet of acetate. The membrane was imaged using an Amersham imager 600 (GE Healthcare, Chicago, IL) and auto exposure, with the exposure time adjusted as necessary to prevent over-exposure. The membrane was removed and washed in PBS. If a second staining round was necessary, the membrane was covered with stripping buffer (Thermofisher, 46430) and incubated for 5 min at room temperature on an orbital shaker. The membrane was washed three times in TBS-T and the process repeated from blocking.

2.8 Plasmid DNA amplification

The *pEGFP-Arl13b* plasmid was generously donated by Dr Judith Paridaen in the Huttner lab (Max Planck Institute, Dresden, Germany) and n-terminal (Clontech, 632523) and c-terminal (Clontech, 632524) mCherry fusion vectors purchased from Clontech (Mountain View, CA).

2.8.1 Transformation

DSHΔ chemically competent *E.coli* were thawed on ice. 1µl of 500ng/µl plasmid DNA, 50µl ice-cold KCM (10mM KCl, 30mM $CaCl_2$, 50mM $MgCl_2$), and 50µl of thawed DSHΔ cells were

combined and incubated at 42°C for 60 sec, and rapidly transferred to ice for a further 5 min. 1ml of antibiotic-free luria broth (LB; Appendix 1) was added and the tube, and incubated at 37°C for 45 min. Cells were spun down in a benchtop centrifuge at 700 rpm for 1 min to pellet, and all but 100µl of medium removed. Cells were then plated onto agar plates (Appendix 1) containing 100µg/ml Kanamycin (Thermo Fisher, 11815024) and incubated at 37°C overnight. Bacterial plates were then stored at 4°C to prevent further growth.

2.8.2 DNA minipreps and glycerol stocks

Individual colonies were picked from bacterial plates, using a 200µl pipette tip with the end partially melted. Each tip was dropped into a 50µl centrifuge tube, with 15ml of LB (Appendix 1) containing 100µg/ml Kanamycin. Tubes were then incubated at 37°C on a shaker overnight or until the LB had turned cloudy. 2-3ml of bacterial broth was pelleted by centrifugation and and the DNA extracted using a QIAprep spin miniprep kit (QIAGEN, 27104) according to the manufacturer's instructions. DNA was eluted into MilliQ H_2O and stored at -20°C. For long-term storage of the transformed bacterial clones, 150µl of glycerol (Sigma, G2025) and 800µl of the bacterial broth were combined in a 1ml cryotube and stored at -80°C.

2.8.3 Digesting and ligating plasmid DNA

Plasmid DNA was digested using N.E.B. enzymes and buffers (New England Biolabs, Ipswich, MA). 5-10µg of DNA was digested by with 5µl of the required enzyme in 10µl of the appropriate 10x enzyme buffer and 10µl of 1:10 BSA, made up to 100µl with nuclease free water and incubated at 37°C for two hours. As a precaution, to guard against the self-ligation of any partially digested vector products, the linearized DNA was treated with Antarctic Phosphatase (New England Biolabs, Ipswich, MA) as per the manufacturer's instructions.

2.9 RNA probe synthesis and *in situ* hybridisation

2.9.1 Generating an RNA probe template

Stab cultures of *E.coli* containing plasmids coding for *SMO, sentan (SNTN), intraflagellar transport protein 81 (IFT81), patched 2 (PTCHD2), Kif3a* and *PDGFRα* were purchased from Source Biosciences (Nottingham, UK)(table 2.1). Each clone was streaked onto a 0.5% (w/v) agar plate containing the appropriate antibiotic and incubated at 37°C overnight (see table 2.1 for antibiotics). DNA was amplified, purified and digested using methods described in 2.8. The restriction enzyme selected, cut the DNA at the 5' end of the coding sequence (see table 2.1 for restriction enzymes).

Plasmid	Vector	Enzyme 1	Enzyme 2	Buffer	Antibiotic resistance
pEGFP-Arl13b-C1	*pEGFP-C1*	Kpn1	Pst1	N.E.Buffer 2	Kan
pmCherry-C1	*pmCherry-C1*	Kpn1	Pst1	N.E.Buffer 2	Kan
pmCherry-N1	*pmCherry-N1*	Kpn1	Pst1	N.E.Buffer 2	Kan
Kif3a clone	*pFLC1*	Not1	-	N.E.Buffer 3	Amp
Ift81 clone	*pYX-Asc*	Sal1	-	N.E.Buffer 3	Amp
Smo clone	*pCMV-SPORT6*	Sal1	-	N.E.Buffer 3	Amp
Ptchd2 clone	*pYX-Asc*	EcoR1	-	EcoR1	Amp
Sntn clone	*pCR-Blunt2-TOPO*	Not1	-	N.E.Buffer 3.1	Kan

Table 2.1 Restriction digests used for digesting plasmids

Table showing restriction digests performed when generating mCherry plasmids and In situ probes. Columns show the generated plasmid that was being digested, the vector that the plasmid was contained in, the enzymes used and the buffer the digest was performed in.

The linearised DNA template was purified using a QIAquick PCR purification kit (QIAGEN,28104) according to the manufacturer's instructions. Briefly, buffer PB was added to the digested DNA in a ratio of 5:1. The solution was transferred to a spin column, placed within a collection tube and centrifuged for 30-60 seconds at 13,000rpm. The eluent was discarded. 750µl of buffer PE was added to the spin column and centrifuged for 30-60 seconds at 13,000rpm. The flow through was discarded and the spin column centrifuged for a further 1 min at 13,000rpm. The spin column was transferred to a clean microcentrifuge tube and 30µl MilliQ added to the membrane. The samples were incubated for 1 min and centrifuged for 1 min at 13,000rpm to elute the linearised DNA. The quality of the DNA template was evaluated by running 5µl on a 1% agarose gel at 100V for 30 min.

2.9.2 RNA probe synthesis

Ribonucleic acid (RNA) probes were synthesised from linearised DNA template using either T7, T3 or SP6 RNA polymerase (Promega, M0251S, P4024 and M0251S) according to the manufacturer's instructions. For each synthesis reaction, 2µl of water was combined with 5µl of template DNA, 5µl of 5x transcription buffer, 7.5µl of DTT (Sigma Aldrich, D0632), 2.5µl of the digoxigenin (DIG) labelling mix (Roche, 11277073910, 1µl of RNAsin (Promega, N26611) and 2µl of the required RNA polymerase (table 2.1), and incubated at 37°C for 2 hours. 75µl of diethyl pyrocarbonate (DEPC)-treated MilliQ water was added to each reaction and the probe stored on ice until its quality could be verified, by running 5µl of the RNA probe on a 1% agarose gel at 100V for 30 min. Quality RNA probes were stored at -80°C until required.

2.9.3 *In situ* hybridisation

The RNA probe was combined 1:500 with pre-heated hybridisation solution (Appendix 1) and incubated at 70°C for 5 min. 300µl of the RNA probe-hybridisation buffer solution was applied to each 13mm coverslips, containing 7-10 DIV OPCs, placed in the central wells of a 12 well plate, with the cell surface facing up. 1ml of PBS was added to all empty wells and Parafilm (Beemis, PM996) placed over the top of the plate before the lid was placed on. The plate was sealed with masking tape and incubated overnight at 65°C in a hybridisation oven. The RNA probe-hybridisation solution was removed, replaced with 1ml pre-heated wash solution (Appendix 1) and incubated at 65°C for 30 min. Three additional 30 min wash steps were performed at 65°C followed by 2 x 10 min maleic acid buffer-Tween 20 (MABT) (Appendix 1) washes at ~21°C. MABT was removed, replaced with 500ml *in situ* blocking solution (Appendix 1) and incubated at ~21°C for 1 hour. Anti-DIG- alkaline phosphatase (AP) (Roche, 11093274910), was applied in blocking solution at 1:1500 and incubated

overnight at 4°C. Antibody was removed and 3 x 15 min MABT washes performed at ~21°C, followed by 2 x 5 min washes in 1x pre-staining buffer (Appendix 1). Pre-staining buffer was removed and replaced with staining buffer (Appendix 1), and the plate covered with foil and incubated at 37°C in a hybridisation oven for 2 hours or until a blue colour was visible, before the reaction was stopped by replacing the staining buffer with MilliQ. Coverslips were EtOH dehydrated, dipped in xylene and mounted using DPX (Sigma, 44581).

2.10 Mouse behavioural testing

2.10.1 Handling and habituation

Mice were handled and weighed daily from P40 until the commencement of optomotor training (P54-P56), after which point, mice were weighed weekly. Before all motor tests, mice were transferred to the test room at least 60 min prior to testing. For the forced swim test, mice were moved to the testing room 1 hour prior to the light cycle change and testing did not begin until 1 hour after. The elevated plus maze, T-maze, open field test and novel object recognition test were conducted during the dark cycle i.e. when the mice were awake and active. During this habituation period, any lights that would illuminate the arena during testing, were turned on.

2.10.2 Optokinetic reflex testing

The rotating optomotor drum is 30cm in diameter and consists of a series of alternating black and white lines at spatial frequency of 0.26 cycles per degree (cpd), which is the most effective frequency for optokinetic reflex testing in C57Bl6 mice (Abdeljalil et al., 2005). Each mouse was placed on a raised central podium within a dimly lit, closed arena and allowed to habituate for 5 min with the drum stationary. Any mouse that left the podium was placed back on the podium during this period. After habituation, the drum was turned on, so that the stripes moved clockwise (CW) and counterclockwise (CCW) for two minutes each way, with a 1 min break between directions. The start direction alternated between trials, to remove order bias. Each trial was video recorded for later analysis. Mice were trained for 2 days and baseline recorded prior to Tx gavage. Following Tx administration mice underwent optokinetic reflex testing weekly. To analyse optokinetic reflex performance the number of ‘head movements’ made by the mouse over the 2 min period was recorded for each direction. A head movement was defined as clear movement of the head in the direction of the rotating stripes, followed by a short, rapid ‘reset’ head movement in the opposite direction.

2.10.3 Gait analysis

Gait analysis was performed using a Digigait™ Imaging System (Mouse Specifics, USA). Mice were habituated to the treadmill with the treadmill lights on for five min. The treadmill was then activated, and mice were video recorded as they ran at 18cm/s, 22cm/s and 26cm/s. Mice ran at each speed for approximately 30 seconds before being slowly ramped up to the next testing speed. Mice were then allowed to rest before testing was repeated at an incline of 3° and then a decline of -3°. Gait analysis was carried out on video segments, in which mice ran for 2-3 seconds without obvious acceleration using Digigait analysis software (Mouse Specifics, MA, USA). Digigait testing was performed once prior to Tx gavage and at 7, 14, 21, 28, 35 and 43 days post gavage.

2.10.4 Grip strength

Grip strength can be used as a measure of decline in muscle strength and coordination (Clark et al., 2018). The protocol was adapted from Clark et al. (2018) and measured using a Chatillon grip strength meter (Columbus Instruments, OH, US). Grip strength testing was performed once prior to Tx gavage and at 7, 14, 21, 28, 35 and 43 days post gavage. Mice were held by the base of the tail and gently but firmly pulled directly backward along the grid allowing contact with only their fore-paws or with all four paws. At each test-point grip strength was recorded five times each for the fore-paws and all four paws and the maximum result was recorded.

2.10.5 Marble bury test

The marble bury test can be used to examine anxiety and OCD-like behaviours in rodents, with an increase in marble burying behaviour indicating increased anxiety (Angoa-Pérez et al., 2013; Kedia and Chattarji, 2014). The protocol was adapted from Deacon et al. (2005). Mice were individually placed in a clean Optimice cage (Animal Care Systems, CO, USA) containing 5cm deep bedding, that was pressed flat and 10 marbles (1.5cm diameter). Marbles were placed on the surface of the bedding, evenly spaced at ~4cm apart. Individual mice were placed in the cage and left undisturbed for 30 min, then returned to their original cage. The number of marbles that were more than 50% submerged in substrate was recorded.

2.10.6 Forced swim test

The forced swim test protocol was adapted from Can et al. (2012). A clean glass beaker (15cm diameter) was filled with 24 ± 1°C water to a depth of 15cm. Mice were individually placed in the water, back feet first and left to swim for 5 min before being gently dried off and

returned to their home cage. The amount of time spent actively swimming, passively swimming, climbing and floating was recorded. Active swimming was defined as swimming with movement of three or more paws, passive swimming involved movement with only one or two paws and floating was defined as no movement of any limbs. Climbing was defined as upward movement of the mouse while facing at a 90° angle against glass of the beaker. Ethovision software was used to record video, track mice and perform manual scoring of behaviours.

2.10.7 Elevated plus maze

The elevated plus maze is a measure of anxiety and was performed as previously described in Walf and Frye (2005). Mice were individually placed in the centre of a plus shaped maze consisting of two open arms, 30cm x 5cm with a light intensity of 70 lux and two closed arms 30cm x 5cm x 15cm with a light intensity of 20 lux. The maze was elevated 50cm from ground level. Mice were positioned in the centre of the maze facing towards an open arm and allowed to explore the maze for a single 5 min trial, before being returned to their home cage. The time spent in each of the open and closed arms was recorded. Ethovision software was used to record video, track mice and perform manual scoring of behaviours. Manually scored behaviours can give a further indication of changes in anxiety-like behaviour (Kulesskaya and Voikar, 2014) and included head dipping, when the mouse dips its head below the level of the platform; supported rear, when the mouse rears onto its hindpaws while supporting its body weight on the maze walls; unsupported rear when the mouse rears onto its hindpaws without supporting itself on the maze; and grooming .

2.10.8 T-maze

The T-maze protocol was adapted from Deacon and Rawlins (2006). Mice were individually placed in the start arm of a T-shaped maze with 30cm long arms and allowed to make a decision as to which of the other ‘choice’ arms it entered. Once the mouse had entered one of the ‘choice’ arms the entrance was blocked off and the mouse allowed to explore the arm for 1 min. The mouse was then removed, the blocked arm reopened and the mouse returned to the start arm. Each mouse was allowed to make a total of 10 decisions during the duration of the testing process. Re-entering the same arm as the previous trial was considered an ‘error’ in alternation and the total number of errors made over the 10 trials was recorded.

2.10.9 Open field test

The open field test measures anxiety and exploratory behaviours (Ennaceur, 2014). It was adapted from (Kulesskaya and Voikar, 2014). Mice were individually placed in a 30cm x

30cm arena, that was divided into a brightly lit centre (250 lux) and a shaded perimeter. The mice were allowed to explore the box for a single 10 min trial, then returned to their home cage. The amount of time spent in the centre and perimeter zones was recorded. Ethovision software was used to record video, track mice and perform manual scoring of behaviours. Manually scored behaviours included supported rearing, unsupported rearing and grooming.

2.10.10 Novel object recognition

The novel object recognition test protocol was adapted from Taglialatela et al. (2009). Novel object recognition testing was performed in the same 30cm x 30cm arena used for the open field test. Mice were habituated to the arena during open field testing, which was performed 24 hours before the first day of novel object testing. For novel object testing the lighting was reduced to 35 lux in the centre zone. On the first day of testing mice were individually placed into the arena with two identical objects (duplo towers). Mice were allowed to explore the box for ten min, then returned to their home cage. The amount of time each mouse spent interacting with each object was recorded. 24 hours later, the test was repeated but, one of the objects replaced with a novel object of similar size, but different shape and colour (a duplo figure). The amount of time each mouse spent interacting with the novel and familiar objects was recorded. Ethovision software was used to record video, track mice and perform manual scoring of behaviours. The position of the two objects was swapped between trials on both day 1 and day 2 of testing. Manually scored behaviours included supported rearing, unsupported rearing, climbing of the objects and grooming.

2.11 Immunohistochemistry

Cryosections (30µm) were collected as floating sections from brain, spinal cord, eye, spleen, liver, kidney, heart, adrenal gland and pituitary gland. Cryosections of sciatic nerve, gastrocnemius, intestine, and bone marrow (tail) were collected directly onto glass microscope slides. Sections were processed for immunohistochemistry as previously described (Young et al., 2010), using primary antibodies at concentrations specified in Table 1. Primary antibody binding was visualised by applying secondary antibodies conjugated to Alexa Fluor-488, -568, -594 or -637 (Appendix 2: Table 2). Tissue was also exposed to Hoechst 33342 (Invitrogen; 1:10,000 dilution) to visualise the cell nuclei. Floating sections were mounted onto glass microscope slides and the fluorescence of all slides preserved by the application of fluorescent mounting medium during coverslipping (Dako, S3023).

2.11 Microscopy

2.11.1 Light microscopy

Light microscopy was performed using 40x and 60x air objectives on an Axio Lab.A1 (Zeiss, Germany) microscope with a Axiocam ICc5 (Zeiss, Germany) camera and Axiocam (Zeiss, Germany) software.

2.11.2 Live imaging

Live imaging was performed using a Nikon Eclipse TI microscope (Tokyo, Japan). The live imaging protocol was adapted from Paridaen et al. (2013). Live videos were recorded for 8-12 hours using differential interference contrast (DIC), 488 and 568 emission filters and a 60x water immersion lens. Images were acquired every 10 min and at 1µm z-plane slices with an Andor Zyla camera (Andor Technology, Belfast, Northern Ireland). Cells were maintained at 37°C and 5% CO_2 during the imaging period. Videos were analysed using NIS Elements software (Nikon, Tokyo, Japan).

2.11.3 Confocal microscopy

Confocal images were collected using an UltraView spinning disk confocal microscope with Volocity Software (Perkin Elmer, Massachusetts, USA) with standard excitation and emission filters for DAPI (Hoechst 33342), FITC (Alexa Fluor-488), TRITC (Alexa Fluor-568) and far red (Alexa Fluor-647). When imaging tissue sections, Hoechst 33342 was used to consistently define the region of interest within the tissue section. For *Pdgfrα-CreER*^{T2} characterisation (Chapter 4), a single z plane image was collected using the 20x air objective, and images were stitched together in the x-y planes using Volocity software. For primary cilium quantification *in vitro* and *in vivo*, confocal z-plane images were collected at 0.5µm intervals, using the 40x water and 60x oil objectives, and stitched together (in z-y-z planes) using Volocity software. For all other immunocytochemistry and immunohistochemistry, confocal stacks were collected 2µm apart using the 20x air and 40x water objectives, and stitched using Volocity software.

Cell counts were performed manually from exported images, viewing the images in ImageJ software version 1.46r (NIH, Washington DC, USA) and Adobe Photoshop CS6. Images were collected from each relevant area, across a minimum of 3 cryosections per mouse, and a minimum of 3 biological replicates per treatment condition.

2.12 Statistical analysis

Statistical analyses were performed in GraphPad Prism 6 (GraphPad, La Jolla, CA, USA). Data was first tested to determine whether it was normally distributed. All data was normally distributed and were analysed according to need, by performing a two tailed t-test, one-way analysis of variance (ANOVA), two-way ANOVA or repeated measures ANOVA, followed by a Bonferroni multiple comparisons post-hoc test. Data are presented as mean ± standard deviation (std dev) unless otherwise stated and analyses were performed in $n \geq 3$ mice in each case.

Chapter 3: *Kif3a* is required for primary cilia assembly by OPCs, and regulates OPC proliferation *in vitro*

3.1 Introduction

Developmental and adult OPCs are highly proliferative *in vitro* (Wu et al., 2011) and *in* vivo (Levison et al., 1999; Horner et al., 2000; Dawson et al., 2003; Lasiene et al., 2009; Clarke et al., 2012), and at ~5% of all cells, are the largest proliferative cell population in the mature CNS (Dawson et al., 2003). Despite primary cilia being a feature common to many proliferative cell types (reviewed in Goto et al., 2017), assembled and disassembled as the cells progress the cell cycle (Han et al., 2008; Spassky et al., 2008; Tong et al., 2014), the presence of primary cilia on the surface of OPCs has not been explored.

Microarray and RNA sequencing studies, comparing gene expression profiles from CNS cell types in the early mouse cortex, indicate that OPCs express genes critical to primary cilia assembly, such as *Kif3a* and *Ift81*, and the Shh receptors, *Ptchd2* and *Smo*, that are known to localize at primary cilia (Cahoy et al., 2008; Zhang et al., 2014). Furthermore, these genes are more highly expressed by OPCs than mature, myelinating oligodendrocytes (Cahoy et al., 2008; Zhang et al., 2014), suggesting that primary cilia are assembled on OPCs and disassembled during differentiation. Therefore, in this thesis Chapter, I will test the hypothesis *that primary cilia on the surface of OPCs are dynamic, and assembled and disassembled with the cell cycle.*

Kif3a$^{fl/-}$ transgenic mice (Marszalek et al., 2000) have been used to interrogate the role of primary cilia on a variety of cell types, as they can be used to prevent primary cilium assembly in a cell-specific manor. For example, the deletion of *Kif3a* from cerebellar granule cell precursors, reduces the developmental, Shh-mediated expansion of this progenitor pool (Spassky et al., 2008). This phenotype is similar to that observed in humans diagnosed with the ciliopathy known as Joubert syndrome, which results in abnormal cerebellar development (Spassky et al., 2008). When cilia assembly or disassembly was instead prevented in radial astrocytes in the hippocampal dentate gyrus of the developing mouse brain (Han et al., 2008) (Tong et al., 2014), neurogenesis was compromised.

In this chapter, I will examine OPCs cultured from early postnatal *Pdgfrα-histGFP* transgenic mice, to determine whether cells of the oligodendrocyte lineage assemble primary cilia *in vitro.* I will then generate OPC cultures from *Pdgfrα-histGFP::Kif3a*$^{fl/fl}$ mice and treat them

with tat-Cre and EdU in order to determine the ability of the primary cilium to regulate OPC proliferation.

3.2 Results

3.2.1 OPCs can be purified from mixed glial cultures by flow cytometry

To determine whether cultured OPCs express genes associated with primary cilia assembly / disassembly or signalling, I generated mixed primary glial cultures from the cortex of P0-P3 *Pdgfrα-histGFP* transgenic mice (see methods). In cells derived from *Pdgfrα-histGFP* mice, the *Pdgfrα* gene promoter drives expression of a histone-targeted form of GFP, such that PDGFRα$^+$ OPCs can be identified by their GFP-labelled nucleus. After 7 DIV the mixed glial cultures, containing both GFP$^+$ and GFP-negative cells (**Fig. 3.1 a**), were enzymatically dissociated and treated with PI to identify dying cells. Using fluorescence activated cell sorting, I set forward- and side-scatter gates to exclude cell doublets and debris, and fluorescent gates to collect the GFP$^+$ PI-negative healthy OPCs (**Fig. 3.1 b**).

The number of cells collected was quantified using a haemocytometer, and the number of cells recovered equated to 7.1 ± 4.9 % of the collected events (avg ± std; n=3 cultures). The cells were plated onto PDL-coated glass coverslips at 30,000 cells per well, and were cultured for a further 3 days. At 10 DIV, each culture was fixed by exposure to 4% PFA and the identity of the purified cells confirmed by immunocytochemistry. 90 ± 3% of the cells identified by Hoescht 33342 staining were GFP$^+$ PDGFRα$^+$ (avg ± std; n=3 cultures), confirming that they were indeed OPCs (**Fig. 3.1 c**). The remaining cells were negative for both GFP and PDGFRα and had the morphological characteristics of astrocytes.

3.2.2 OPCs express genes associated with primary cilium structure and function

In order to determine whether OPCs have the potential to assemble primary cilia, 10 DIV OPC cultures were fixed and *in situ* hybridisation performed to detect mRNA coding for proteins integral to primary cilium assembly / disassembly or primary cilium-associated signalling pathways (**Fig. 3.2**; blue). A haemotoxylin (Htx) counterstain was also applied to each coverslip to ensure that all cells could be visualised (**Fig. 3.2**; pink). An anti-sense *Pdgfrα* RNA probe acted as a positive control for the *in situ* hybridization protocol. *Pdgfrα* mRNA was detected in the same proportion of cells known to be OPCs (~91%; **Fig 3.2 a, b, l**). It was highly expressed in the cell body, but mRNA expression also extended along the OPC processes (**Fig. 3.2 b**). An anti-sense *SNTN* RNA probe was used as a negative control for this experiment, as *SNTN* is only expressed by motile cilia, not primary cilia. As

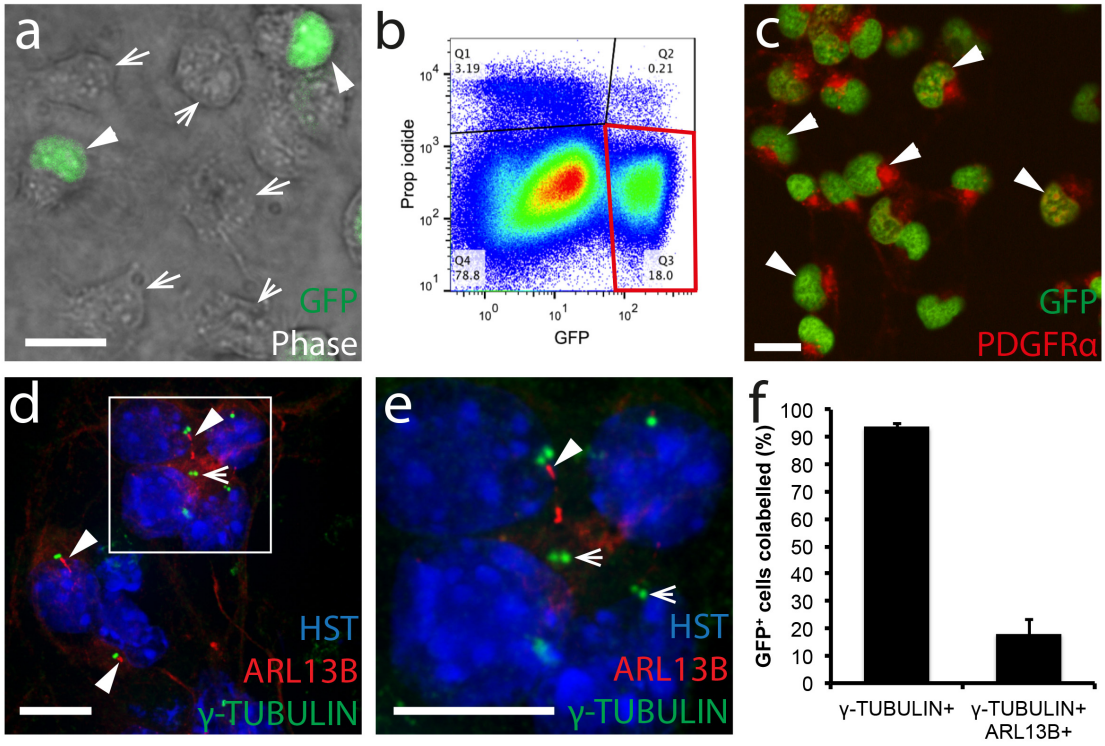

Figure 3.1: OPCs assemble primary cilia in vitro.
*(**a**) 5 DIV mixed glial cultures (phase, greyscale), derived from Pdgfrα-histGFP mice express GFP (green). Arrow heads denote GFP⁺ cells. Arrows denote GFP-negative cells. (**b**) Fluorescence activated cell sorting dot plot for 7 DIV mixed glial cultures derived from Pdgfrα-histGFP mice. Red box denotes GFP⁺ PI-negative cells to be isolated. (**c**) GFP⁺ cells purified from mixed glial at 7DIV, grown for a further 3 days and immunostained to detect GFP (green) and Pdgfrα (red). Low (**d**) and high (**e**) magnification images of 10 DIV OPC cultures immunostained to detect Arl13b (red), γ-tubulin (green) and Hoescht 33342 (HST, blue). Arrow heads denote γ-tubulin⁺ Arl13b⁺ primary cilia. Small arrows indicate unciliated basal bodies (γ-tubulin alone). (**f**) Quantification of the GFP⁺ OPCs with γ-tubulin⁺ basal bodies and Arl13b⁺ γ-tubulin⁺ primary cilia (avg ± std; n=3 cultures). Scale bars = 20 μm.*

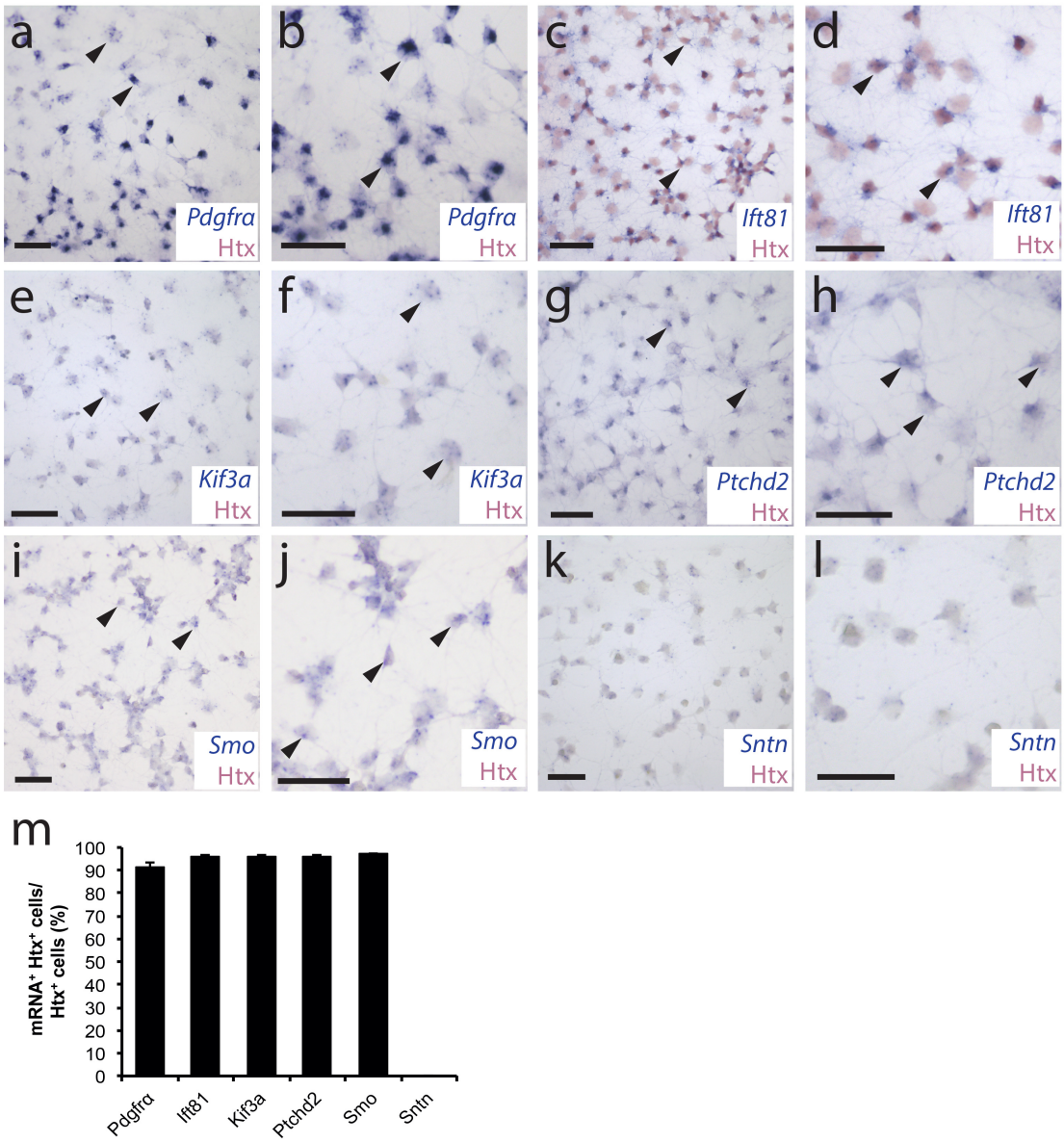

Figure 3.2: OPCs express primary cilium-associated genes
*(**a, b**) Low and high magnification images of OPCs probed to detect Pdgfrα mRNA (purple). (**c, d**) Low and high magnification images of OPCs probed to detect Ift81 mRNA (purple). (**e, f**) Low and high magnification images of OPCs probed to detect Kif3a mRNA (purple). (**g, h**) Low and high magnification images of OPCs probed to detect Ptchd2 (purple). (**i, j**) Low and high magnification images of OPCs probed Smo mRNA (purple). (**k, l**) Low and high magnification images of OPCs probed to detect Sentan mRNA (Sntn, purple). (**m**) Quantification of the proportion of cells in each culture that were positive for each mRNA. Haematoxylin counterstain (pink). Black arrowheads indicate representative mRNA positive cells. Scale bars = 60μm.*

predicted, even after an extended developing period, I found no evidence that this gene was expressed by OPCs (**Fig. 3.2 k**).

The first primary cilium-associated gene that I investigated was *Ift81*, a protein which is necessary for maintenance of the cilium cytoskeleton (Lucker et al., 2005). *Ift81* mRNA was expressed by all OPCs (~96% of cells; **Fig. 3.2 c, d, l**). Like *Pdgfrα* mRNA, *Ift81* mRNA appeared to be expressed throughout the cytoplasm, including in the processes, and some cells displayed regions of dense expression in the cell body (**Fig. 3.2 d**). The *Kif3a* gene is involved in primary cilium assembly (Rosenbaum and Witman, 2002; Huangfu et al., 2003; Huangfu and Anderson, 2005), and *Kif3a* mRNA was highly expressed throughout each OPC (~96% of cells; **Fig. 3.2 e, f, l**), with a small number of discrete sites showing a particularly high level of expression within each cell. As both of these genes are essential for primary cilia construction, and the deletion of either gene results in primary cilia ablation, these data suggest that OPCs are likely to have a primary cilium assembled on their cell surface.

As components of the Shh signalling pathway localize to the primary cilium, I predicted that genes associated with Shh signalling would also be expressed by OPCs. To investigate this possibility, I used an anti-sense *PTCHD2* RNA probe and an anti-sense *SMO* RNA probe to examine expression of mRNAs coding for these Shh receptors in OPC cultures. *PTCHD2* mRNA was expressed by 96 ± 0.56% of cells in these cultures (**Fig. 3.2 g, h, i**). Expression was evident at low levels throughout the soma and to a lesser extend in the processes (**Fig. 3.2 h**). *SMO mRNA* was expressed by an equivalent proportion of OPCs (~97% of cells; **Fig. 3.2 i, j, l**), however, this mRNA was distributed throughout each cell (**Fig. 3.2j**). The expression of Shh signalling genes by OPCs further supports the idea that these cells have assembled primary cilia *in vitro*.

3.2.3 Only a subset of OPCs have assemble primary cilia *in vitro*

As OPCs express genes associated with primary cilium structure and function, I next performed immunocytochemistry on 10 DIV *Pdgfrα-histGFP* OPC cultures, to detect GFP (not shown), the cilia markers ADP-ribosylation factor-like protein 13b (Arl13b) (red) and γ-tubulin (green), and the nuclear marker Hoescht 33342 (blue) (**Fig 3.1. d, e**). γ-tubulin is a protein present in the basal body, while Arl13b is present in the membrane of the primary cilium. As the basal body is a structure associated with primary cilia assembly, but also forms the centrioles during cell division, it was not surprising that ~94% of cultured OPCs had a γ-tubulin$^+$ puncta (green) (**Fig. 3.1 f**). When viewed at high magnification the γ-tubulin$^+$ puncta appeared to consist of two distinct, but closely associated, dots of staining in some cells, suggesting that each cell possesses two conjoined centrioles. This configuration has

been reported in other cells, and includes the mother centriole, which forms the basal body of the primary cilium, and the daughter centriole (reviewed in Winey and O'Toole, 2014). A low level of Arl13b staining was detected throughout the cytoplasm of some OPCs, but the intense Arl13b$^+$ puncta (red), associated with a γ-tubulin$^+$ basal bodies and indicative of primary cilia, were only detected on a subset of OPCs (~18% of GFP$^+$ cultured OPCs; **Fig 3.1 f**). The Arl13b$^+$ primary cilia varied in length, with some being quite short and circular and others linear, perhaps reflecting different states of assembly and disassembly.

3.2.4 Generation of a *CMV-mCherry-Arl13b* plasmid to label primary cilia with a red fluorescent protein

It has been reported that primary cilia are disassembled as cells enter the cell cycle. As OPCs are highly proliferative (Wu et al., 2011), it is therefore possible that those without primary cilia were in the process of dividing. Primary cilia assembly and disassembly has been visualized in HEK293T cells in real time by fluorescently tagging the primary cilia using a plasmid (*CMV-eGFP-Arl13b*) to drive expression of an eGFP-Arl13b fusion protein (Paridaen et al., 2013). When HEK233 cells were transfected with the *CMV-eGFP-Arl13b* plasmid (a kind gift from Dr Judith Paridaen, in the Huttner lab, Max Planck Institute, Dresden, Germany), eGFP-tagged primary cilia could be visualized on the cell surface (**Fig. 3.3 a**). To instead visualize primary cilia on the surface of histGFP-labelled OPCs, I used the DNA sequence coding for *Arl13b*, to generate *CMV-mCherry-Arl13b* (**Fig. 3.4**) and *CMV-Arl13b-mCherry* (**Fig. 3.5**) plasmids, that would instead have mCherry-labelled primary cilia.

The *Arl13b* fragment was excised from the *CMV-eGFP-Arl13b* plasmid by performing a restriction digest with the enzymes Pst1 and Kpn1, followed by gel purification of the ~1300bp band (**Fig. 3.3 b**). The *CMV-N1-mCherry* vector (Clontech, 632523), which has a multiple cut site (MCS) at the N-terminal end of the *mCherry* sequence, and the *CMV-mCherry-C1* vector (Clontech, 632524; **Fig. 3.3 c, d**), which has an MCS at the C-terminal end of the *mCherry* sequence, were linearized by performing a restriction digest with Pst1 and Kpn1 (**Fig. 3.3 e**). As a precaution, to guard against the self-ligation of any partially digested vector products, the linearized DNA was treated with Antarctic Phosphatase (New England Biolabs, Ipswich, MA) as per the manufacturer's instructions. The *Arl13b* DNA fragment was then ligated into the linearized *CMV-mCherry-Arl13b* and *CMV-Arl13b-mCherry* plasmids and the resulting plasmids transformed into *E.coli*.

DNA was purified from ~5 bacterial clones and diagnostic restriction digests performed to confirm the successful generation of the *CMV-mCherry-Arl13b* and *CMV-Arl13b-mCherry* plasmids (**Fig 3.3 f**). Glycerol stocks were generated from bacterial clones containing the

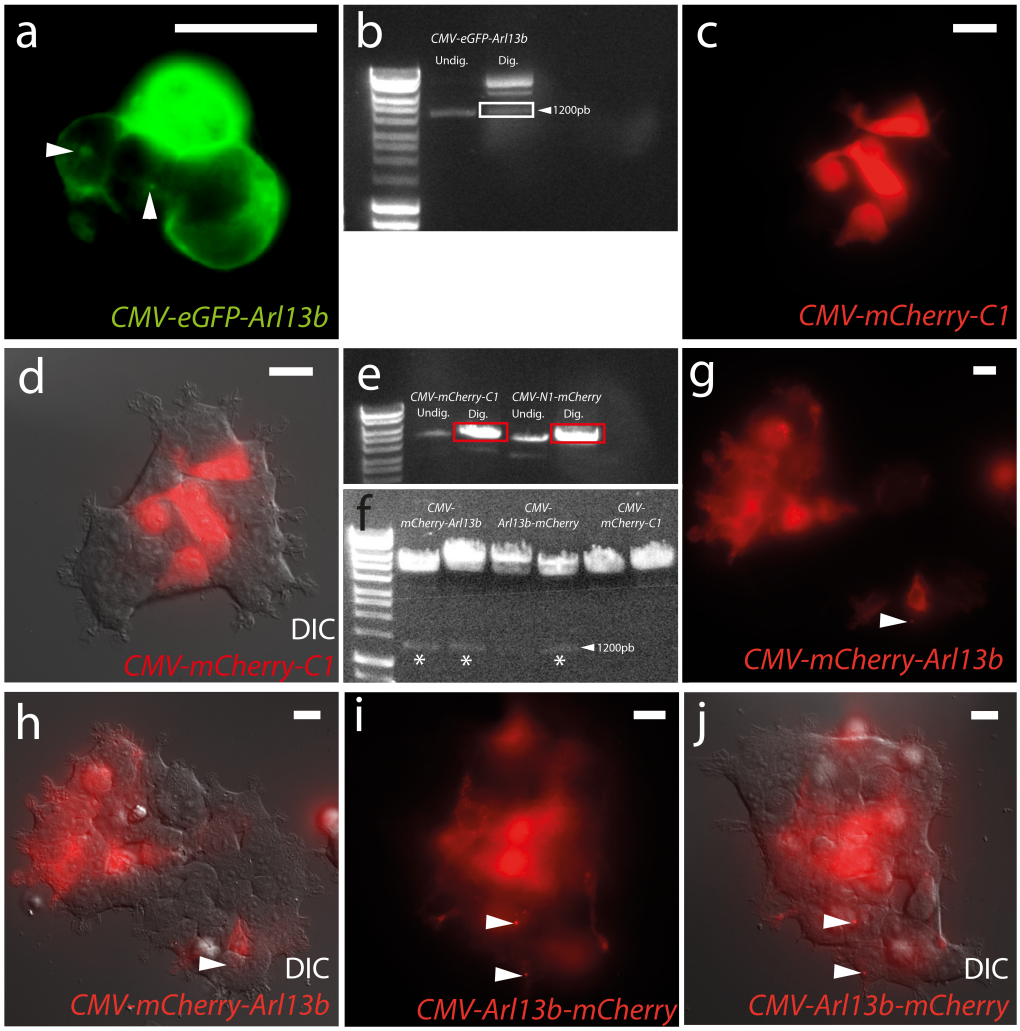

Figure 3.3: Visualizing primary cilia in real-time

*(**a**) Photomicrograph of HEK cells transfected with CMV-eGFP-Arl13b. White arrow heads denote eGFP⁺ primary cilia. (**b**) DNA gel showing undigested CMV-eGFP-Arl13b and Kpn1 / Pst1 digested CMV-eGFP-Arl13b, with the liberated ~1300bp Arl13b fragment (white box) and ~4722bp vector backbone. (**c, d**) HEK cells (DIC, greyscale) transfected with CMV-mCherry-C1 (red). (**e**) DNA gel showing undigested CMV-mCherry-C1 and CMV-N1-mCherry plasmids and Kpn1 / Pst1 linearized CMV-mCherry-C1 and CMV-N1-mCherry plasmids (red box). (**f**) DNA gel showing CMV-mCherry-Arl13b and CMV-Arl13b-mCherry, but not CMV-mCherry-C1, digested with Kpn1 / Pst1, liberates the Arl13b fragment (white asterisk). (**g, h**) HEK cells (DIC, grey scale) transfected with CMV-mCherry-Arl13b (red). (**i, j**) HEK cells (DIC, greyscale) transfected with CMV-Arl13b-mCherry (red). White asterisks denote primary cilia. Scale bars represent 15µm.*

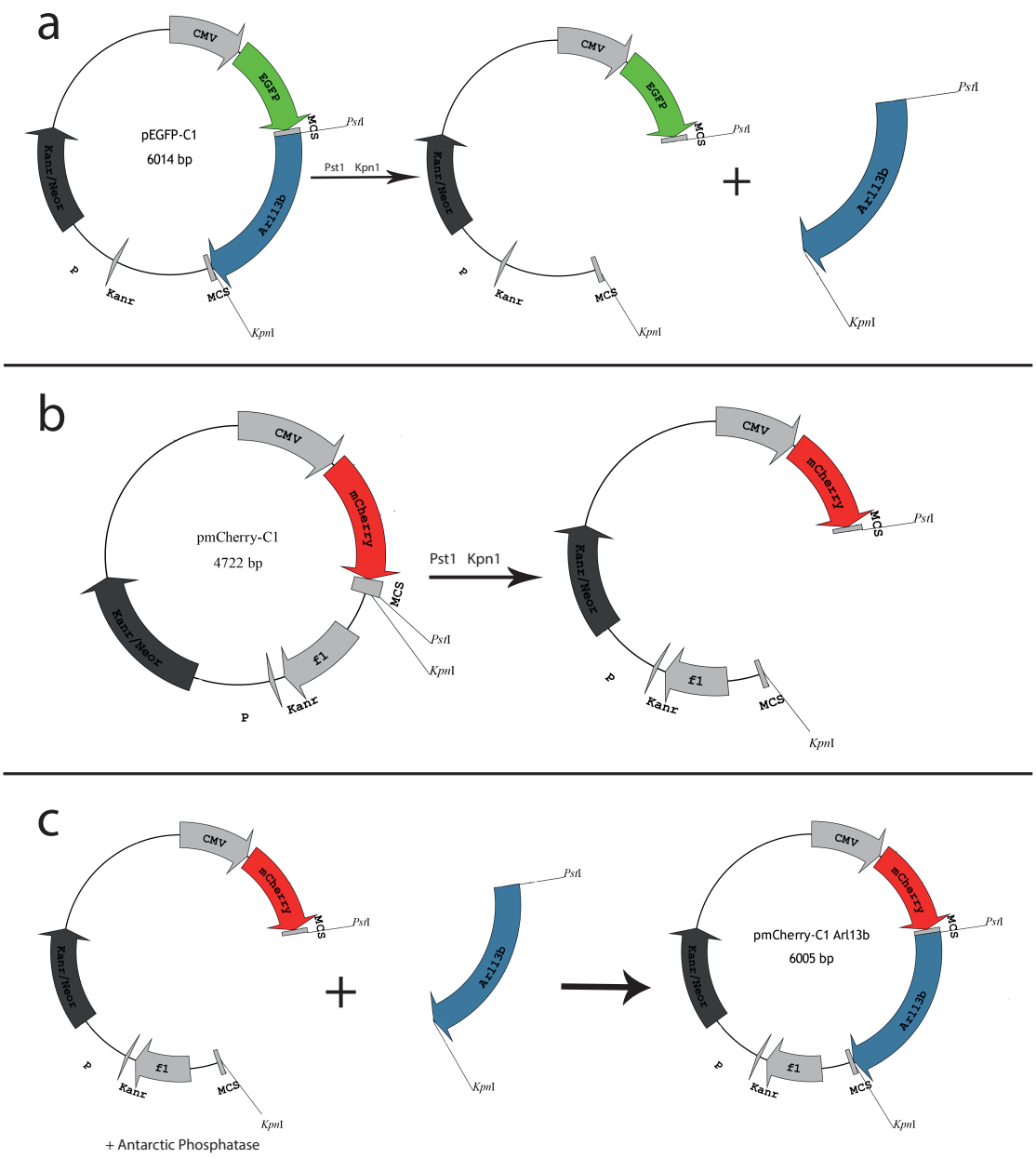

Figure 3.4: Schematic of CMV-mCherry-Arl13b synthesis
*(**a**) Schematic depicting the Kpn1 / Pst1 restriction digest of CMV-eGFP-Arl13b to excise Arl13b. (**b**) Schematic depicting Kpn1 / Pst1 restriction digest of CMV-C1-mCherry to linearise the vector. (**c**) Schematic depicting the ligation of the linearised CMV-C1-mCherry vector and the Arl13b DNA fragment creating an CMV-mCherry-Arl13b plasmid.*

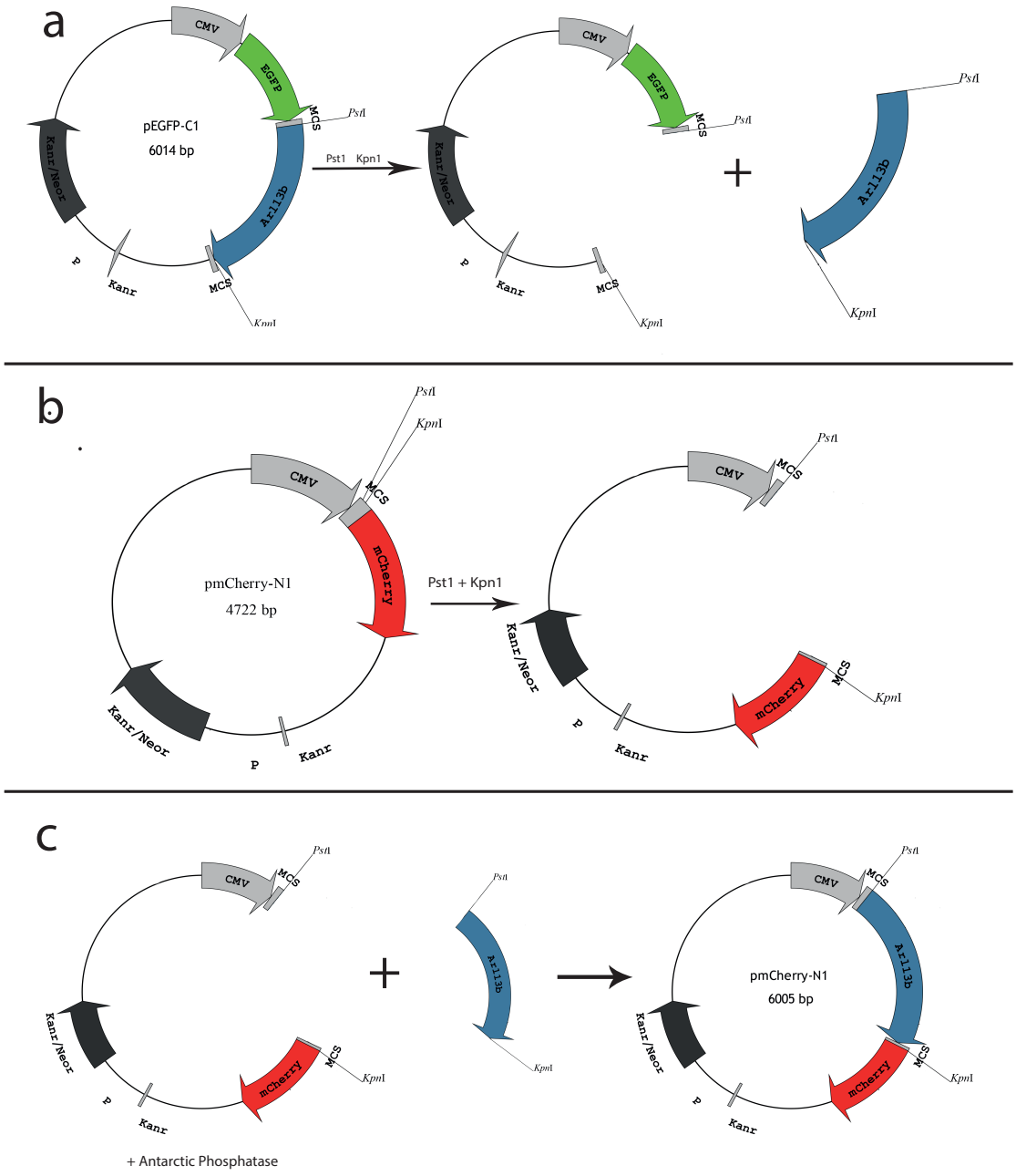

Figure 3.5: Schematic of CMV-Arl13b-mCherry synthesis
*(**a**) Schematic depicting the Kpn1 / Pst1 restriction digest of CMV-eGFP-Arl13b to excise Arl13b. (**b**) Schematic of Kpn1 / Pst1 restriction digest of CMV-mCherry-N1 to linearise the vector. (**c**) Schematic depicting the ligation of linearised CMV-N1-mCherry and the Arl13b DNA fragment to create CMV-Arl13b-mCherry.*

CMV-mCherry-Arl13b and *CMV-Arl13b-mCherry* plasmids, before progressing to validate the ability of each plasmid to fluorescently label primary cilia in a cellular expression system.

After 24 hours, HEK293 cells transfected with the *CMV-mCherry-Arl13b* (**Fig. 3.3 g, h**) or *CMV-Arl13b-mCherry* (**Fig. 3.3, i, j**) plasmids had very low levels of cytoplasmic mCherry expression (**Fig. 3.3 g-i**), when compared with HEK293T cells transfected with either empty vector (**Fig. 3.3 c, d**). Consistent with the labelling obtained using the *CMV-eGFP-Arl13b* plasmid, a single point of intense mCherry expression was also observed on a number of the transfected cells. When performing live imaging of the transfected cultures, the mCherry-labelled primary cilia could be visualized and tracked most readily, in cultures transfected with the *CMV-Arl13b-mCherry* plasmid. Therefore, this plasmid was used for further experiments.

3.2.5 Primary cilia are disassembled and reassembled as OPCs progress through the cell cycle

In order to determine whether primary cilia are dynamically assembled and disassembled on the surface of OPCs as they proliferate, 8 DIV *Pdgfrα-histGFP* OPC cultures were transfected with the *CMV-Arl13b-mCherry* plasmid. After 24 hours, 53 OPCs with an mCherry$^+$ primary cilium were selected for live imaging at high magnification, collecting mCherry, GFP and differential interference contrast (DIC) images every 15 min for 8-12 hours (**Fig. 3.6**). Of the 53 transfected OPCs, only 2 divided during the imaging period, and the assembled primary cilium was disassembled immediately prior to nuclear chromatin condensation (**Fig. 3.6 c, d**). Furthermore, the mCherry$^+$ primary cilium was reassembled by a daughter OPC, once cell division was complete (**Fig. 3.6 g, h)**.

The second daughter OPC did not have an mCherry$^+$ primary cilium immediately after cell division (**Fig. 3.6 g, h**), and this is to be expected. During cell division the primary cilium is disassembled from the basal body, which forms the centriole and is preferentially inherited by one daughter cell following a cell division (Paridaen et al., 2013). That daughter cell can use the basal body to immediately reassemble a primary cilium, while the other daughter cell must synthesize a basal body before it can assemble a primary cilium. These data show that the primary cilium is disassembled by OPCs as they enter the cell cycle *in vitro* and reassembled once they exit

3.2.6 Tat-Cre activates the cre-sensitive Rosa26-YFP reporter *in vitro*

Having determined that OPCs have primary cilia that are assembled on their surface between cell divisions, I next hypothesized that these primary cilia are critical regulators of

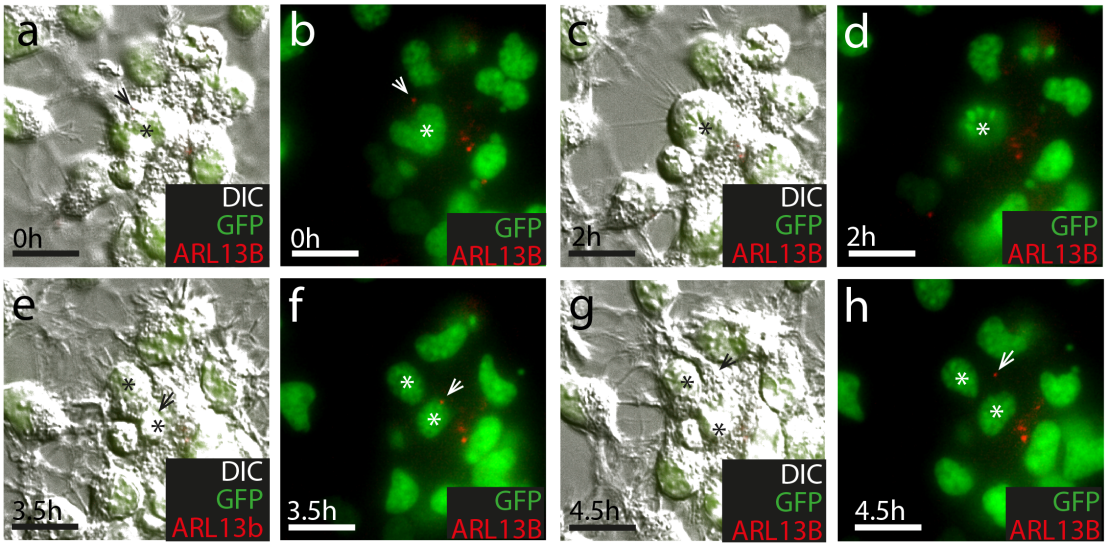

Figure 3.6: OPCs disassemble primary cilium as they enter the cell cycle
*Still frames from a representative time-lapse movie, depicting a dividing OPC. 10DIV Pdgfrα-histGFP OPC cultures were transfected with CMV-Arl13b-mCherry and imaged to visualise GFP (green), Arl13b (red) and DIC (greyscale). A GFP⁺ OPC before (**a**, **b**), during (**c**, **d**) and after cell division (**e**, **f**), and after assembly of the primary cilium by one of the two a daughter cells (**g**, **h**). Asterisk denotes dividing cell and daughter cells. Arrows indicate primary cilia. Scale bars = 20μm*

OPC division *in vitro*. To test this directly, I aimed to use a Cre-lox approach to delete the *Kif3a* gene from OPCs, and prevent primary cilia assembly.

When Cre recombinase is fused to a tat linker peptide (tat-Cre), it is able to cross the cell membrane, enter the nucleus, recognize lox-p sites, and facilitate DNA recombination (reviewed in Van Duyne, 2015). To assess the efficacy of this tat-Cre for inducing recombination in glial cells, it was added into the culture medium of mixed glial cultures generated from *Rosa26-YFP* cre-sensitive reporter mice, for 90 min, at a concentration of 0, 0.5 or 1μM. The cells were fixed at 24, 48 or 72 hours post-treatment and immunocytochemistry performed to detect the recombined (YFP^+) cells (anti-GFP antibody; green), OPCs within the culture (PDGFRα; red) and the nuclear marker Hoescht 33342 (blue). Cultures exposed to 0μM tat-Cre (diluent alone) lacked YFP expression at all time-points (**Fig. 3.7 a, f**). YFP-labelled glia, including YFP-labelled OPCs, were visible within 24 hours of treatment, in cultures exposed to both 0.5μM (**Fig. 3.7 b, c, f, h**) and 1μM tat-cre (**Fig. 3.7 d, e, g, h**). ~57% of OPCs became YFP-lablled when exposed to 0.5μM tat-Cre and ~88% when exposed to 1μM tat-Cre (**Fig. 3.7 f**). This was largely unchanged at 48 and 72 hour (**Fig. 3.7 h**).

3.2.7 *Kif3a* knockout reduces OPC primary cilium assembly and proliferation *in vitro*

Having determined that tat-Cre can effectively induce DNA recombination in cultured OPCs, I isolated OPCs from glial cultures grown from early postnatal *Pdgfrα-histGFP::Kif3a*$^{fl/fl}$ mouse pups, in which both copies of the *Kif3a* gene are flanked by loxP sites, rendering them susceptible to Cre-mediated gene deletion. I treated 8 DIV *Pdgfrα-histGFP::Kif3a*$^{fl/fl}$ OPCs with 0 (diluent only), 0.5, 1 and 2μM tat-Cre, and cultured them for a further 5 days, before generating protein lysates to determine KIF3a expression by western blot (**Fig. 3.8 a, b**). When KIF3a expression was normalized to β-actin expression, there was no significant difference between control cultures (0μM tat-Cre) and those treated with 0.5 or 1μM tat-Cre (**Fig. 3.8 a, b**). However, when *Pdgfrα-histGFP::Kif3a*$^{fl/fl}$ OPCs were treated with 2μM tat-Cre, KIF3a expression was reduced to ~43% of controls (**Fig. 3.8 a, b**). These data suggest that treatment of *Pdgfrα-histGFP::Kif3a*$^{fl/fl}$ OPC cultures with 2μM tat-Cre successfully induces *Kif3a* deletion *in vitro*.

To determine whether the deletion of *Kif3a* prevents primary cilia assembly by cultured OPCs, 8-9 DIV *Pdgfrα-histGFP::Kif3a*$^{fl/fl}$ OPC cultures were treated with 0 or 2μM tat-Cre for 90 min, and cultured for a further 5 days. The OPCs were fixed and immunocytochemistry performed to detect GFP (blue), as well as γ-tubulin (green), Arl13b (red) and Hoescht 33342 (not shown). In these control cultures, ~40% of the GFP^+ OPCs had an assembled primary cilia (**Fig. 3.8 c, e**) and this was significant reduced in the 2μM tat-Cre treated

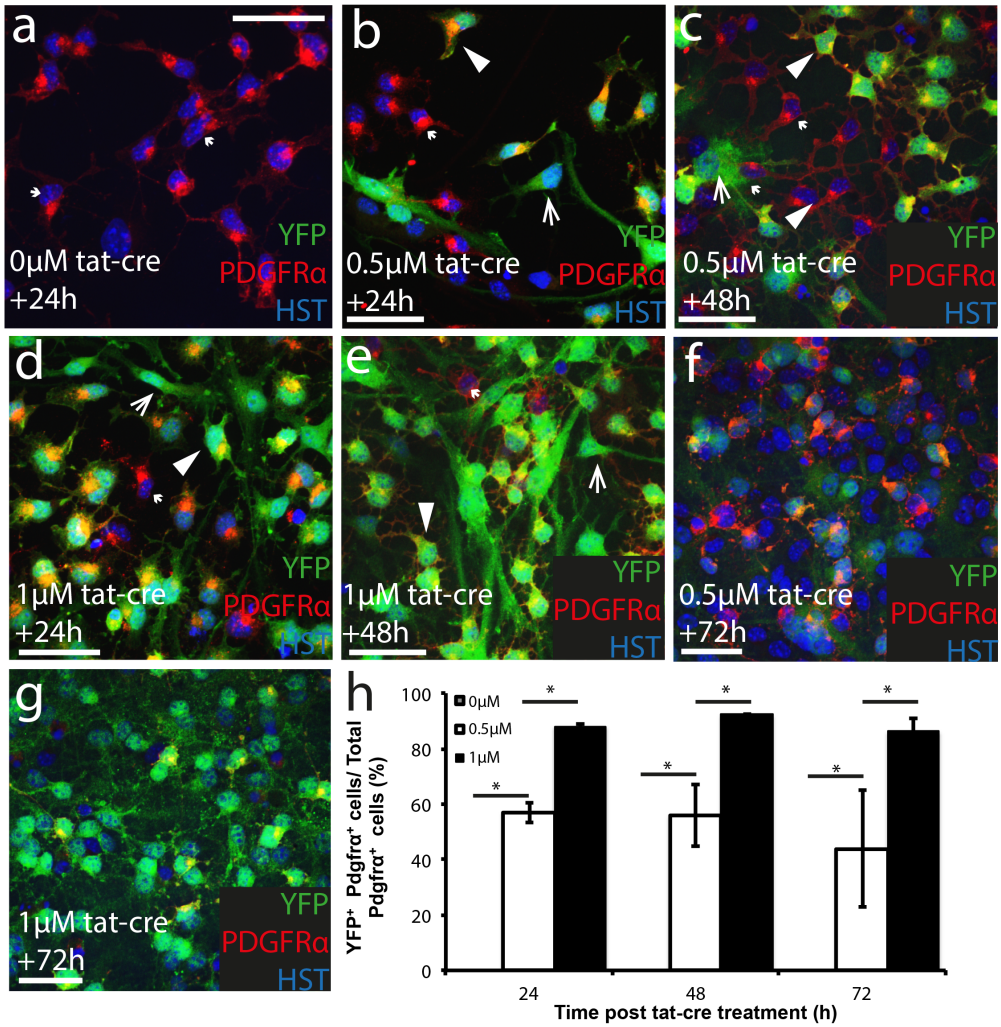

Figure 3.7: Tat-Cre recombines the cre-sensitive Rosa26-YFP transgene in mixed glial cultures

*(**a**) Confocal image (single z plane) of a 10DIV mixed glial culture, derived from Rosa26-YFP mice, immuno-stained to detect YFP (green), PDGFRα (red) and HST (blue). Confocal images (single z plane) of Rosa26-YFP mixed glial culture treated with 0.5μM tat-Cre at 9DIV and fixed at 24 (**b**), 48 (**c**) and 72 **(f)** hours post-treatment. Cultures were immuno-stained to detect YFP (green), PDGFRα (red) and HST (blue). Confocal images (single z plane) of Rosa26-YFP mixed glial cultures, treated with 1μM tat-Cre at 9DIV and fixed at 24 (**d**), 48 (**e**) and (**g**) hours post treatment. Cultures were immuno-stained to detect YFP (green), PDGFRα (red) and HST (blue). (**h**) Quantification of the percentage of OPCs, in mixed glial cultures, that became YFP-labelled following tat-cre treatment (avg ± std, n=3 cultures; p<0.02, two-way ANOVA with Bonferroni correction). Large arrowheads indicate YFP⁺ PDGFRα⁺ OPCs. Arrows represent YFP⁺ PDGFRα-negative cells. Small arrowheads indicate YFP-negative PDGFRα⁺ cells. Scale bars = 60μm.*

Figure 3.8: Deleting Kif3a from cultured OPCs reduces their proliferation

*(**a**) Image of a western blot detecting KIF3A protein in protein lysates generated from diluent- and tat-Cre-treated (0.5, 1, and 2μM tat-cre for 90 minutes) OPC cultures derived from Pdgfrα-histGFP :: Kif3a$^{fl/fl}$ transgenic mice. (**b**) Quantification of KIF3a protein expression by western blot (avg ± std, n=3 cultures; p<0.05, t-test). (**c**) Confocal image of diluent-treated Pdgfrα-histGFP :: Kif3a$^{fl/fl}$ OPC cultures stained to detect γ-tubulin (green), Arl13b (red) and GFP (blue). (**d**) Confocal image of 2μm tat-cre-treated Pdgfrα-histGFP :: Kif3a$^{fl/fl}$ OPC cultures, stained to detect γ-tubulin (green), Arl13b (red) and GFP (blue). (**e**) Quantification of the percentage of GFP^{+} OPCs with assembled primary cilia in diluent- and tat-cre-treated cultures (avg ± std, n=4 cultures; p<0.0001, t-test). Arrowheads represent assembled primary cilia. Arrows represent Arl13b-negative γ-tubulin^{+} basal bodies. (**f-h**) Confocal image (single z plane) of diluent-treatd Pdgfrα-histGFP :: Kif3a$^{fl/fl}$ OPC cultures that received EdU for 12 hours and were immuno-stained to detect GFP (green), PDGFRα (red) and EdU (blue). (**i-k**) Confocal image (single z plane) of 2μM tat-Cre-treated Pdgf-histGFP/Kif3a$^{fl/fl}$ OPC cultures, treated with EdU for 12 hours, and immuno-stained to detect GFP (green), PDGFRα (red) and EdU (blue). Arrowheads indicate GFP^{+} PDGFRα^{+} EdU^{+} cells. Arrows indicate GFP^{+} PDGFRα^{+} EdU-negative cells. (**l**) Quantification of the percentage of OPCs that are EdU^{+} after treatment with 0μm or 2μM tat-Cre (avg ± std, n=3 cultures; p<0.05, t-test). Scale bars represent 25μm (d, e) and 50μm (i-k).*

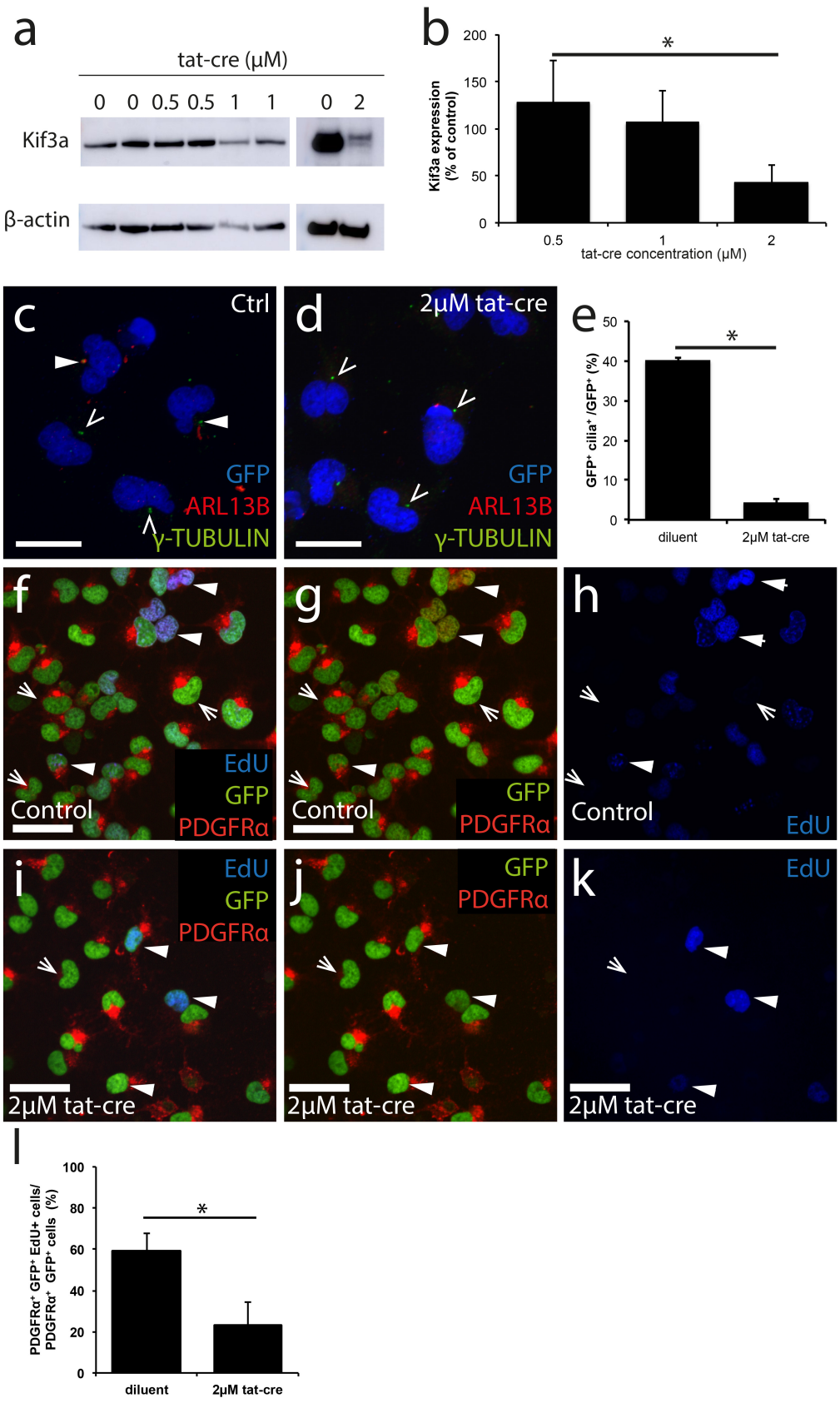
a
tat-cre (μM)
0 0 0.5 0.5 1 1 0 2
Kif3a
β-actin
b
Kif3a expression (% of control)
200
150
100
50
0
*
0.5
1
2
tat-cre concentration (μM)
c
Ctrl
GFP
ARL13B
γ-TUBULIN
d
2μM tat-cre
GFP
ARL13B
γ-TUBULIN
e
GFP+ cilia+ /GFP+ (%)
50
40
30
20
10
0
*
diluent
2μM tat-cre
f
EdU
GFP
PDGFRα
Control
g
GFP
PDGFRα
Control
h
Control
EdU
i
EdU
GFP
PDGFRα
2μM tat-cre
j
GFP
PDGFRα
2μM tat-cre
k
EdU
2μM tat-cre
l
PDGFRα+ GFP+ EdU+ cells/ PDGFRα+ GFP+ cells (%)
100
80
60
40
20
0
*
diluent
2μM tat-cre

cultures (**Fig. 3.8 c, d, e**). These data likely indicate that the deletion of *Kif3a* prevents primary cilium assembly by OPCs, however a similar phenotype would be observed if *Kif3a* deletion instead increased the rate of OPC proliferation i.e. more cells enter the cell cycle and have disassembled primary cilia.

To examine this possibility, 8-9 DIV *Pdgfrα-histGFP::Kif3a*$^{fl/fl}$ OPC cultures were treated with 2μM tat-Cre and incubated for 5 days. For the final 12 hours, EdU was added to the culture media. EdU is a thymidine analog, which is taken up by cells in S-phase of the cell cycle, effectively labeling all OPCs that divide during the labelling period. Immunocytochemistry was performed to detect GFP$^+$ (green), PDGFRα$^+$ (red) OPCs, EdU$^+$ proliferating cells (blue) and a Hoescht 33342 nuclear stain. ~59% of PDGFRα$^+$ GFP$^+$ OPCs were EdU labeled in diluent treated cultures (**Fig. 3.8 f-h, l**), compared with only ~22% of PDGFRα$^+$ GFP$^+$ OPCs in the tat-Cre treated cultures (**Fig. 3.8 i-k, l**). These data indicate that the deletion of *Kif3a* effectively prevents primary cilia assembly on OPCs and reduces the proliferation of these cultures.

3.3 Discussion

3.3.1 OPCs have assembled primary cilia that are disassembled for cell cycle reentry

My findings show that ~18% of 10DIV and ~40% of 13 DIV cultured OPCs have assembled primary cilia, at any one time. As primary cilia are only assembled on the surface of OPCs not actively dividing (**Fig. 3.6 c, d**), these data suggest, that a higher fraction of OPCs are actively proliferating in 10 DIV cultures, when compared with 13 DIV cultures. This is entirely feasible, as the proliferation rate of OPCs slows daily *in vivo* (Psachoulia et al., 2009), and the proliferation rate of OPCs slows as the cultures expand, prior to the onset of differentiation (Barres et al., 1994).

Using live-cell imaging, I was able to follow individual OPCs as they underwent division. Prior to cell division, an individual mCherry-labelled primary cilium shortened on the surface of the OPC, before becoming a small puncta that moved from the cell surface into the nucleus. mCherry labelling disappeared completely during division, but was reassembled by one of the daughter cells upon cell cycle exit. This observation is consistent with the findings of studies conducted in other cell types, that the primary cilium must be disassembled for the cell to re-enter the cell cycle, and that once the cilium is disassembled, the basal body migrates away from the cell surface and into the cytoplasm where it converts into the centriole (Seeley and Nachury, 2010; Garcia-Gonzalo and Reiter, 2012; Kim and Dynlacht, 2013). A small amount of Arl13b is contained within a membrane vesicle and associated with the centrosome after disassembly, while it migrates to the nucleus, resulting in Arl13b

labeling of the migrating basal body (Paridaen et al., 2013). Once division is complete, the centriole is transported back to the cell surface, where it again acts as the basal body for primary cilium reassembly (Kobayashi and Dynlacht, 2011; Garcia-Gonzalo and Reiter, 2012). It is likely that the second daughter cell, that did not have a visible mCherry^{+} primary cilium, corresponds to the cell that did not inherit the mother centriole. With every cell division, one daughter cell inherits the mother centriole from the parent cell, and can immediately assemble a primary cilium, while the other daughter cell must first assemble a basal body and subsequently assemble a primary cilium (Paridaen et al., 2013). Given time, it is likely that the second daughter cell would also assemble an mCherry^{+} primary cilium (Paridaen et al., 2013).

Kif3a deletion from OPCs *in vitro*, prevented primary cilia assembly and impaired OPC proliferation. *Kif3a* deletion could reduce proliferation by producing a physical barrier to cell cycle re-entry, by keeping the basal body at the cell surface and preventing the centriole from migrating to the nucleus. However, it is also possible that in preventing cilium assembly, *Kif3a*-deletion prevents signalling that would otherwise occur within the primary cilium (Schneider et al., 2005; Christensen et al., 2008; Lancaster et al., 2011; Ruat et al., 2012). For example, Shh signaling is reliant upon the presence of a primary cilium, and Falcón-Urrutia et al. (2015) demonstrated that knocking out Shh signaling, using the Smo inhibitor cyclopamine, significantly reduced OPC proliferation *in vitro* (Falcón-Urrutia et al., 2015). It would be particularly interesting to determine whether *Kif3a*-deleted OPCs are still able to undergo Shh-induced proliferation *in vitro*.

3.3.2 Does Shh signalling directly influence OPC behaviour?

I have shown that OPCs express mRNA for the *Shh* receptors *PTCHD2* and *SMO* (**Fig. 3.2**). These data are consistent with RNA sequencing data, showing that OPCs express Shh-associated genes (Zhang et al., 2014). During development, Shh is a key factor regulating the differentiation of OPCs from multipotent stem cells in the spinal cord (Zhou et al., 2001) and the preoptic area of the developing optic nerve (Merchán et al., 2007). Shh treatment of embryonic stem cells *in vitro*, also drives their differentiation from pluripotent stem cells into OPCs (Shin et al., 2007; Bian et al., 2016). However, more important for this study, blocking Shh signaling in cultured OPCs, by treating with the SMO inhibitor cyclopamine, reduces OPC proliferation (Tekki-Kessaris et al., 2001; Falcón-Urrutia et al., 2015). As cyclopamine reduces the proliferation of OPCs, even in the absence of exogenous Shh application (Falcón-Urrutia et al., 2015), this suggests that OPCs can themselves produce Shh. As OPCs express *Shh* mRNA (Zhang et al., 2014), and OLIG2+ cells upregulate Shh protein is naturally upregulated within lysolecithin-induced lesions during remyelination (Ferent et al.,

2013), making it possible that they secreted Shh into the culture medium, where it can act as an autocrine or paracrine signal to promote proliferation.

These data indicate that Shh signalling is important for OPCs, with Shh driving their specification from stem cells, as well as encouraging proliferation and differentiation. Further culture experiments could be performed, however, to confirm and further elucidate the exact relationship between Shh signalling, the primary cilium and OPCs. Such as examining the response of cultured OPCs to both cyclopamine addition and *Kif3a* gene deletion. If the simultaneous addition of cyclopamine and deletion of the *Kif3a* gene is not found to have a greater change in proliferation than only the addition of cyclopamine, this indicates that preventing primary cilium assembly is only affecting Shh signalling, and not other pathways such as PDGFRα or Wnt. Additionally, further experiments should be performed to observe the effect of tat-cre treatment on wild-type OPCs in culture, to confirm that proliferation changes were the result of preventing cilium assembly rather than an effect of the tat-cre itself.

3.3.3 Do mature oligodendrocytes assemble primary cilia?

Essentially all OPCs, irrespective of whether they had an assembled primary cilium or not, stained for γ-tubulin. Alone, γ-tubulin is not a marker of primary cilia, as the cilium basal body is the same structure that forms the centriole during a cell division (Paridaen et al., 2013). However, cultured rat OPCs lose γ-tubulin staining as they differentiate into MBP^+ oligodendrocytes (Falcón-Urrutia et al., 2015) and the loss of the basal body / centrioles has also been reported to occur during the differentiation of other cell types, including some neurons (Cunha-Ferreira et al., 2009; Debec et al., 2010). Cells lacking γ-tubulin, therefore likely correspond to cell that are no longer capable of successfully re-entering the cell cycle, and the complete loss of γ-tubulin from mature oligodendrocytes, suggests that these cells do not assemble primary cilia. This possibility is further supported by microarray (Cahoy et al., 2008) and RNA sequencing (Zhang et al., 2014) gene expression data, indicating that OPCs express the major cilium cytoskeleton-associated genes, such as *Kif3a*, the IFT proteins *Ift81*, *Ift57, Ift172 and Ift88,* the basal body associated proteins *Cep290* and *Cep97* and the cilium membrane associated protein *Arl13b* more highly than oligodendrocytes.

3.4 Conclusions

In this Chapter, I have demonstrated that OPCs *in vitro* assemble and disassemble primary cilia as they progress through the cycle and that disruption of primary cilium assembly *in vitro*, by the deletion of *Kif3a*, leads to a reduction in proliferation. I would predict that Kif3a deletion will similarly affect OPCs in vivo, where they remain highly proliferative, and by

extension, may play a critical role in regulating oligodendrogenesis. In order to examine this relationship, it will be necessary to conditionally delete *Kif3a* from adult OPCs. This could be achieved using a *Pdgfrα-CreER*^{T2} transgenic mouse line, so long as it preferentially induces gene deletion in OPCs, without affecting PDGFRα^{+} cell populations outside of the CNS.

Chapter 4: Evaluating tissue-specific recombination in a *Pdgfrα-CreER^{T2}* transgenic mouse line

4.1 Introduction

PDGFR was first identified in 1982, as a protein expressed by fibroblasts and arterial smooth muscle cells (Bowen-Pope and Ross, 1982). It was shown to facilitate normal growth and development by regulating critical cell processes including proliferation and differentiation (Boström et al., 1996; Soriano, 1997; Fruttiger et al., 1999; Karlsson et al., 1999; Gnessi et al., 2000; Karlsson et al., 2000), and mutations in this receptor were strongly associated with tumour growth (Hermanson et al., 1992; 1996; Nakamura et al., 1997). In 1988, it was discovered that PDGFR was actually two receptors, named PDGFRα and PDGFRβ, that bind dimers of the PDGFs with different affinities (Hart et al., 1988). PDGFRα is capable of binding all PDGFs except PDGF-DD (Hart et al., 1988; Cao et al., 2008), but has a strong affinity for the PDGF-A homodimer (Glenn et al., 1982). In the CNS, PDGFRα is selectively expressed by OPCs (Pringle et al., 1992), and its activation by PDGF-AA regulates the proliferation, migration and differentiation of this cell type in normal development, as well as in response to demyelination (Woodruff et al., 2004).

The high specificity of PDGFRα expression by OPCs in the CNS, has made the *Pdgfrα* gene promoter useful for manipulating gene expression exclusively in OPCs without affecting other CNS cell types. For example, Rivers et al. (2008) generated a bacterial artificial chromosome (BAC) transgenic mouse line, the *Pdgfrα-CreER^{T2}* transgenic mouse, which expresses Cre recombinase fused to the oestrogen-receptor type II, under the control of the *Pdgfrα* promoter. Tx administration to adult *Pdgfrα-CreER^{T2}::Rosa26-YFP* transgenic mice resulted in ~50% of the OPCs in the brain (Tripathi et al., 2010), ~40% of the OPCs in the spinal cord and ~20% of OPCs in the optic nerve being labelled with yellow fluorescent protein (YFP; (Young et al., 2013). A second BAC transgenic *Pdgfrα-CreER^{T2}* mouse line was subsequently developed by Kang et al. (2010), which achieves Cre-mediated gene recombination in ≥ 90% of OPCs in the brain and spinal cord (Kang et al., 2010). Both *Pdgfrα-CreER^{T2}* mouse lines have been widely used to label OPCs and trace their progeny *in vivo*. These studies largely report that OPCs continually generate new myelinating oligodendrocytes in the mature healthy CNS, and a small number indicate that OPCs differentiate into astrocytes (or astrocyte-like cells) and even Schwann cells in the CNS under certain pathological conditions (Richardson et al., 2011).

More recently the *Pdgfrα-CreER^{T2}* transgenic mouse line produced by Rivers et al. (2008) was used to conditionally ablate *Myrf* from OPCs (McKenzie et al., 2014). *Myrf* is not widely expressed outside of the CNS, which reduced the likelihood that this strategy would inadvertently affect the function of PDGFRα$^+$ cell populations outside of the CNS. However, when using the *Pdgfrα-CreER^{T2}* transgenic mouse line to conditionally delete genes with a less discrete expression pattern, this is an important consideration. To assess the ability of *Pdgfrα-CreER^{T2}* transgenic mice to induce recombination in PDGFRα$^+$ cells within and outside of the CNS, we crossed *Pdgfrα-CreER^{T2}* transgenic mice (Kang et al., 2010) with *Rosa26-YFP* transgenic mice (Srinivas et al., 2001) and administered Tx to adult *Pdgfrα-CreER^{T2}::Rosa26-YFP* offspring. The pattern of YFP labelling was then examined in a variety of tissues. I report that *Pdgfrα-CreER^{T2}* transgenic mice are highly suitable for OPC-directed gene recombination in the CNS, as they induce robust recombination in OPCs, moderate recombination in PDGFRα$^+$ bone marrow stromal cells, and have a minimal effect on other PDGFRα$^+$ cell populations.

4.2 Results

4.2.1 *Pdgfrα-CreER^{T2}* transgenic mice can be used to specifically and efficiently induce recombination in OPCs in the CNS

To confirm that OPCs are the only cell type to undergo recombination in the CNS of *Pdgfrα-CreER^{T2}* transgenic mice, adult *Pdgfrα-CreER^{T2}::Rosa26-YFP* transgenic mice were treated with Tx, and perfusion fixed 7 days later (P57+7). The brain, spinal cord, retina and optic nerve were cryosectioned and immunohistochemistry performed to detect cells expressing PDGFRα (red), YFP (anti-GFP, green) and the nuclear marker Hoescht 33342 (**Fig. 4.1**). PDGFRα$^+$ OPCs were found throughout the CNS (**Fig. 4.1 a-g**) with the exception of the retina (**Fig. 4.1 h**). The density of PDGFRα$^+$ OPCs was equivalent in the cortex (104 ± 27 cells/mm^2), CC (123 ± 20 cells/mm^2) and spinal cord (87 ± 17 cells/mm^2) ($P>0.9$ ANOVA; **Fig. 4.1 m**). The vast majority of OPCs became YFP-labelled in the CNS (**Fig. 4.1 n**) allowing clear visualization of their typical stellate morphology in the cortex (**Fig. 4.1 b**), CC (**Fig. 4.1 d**) and spinal cord (**Fig. 4.1 g**). Few PDGFRα$^+$ OPCs escaped recombination as ~97% of PDGFRα$^+$ OPCs were YFP-labelled in the cortex, ~96% in the CC, ~92% in the spinal cord (**Fig. 4.1 n**) and ~97% in the optic nerve (75 of 77 YFP$^+$ cells counted). The retina lacked PDGFRα$^+$ OPCs, and no YFP-labelled cells were detected (**Fig. 4.1 h, m**).

In addition to YFP-labelled OPCs, we identified a number of YFP$^+$ cells that were PDGFRα-negative in the brain (**Fig. 4.1 e**) and spinal cord (**Fig. 4.1 g**), and these cells had the morphological characteristics of oligodendrocytes. Given that OPCs are known to give rise

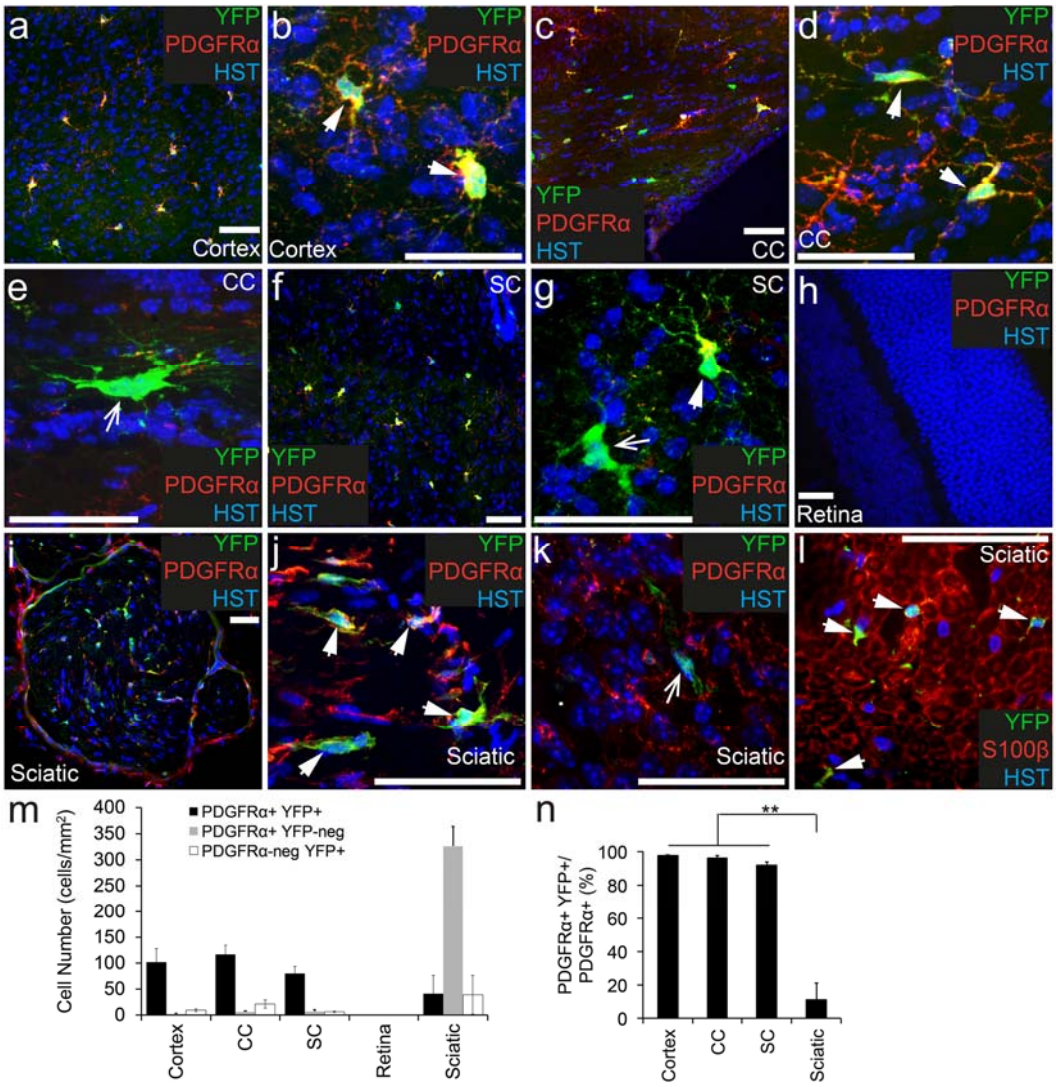

Figure 4.1: PDGFRα⁺ OPCs become YFP-labelled throughout the nervous system of adult Pdgfrα-CreER^{T2} :: Rosa26-YFP transgenic mice

*Cryosections from P57+7 Pdgfrα-CreER^{T2} :: Rosa26-YFP transgenic mice were immunostained to detect PDGFRα (red), YFP (green) and Hoescht 33342 (HST, blue). Confocal image (single z plane) of the motor cortex at low (a) and high (b) magnification. Confocal image (single z plane) of the corpus callosum (cc) at low (c) and high (d, e) magnification. Confocal image (single z plane) of a transverse spinal cord section at low (f) and high (g) magnification. Confocal image (single z plane) of the retina (h). Confocal image (single z plane) of a transverse sciatic nerve section at low (i) and high (j, k) magnification. Cryosection from P57+7 Pdgfrα-CreER^{T2} :: Rosa26-YFP transgenic mouse immunostained to detect S100β (red), YFP (green) and HST (blue) (l). m) The number of PDGFRα⁺ YFP⁺, PDGFRα⁺ YFP-negative and PDGFRα-negative YFP⁺ cells quantified from confocal images (single z plane) of nervous system tissue, expressed as the number of cells per mm². n) The proportion of PDGFRα⁺ cells that become YFP-labelled (PDGFRα⁺ YFP⁺ cells / total PDGFRα⁺ cells x 100) quantified from confocal images (single z plane) of nervous system tissue. Error bars represent mean ± std dev from n=3 mice. ** P<0.001, ANOVA. PDGFRα⁺ YFP⁺ cells (and S100β⁺ YFP⁺ cells) are denoted by arrowheads. PDGFRα-negative YFP⁺ cells are denoted by arrows. Scale bars = 50μm*

to new oligodendrocytes, producing new differentiated PDGFRα-negative cells even within 1 week of labelling (Rivers et al., 2008), this was to be expected. The oligodendroglial identity of the YFP$^+$ PDGFRα-negative cells was confirmed by performing immunohistochemistry to detect YFP and the oligodendrocyte lineage marker OLIG2. In the CC all YFP$^+$ cells were also OLIG2$^+$ GFAP-negative (639 YFP$^+$ cells analyzed), confirming that the YFP$^+$ PDGFRα-negative cells identified in this region were indeed oligodendrocytes. In the cortex, essentially all YFP$^+$ cells were OLIG2$^+$, with the exception of very rare YFP$^+$ cells that instead co-labelled for the neuronal marker, NeuN (2 of 2035 YFP$^+$ cells analyzed). A similarly small number of cortical neurons are GFP labelled in *Pdgfrα-histGFP* knock-in mice, despite their lack of PDGFRα expression (Clarke et al., 2012). Therefore, the YFP$^+$ NeuN$^+$ cells that we observe may be rare neurons that experience *Pdgfrα* gene promoter activity, but no PDGFRα protein translation.

These experiments confirm that the *Pdgfrα-CreER^{T2}* transgene is expressed by OPCs, and that Tx administration efficiently leads to DNA recombination in these cells.

4.2.2 A small number of PDGFRα$^+$ Schwann cells undergo recombination in the sciatic nerve of *Pdgfrα-CreER^{T2}::Rosa26-YFP* transgenic mice

To determine whether cells within the peripheral nervous system express PDGFRα and / or undergo recombination in adult *Pdgfrα-CreER^{T2}*::*Rosa26-YFP* transgenic mice, we processed cryosections from the sciatic nerve to detect PDGFRα (red), YFP (anti-GFP, green) and Hoescht 33342 (**Fig. 4.1 i-k**). PDGFRα$^+$ cells were detected throughout the sciatic nerve, and at the edge of each nerve bundle (**Fig. 4.1 i**). Surprisingly, the density of PDGFRα$^+$ cells was significantly higher in the sciatic nerve (367 ± 17 cells/mm^2) than any of the CNS regions examined (P<0.0001, ANOVA; **Fig. 4.1m**). However, only ~11% of the PDGFRα$^+$ cell population found in the sciatic nerve was YFP-labelled (**Fig. 4.1 n**). Furthermore, only half of the YFP$^+$ cells examined co-labelled for PDGFRα (**Fig. 4.1 k, m**; 52% ± 5.7% of YFP$^+$ cells co-expressed PDGFRα), indicating that the *Pdgfrα-CreER^{T2}* transgene also induced recombination in a small number of unidentified cells in the peripheral nervous system. Some Schwann cells in the sciatic nerve have been shown to express PDGFRα (Eccleston et al., 1993), and by performing immunohistochemistry to detect YFP (green) and the Schwann cell marker S100β (red; **Fig. 4.1 l**), we determined that all of the YFP$^+$ cells present in the sciatic nerve of adult *Pdgfrα-CreER^{T2}::Rosa26-YFP* transgenic mice were Schwann cells.

4.2.3 Fewer than 1% of PDGFRα$^+$ cells become YFP-labelled in the endocrine glands of adult *Pdgfrα-CreER^{T2}::Rosa26-YFP* transgenic mice.

To determine whether Tx administration to adult *Pdgfrα-CreER^{T2}::Rosa26-YFP* transgenic mice can induce YFP-labelling in PDGFRα$^+$ cells within the endocrine system, cryosections of the adrenal and pituitary glands were examined following immunohistochemistry to detect PDGFRα$^+$ (red), YFP (green) and the nuclear marker Hoescht 33342 (**Fig. 4.2 a-d**). PDGFRα$^+$ cells were present throughout the adrenal (**Fig. 4.2 a-b**) and pituitary (**Fig. 4.2 c-d**) glands at a density of 1086 ± 500 cells/mm^2 and 2237 ± 282 cells/mm^2 respectively (**Fig. 4.2 e**). Of these PDGFRα$^+$ cell populations, only ~0.9% and ~0.4% became YFP-labelled, respectively (**Fig. 4.2 f**). In addition to the small number of YFP$^+$ PDGFRα$^+$ cells detected, a number of YFP$^+$ PDGFRα-negative cells were identified. In the adrenal gland these cells appeared to be clustered (**Fig. 4.2 b**), whereas in the pituitary gland they were more evenly distributed throughout the tissue (**Fig. 4.2 d**), but were still very rare. The YFP$^+$ PDGFRα-negative cells represented 46% ± 24% of the YFP$^+$ cells present in the adrenal gland and 81% ± 2.6% of the YFP$^+$ cells in the pituitary gland. These data indicate that while the extent of recombination and YFP-labelling in the adrenal or pituitary glands of *Pdgfrα-CreER^{T2}::Rosa26-YFP* mice is extremely low, the specificity of this labelling is also poor.

4.2.4 Less than 1.5% of PDGFRα$^+$ cells in the heart or gastrocnemius muscle undergo recombination following Tx administration to adult *Pdgfrα-CreER^{T2}::Rosa26-YFP* transgenic mice

To determine whether cells within the heart or gastrocnemius muscle become YFP-labelled in adult *Pdgfrα-CreER^{T2}::Rosa26-YFP* transgenic mice, cryosections of each were stained to detect PDGFRα$^+$ (red), YFP (green) and the nuclear marker Hoescht 33342 (**Fig. 4.3 a-d**). PDGFRα$^+$ cell populations were identified in the heart (**Fig. 4.3 a-b**) and gastrocnemius muscle (**Fig. 4.3 c-d**) at a similar density (**Fig. 4.3 e**) and these cells had a similar morphology (compare **Fig. 4.3 b, d**). The location and morphology of the PDGFRα$^+$ cells in the heart and gastrocnemius muscle, are consistent with that of PDGFRα$^+$ cardiac progenitors (Noseda et al., 2015) and PDGFRα$^+$ fibro/adipogenic progenitors (FAPs) (Contreras et al., 2016) previously characterized. In the heart, only ~0.5% of the PDGFRα$^+$ cell population became YFP-labelled (**Fig. 4.3 a, b, f**), which was not dissimilar to the ~1.2% of PDGFRα$^+$ cells that became YFP-labelled in the gastrocnemius muscle (**Fig. 4.3 a-d, f**). These data indicate that the *Pdgfrα-CreER^{T2}* transgenic mouse does not enable significant recombination in either of these cell populations.

In addition to the YFP$^+$ PDGFRα$^+$ cells identified in the heart and gastrocnemius muscle, we detected YFP$^+$ PDGFRα-negative cells (**Fig. 4.3 a, d**). In the heart only 44% ± 6.3% of the

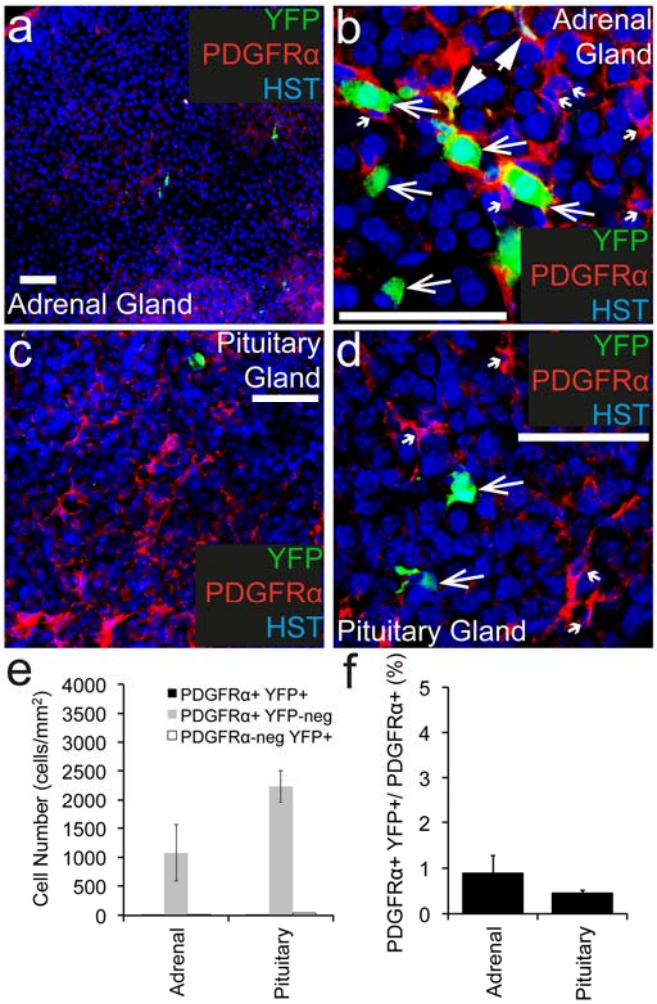

Figure 4.2: PDGFRα⁺ cells recombine at low efficiency in endocrine tissue

Cryosections through the adrenal and pituitary gland of P57+7 Pdgfrα-CreER^{T2} :: Rosa26-YFP were immuno-stained to detect PDGFRα (red), YFP (green) and Hoescht 33342 (blue). Confocal image (single z plane) of the adrenal gland at low (a) and high (b) magnification. Confocal image (single z plane) of the pituitary gland at low (c) and high (d) magnification. (e) The number of PDGFRα⁺ YFP⁺, PDGFRα⁺ YFP-negative and PDGFRα-negative YFP⁺ cells quantified from confocal images (single z plane) of the adrenal and pituitary glands, expressed as the number of cells per mm². (f) The proportion of PDGFRα⁺ cells that become YFP-labelled (PDGFRα⁺ YFP⁺ cells / total PDGFRα⁺ cells, x 100) quantified from confocal images (single z plane) of adrenal and pituitary gland. Error bars represent mean ± std dev from n=3 mice. PDGFRα⁺ YFP⁺ cells are denoted by arrowheads. PDGFRα-negative YFP⁺ cells are denoted by arrows. PDGFRα⁺ YFP-negative cells are denoted by small arrows. Scale bars = 50μm

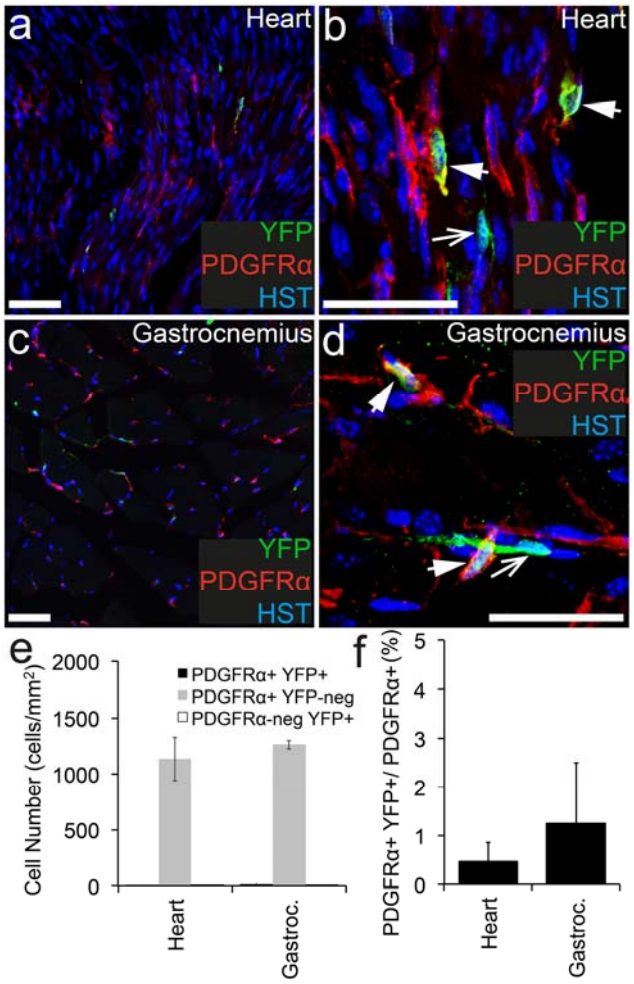

Figure 4.3: PDGFRα⁺ cells recombine at low efficiency in cardiac and skeletal muscle

Cryosections from P57+7 Pdgfrα-CreER^{T2}:: Rosa26-YFP transgenic mice were immuno-stained to detect PDGFRα (red), YFP (green) and HST (blue). Confocal image (single z plane) of the heart at low (a) and high (b) magnification. Confocal image (single z plane) of the gastrocnemius at low (c) and high (d) magnification. (e) The number of PDGFRα⁺ YFP⁺, PDGFRα⁺ YFP-negative and PDGFRα-negative YFP⁺ cells quantified from confocal images (single z plane) of the heart and gastrocnemius expressed as the number of cells per mm². (f) The proportion of PDGFRα⁺ cells that become YFP-labelled (PDGFRα⁺ YFP⁺ cells/ total PDGFRα⁺ cells, expressed as a percentage) quantified from confocal images (single z plane) of the heart and gastrocnemius. Error bars represent mean ± std dev from n=3 mice. PDGFRα⁺ YFP⁺ cells are denoted by arrowheads. PDGFRα-negative YFP⁺ cells are denoted by arrows. Scale bars = 50μm

YFP$^+$ cells expressed PDGFRα, whereas in the gastrocnemius muscle, recombination was more specific with 83% ± 25% of the YFP+ cells co-expressing PDGFRα (**Fig. 4.3 e**). These data suggest that the *Pdgfrα-CreER^{T2}* transgene is ectopically expressed by some cells in the heart. However the extremely low number of YFP$^+$ cells detected in either muscle suggests that the *Pdgfrα-CreER^{T2}* transgenic mouse is largely ineffective in targeting cells in these tissues.

4.2.5 PDGFRα$^+$ cells are present in the liver, lung, spleen and kidney, and recombine at low efficiency in adult *Pdgfrα-CreER^{T2}::Rosa26-YFP* transgenic mice

To determine whether cells within the liver, lung, spleen or kidney undergo recombination and become YFP-labelled in adult *Pdgfrα-CreER^{T2}::Rosa26-YFP* transgenic mice, cryosections were processed to detect PDGFRα$^+$ (red), YFP (green) and the nuclear marker Hoescht 33342 (**Fig. 4.4**). PDGFRα$^+$ cells were dispersed throughout the liver (**Fig. 4.4 a-b**), lung (**Fig. 4.4 c-d**), spleen (**Fig. 4.4 e-f**) and kidney (**Fig. 4.4 g-h**). They were particularly numerous in the lung (4023 ± 1400 cells/ mm^2) and spleen (5189 ± 236 cells/mm^2). Despite each organ containing a higher density of PDGFRα$^+$ cells than any CNS region examined ($P<0.0003$, ANOVA; **Fig. 4.4i**), the number of YFP$^+$ cells detected was extremely low. In the liver only ~1.2% of the PDGFRα$^+$ cell population expressed YFP (**Fig. 4.4 b, j**). This was even lower in the other organs, with ~0.7% of the PDGFRα$^+$ cells in the lung, ~0.3% of the PDGFRα$^+$ cells in the spleen and ~0.2% of the PDGFRα$^+$ cells in the kidney being YFP-labelled (**Fig. 4.4 j**). The YFP$^+$ PDGFRα$^+$ cells in the liver (**Fig. 4.4 b**) and kidney (**Fig. 4.4 h**) have a distinct fibroblast-like morphology. This is entirely consistent with previous reports that tissue fibroblasts express PDGFRα (Chen et al., 2012; Hayes et al., 2014; Liu et al., 2014; Horikawa et al., 2015), and more specifically that hepatic stellate cells express PDGFRα in the adult liver (Hayes et al., 2014; Liu et al., 2014). Similarly, in the lung the YFP$^+$ PDGFRα$^+$ cells were detected in the alveoli (**Fig. 4.4 g**), consistent with previous reports that the PDGFRα$^+$ lung cells are a subpopulation of lung fibroblasts called alveolar fibroblasts (Chen et al., 2012).

Only 18.8% ± 13% of the YFP$^+$ cells in the liver, 22.9% ± 0.9% of the YFP$^+$ cells in lung, 22% ±17% of the YFP$^+$ cells in the spleen and 44% ± 3.8% of the YFP$^+$ cells in the kidney co-expressed PDGFRα (**Fig. 4.4 i**). In the liver, the YFP$^+$ cells (both YFP$^+$ PDGFRα$^+$ as well as YFP$^+$ PDGFRα-negative cells) were unusually distributed – being rare overall, but when they were detected, they always appeared in clusters (as shown in **Fig. 4.4 a**). It is unlikely that the YFP$^+$ PDGFRα-negative cells detected in the liver, lung, spleen and kidney are the result of the proliferation and differentiation of the YFP$^+$ PDGFRα$^+$ cells, as this would require each YFP$^+$ PDGFRα$^+$ cell to undergo between one and three cell divisions within the seven day

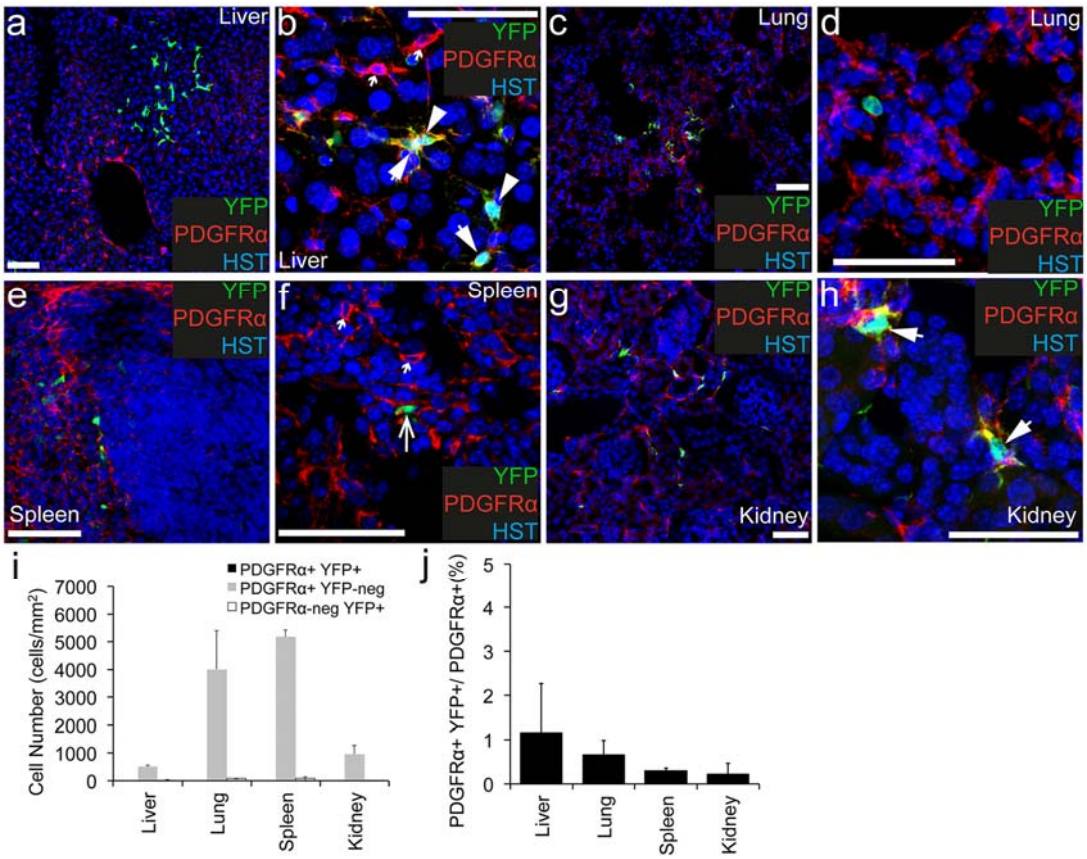

Figure 4.4: PDGFRα⁺ cells recombine at low efficiency in the liver, lung, spleen and kidney

Cryosections from P57+7 Pdgfrα-CreER^{T2}:: Rosa26-YFP transgenic mice were immuno-stained to detect PDGFRα (red), YFP (green) and HST (blue). Confocal image (single z plane) of the liver at low (a) and high (b) magnification. Confocal image (single z plane) of the lung at low (c) and high (d) magnification. Confocal image (single z plane) of the spleen at low (e) and high (f) magnification. Confocal image (single z plane) of the kidney at low (g) and high (h) magnification. (i) The number of PDGFRα⁺ YFP⁺, PDGFRα⁺ YFP-negative and PDGFRα-negative YFP⁺ cells quantified from confocal images (single z plane) of the liver, lung, spleen and kidney expressed as the number of cells per mm². (j) The proportion of PDGFRα⁺ cells that become YFP-labelled (PDGFRα⁺ YFP⁺ cells/ total PDGFRα⁺ cells, expressed as a percentage) quantified from confocal images (single z plane) of the liver, lung, spleen and kidney. Error bars represent mean ± std dev from n=3 mice. PDGFRα⁺ YFP⁺ cells are denoted by arrowheads. PDGFRα-negative YFP⁺ cells are denoted by arrows. PDGFRα⁺ YFP-negative cells are denoted by small arrows. Scale bars = 50μm

labelling and tracing period, which is well above the level of cellgenesis previously reported in these tissues (Chang et al., 2008; Parretta et al., 2008; Seyed-Razavi et al., 2013). The more likely explanation is that the majority of YFP-labelling that occurs in these organs is non-specific. We conclude that the *Pdgfrα-CreER^{T2}::Rosa26-YFP* transgenic mice cannot be used to specifically or efficiently induce gene recombination in the PDGFRα^{+} fiboblast-like cell populations in any of these organs.

4.2.6 PDGFRα^{+} cells are present in the large and small intestine, and a small proportion of them become YFP-labelled in adult *Pdgfrα-CreER^{T2}::Rosa26-YFP* transgenic mice.

The gastrointestinal tract is organized into distinct layers. A special population of PDGFRα^{+} cells, with a largely unknown function, has been previously identified within the mucosal layer of the intestine (Kurahashi et al., 2013). PDGFRα^{+} cells are also present in the muscular layer of the intestine where they mediate communication between the enteric nervous system and smooth muscle cells (Kurahashi et al., 2011; 2014). To determine whether these cells undergo recombination and become YFP-labelled in adult *Pdgfrα-CreER^{T2}::Rosa26-YFP* transgenic mice, cryosections were processed to detect PDGFRα^{+} (red), YFP (green) and the nuclear marker Hoescht 33342 (**Fig. 4.5**). We confirm that PDGFRα^{+} cells are present throughout the small intestine. In particular there was a high density of PDGFRα^{+} cells detected in the lamina propria of the villi (**Fig. 4.5 a-c, g**). PDGFRα^{+} cells were also detected in the smooth muscle layer (**Fig. 4.5 d**), but no PDGFRα^{+} were detected in the epithelial cell layer (**Fig. 4.5 b**). In the large intestine, PDGFRα^{+} cells were similarly observed in the crypts and smooth muscle (**Fig. 4.5 e-f**). However, PDGFRα^{+} cell density was significantly higher in the small (344.3 ± 10 cells/mm^2) relative to the large (184.9 ± 44.6 cells/mm^2) intestine ($P<0.002$, ANOVA).

We next determined that YFP^{+} PDGFRα^{+} cells were present in the small and large intestines, however the proportion of PDGFRα^{+} cells that became YFP-labelled was quite small. Only ~6.4% of the PDGFRα^{+} cells in the villi and crypts of the small intestine and ~5.7% of the PDGFRα^{+} cells in the smooth muscle layer of the small intestine became YFP-labelled. Similarly, only ~2% of the PDGFRα^{+} cells in the large intestine co-expressed YFP (**Fig. 4.5 g**). Furthermore, the specificity of the YFP labelling in the intestine may also be of concern. In the villi and crypts of the small intestine 63% ± 22% of the YFP^{+} cells co-expressed PDGFRα (**Fig. 4.5 b, c, g**). However in the smooth muscle layer only 14% ± 3% of the YFP^{+} cells co-labelled for PDGFRα^{+} (**Fig. 4.5 g**). The YFP^{+} PDGFRα-negative cells in the smooth muscle layer were elongated and had long narrow nuclei, suggesting that they were smooth muscle cells. Therefore, while the *Pdgfrα-CreER^{T2}* transgenic mouse can be

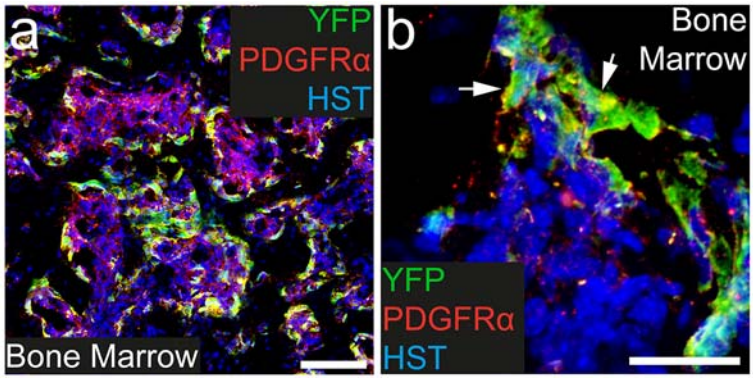

Figure 4.6: A proportion of PDGFRα⁺ cells become YFP- labeled in the bone marrow
Transverse cryosections taken through the tail of P57+7 Pdgfrα-CreER^{T2}:: Rosa26-YFP transgenic mice were immuno-stained to detect PDGFRα (red), YFP (green) and HST (blue). Confocal images (single z plane) of the bone marrow at low (a) and high (b) magnification. PDGFRα⁺ YFP⁺ cells are denoted by arrowheads. Scale bars represent 100μm (a) and 25μm (b).

used to label a small subpopulation of the intestinal PDGFRα$^+$ cell population for lineage tracing studies, it would be ineffective for facilitating conditional gene deletion in these cells.

4.2.7 PDGFRα$^+$ cells are present in the bone marrow and become YFP-labelled following Tx administration to adult *Pdgfrα-CreER^{T2}::Rosa26-YFP* transgenic mice

Within the bone marrow, PDGFRα$^+$ cells are non-hematopoietic stromal cells (Anthony and Link, 2014). To determine whether these PDGFRα$^+$ cells become YFP labelled in adult *Pdgfrα-CreER^{T2}::Rosa26-YFP* transgenic mice, cryosections were taken through the tail and processed to detect PDGFRα (red), YFP (green) and the nuclear marker Hoescht 33342 (**Fig. 4.6**). As expected PDGFRα$^+$ cells were present throughout the bone marrow (**Fig. 4.6 a, b**) at high density (3545.7 ± 619.5 cells/mm^2). Furthermore, 37.9 ± 0.8% of these cells had undergone recombination and were YFP labeled. Within the bone marrow, the YFP-labelling was highly specific, with all YFP-labeled cells expressing PDGFRα$^+$. These data indicate that, outside of the CNS, the most specific and extensive site of recombination and YFP-labelling achieved using the *Pdgfrα-CreER^{T2}::Rosa26-YFP* transgenic mice, is within the bone marrow.

4.3 Discussion

4.3.1 *Pdgfrα-CreER^{T2}* transgenic mice specifically and efficiently induce recombination in OPCs in the CNS

Within the CNS, PDGFRα and the NG2 proteoglycan are both accepted markers for the identification of OPCs, as they are co-expressed by >98% of OPCs (Rivers et al., 2008). While inconsistent with the protein expression data, *Ng2-dsred* transgenic mice not only label OPCs within the CNS, but also robustly label pericytes (Hall et al., 2014), whereas *Pdgfrα-CreER^{T2}* transgenic mice have been used to induce Cre-mediated recombination soley within OPCs (Rivers et al., 2008; Kang et al., 2010). In this study we report that *Pdgfrα-CreER^{T2}* transgenic mice can induce recombination in >90% of OPCs across the CNS, ranging from ~91% in the spinal cord to ~97% in the motor cortex (see **Fig. 4.1**). These data are consistent with previous reports in which the administration of Tx to adult *Pdgfrα-CreER^{T2}::Rosa26-mGFP* transgenic mice resulted in the GFP-labelling of ~94% of OPCs in the dorsal cortex and ~91% of OPCs in the piriform cortex (Kang et al., 2013). Essentially all PDGFRα-negative YFP$^+$ cells observed in the CNS had distinct oligodendrocyte morphology and co-labelled for OLIG2, suggesting that they were newly differentiated oligodendrocytes, generated by the YFP-labelled OPCs. More of these cells were observed in the CC than the cortex, which is also consistent with previous observations

that OPCs within the adult mouse CC proliferate and generate new oligodendrocytes more rapidly than those in the cortex (Rivers et al., 2008).

While these results show that the *Pdgfrα-CreER^{T2}::Rosa26-YFP* transgenic mouse line is highly effective for inducing gene-specific recombination in OPCs throughout the CNS when treated with Tx this study did not address any potential leakiness of the system. Untreated *Pdgfrα-CreER^{T2}::Rosa26-YFP* control mice could be included to determine whether any recombination is occurring without Tx administration. However, if recombination was occurring prior to Tx administration it would be expected that fluorescence would be identified in a greater number of non-oligodendrocyte lineage cells, which had spontaneously recombined prior to differentiating from stem cell populations during development.

We conclude that within the CNS, expression of the *Pdgfrα-CreER^{T2}* transgene faithfully follows that of endogenous PDGFRα expression, in that it specifically facilitates DNA recombination in a high proportion of OPCs. This transgenic mouse can therefore be used to effect gene activation or deletion within OPCs of the CNS, without affecting other CNS cell types. However, its suitability for some experiments, particularly gene deletion experiments, is also dependent on the level of recombination (or lack of recombination) achieved in cells outside of the CNS.

4.3.2 The *Pdgfrα-CreER^{T2}* transgene enables recombination in a small proportion of Schwann cells

We have determined that a small proportion (~11%) of PDGFRα^{+} S100β^{+} Schwann cells, and a small number of PDGFRα-negative S100β^{+} Schwann cells, become YFP-labelled in P57+7 *Pdgfrα-CreER^{T2}::Rosa26-YFP* transgenic mice (see **Fig. 4.1**). This reflects a low recombination efficiency for the Schwann cell population overall. However since the vast majority of peripheral myelin is laid down by P22 (Garbay et al., 2000), and only a small number of Schwann cells are still adding myelin at P57 (Garbay et al., 2000), it is possible that the less mature cells are preferentially labelled using the *Pdgfrα-CreER^{T2}* transgenic mouse. Irrespective of their stage of maturation, this is the first report of Schwann cell labelling in the sciatic nerve of *Pdgfrα-CreER^{T2}* mice. A previous study, using an alternative *Pdgfrα-CreER^{T2}* mouse line, achieved recombination in the sciatic nerve following a crush injury, but the labelled cells were not Schwann cells (Zawadzka et al., 2010). However, given the small proportion of Schwann cells that became YFP-labelled in the *Pdgfrα-CreER^{T2}* mouse line used for this study, and the known capacity of peripheral nerves to regenerate following an injury (Makwana and Raivich, 2005; Mietto et al., 2015), it is unlikely that using the *Pdgfrα-CreER^{T2}* transgenic mouse for conditional gene ablation, irrespective

of the gene, would seriously impact peripheral nerve function or result in a detectable or long-lived Schwann cell phenotype.

4.3.3 *Pdgfrα-CreER^{T2}* transgenic mice induce recombination in a novel PDGFRα$^+$ cell population in the intestine

A unique population of PDGFRα$^+$ cells reside in the mucosal layer of the gastrointestinal tract (Kurahashi et al., 2013). These cells have long, thin cell bodies and processes, and are found in the laminar propria where they form a sheath that extends along the length of the crypts, immediately below the epithelial cell layer. Many of the PDGFRα$^+$ YFP$^+$ cells detected in the villi and crypts of the small and large intestine of *Pdgfrα-CreER^{T2}::Rosa26-YFP* transgenic mice belong to this population of cells. Interestingly, it has been suggested that these subepithelial PDGFRα$^+$ cells may be able to remodel or change their phenotype depending upon cell culture conditions (Kurahashi et al., 2013), and this could be a possible explanation for the occasional YFP$^+$ PDGFRα$^+$ cells in the villi of the small intestine that are morphologically distinct from most of this population (see **Fig. 4.5 c**). However, little is known about this newly discovered cell type and its *in vivo* differentiation capabilities.

In the muscle layers of the small and large intestine, PDGFRα$^+$ cells are a subtype of interstitial cell, also known as “fibroblast-like” cells (Kurahashi et al., 2011). These cells are located near the terminals of enteric motor neurons and communicate information from the enteric nervous system to the smooth muscle cells of the intestine via gap junctions (Kurahashi et al., 2011; 2014). In *Pdgfrα-CreER^{T2}::Rosa26-YFP* transgenic mice, Tx administration induced recombination and YFP-labelling in a very small proportion of PDGFRα$^+$ cells in any muscle type. The intestinal smooth muscle had the highest level of recombination with ~5.7% of PDGFRα$^+$ cells becoming YFP labeled, while in the cardiac and skeletal muscle <2% of PDGFRα$^+$ cells recombined. Morphologically the PDGFRα$^+$ cell population in the smooth muscle is similar to the PDGFRα$^+$ cell populations identified in the heart and gastrocnemius muscle (compare **Fig. 4.3 b, d** with **Fig. 4.5 d**), which is particularly interesting as a number of studies have indicated that the PDGFRα$^+$ cells in the heart (Chong et al., 2013; Noseda et al., 2015) and skeletal muscle (Oishi et al., 2013; Pannérec et al., 2013) are progenitor populations.

While few of the PDGFRα$^+$ cells in the heart and small intestinal smooth muscle underwent recombination, these regions contained a relatively high proportion of YFP$^+$ PDGFRα-negative cells. One possible explanation for these cells is that the YFP$^+$ PDGFRα$^+$ cells represent immature cell populations which, like the OPCs, rapidly divide and mature into cells that no longer express PDGFRα. Even though the PDGFRα$^+$ cells in the heart are multipotent progenitors (Chong et al., 2013), their rate of proliferation and differentiation

could not account for the number of YFP$^+$ PDGFRα-negative cells detected (Senyo et al., 2013). Alternatively, in the intestinal smooth muscle, it is possible that YFP could pass from recombined YFP$^+$ PDGFRα$^+$ cells through the gap junctions to give the appearance of YFP-labelling in PDGFRα-negative cells. However, this seems unlikely as there does not appear to be a close physical association between these two cell populations. The most likely explanation is that the *Pdgfrα-CreER^{T2}* transgene lacks a regulatory element that controls the expression of *Pdgfrα* – one that is not required to regulate gene expression in the CNS, so that it is mis-expressed, resulting in the direct recombination of small numbers of PDGFRα-negative cells in these tissues.

4.3.4 PDGFRα$^+$ stromal cells in the bone marrow become YFP-labelled more efficiently than any other PDGFRα$^+$ cell population outside of the CNS

The bone marrow is a major site of haematopoiesis. However, surrounding the islands of hematopoietic cells, is an extensive network of stromal cells that includes the PDGFRα$^+$ cells of the bone marrow. The PDGFRα$^+$ stromal cells comprise the perivascular CXCL12-abundant reticular (CAR) cells and the PDGFRα$^+$ Sca1$^+$ (PαS) cells (Anthony and Link, 2014). CAR cells are adipo-osteogenic progenitors that secrete factors essential for haematopoietic stem and progenitor cell maintenance (Sugiyama et al., 2006; Omatsu et al., 2010; Ding et al., 2012), while PαS cells are a population enriched in bone marrow mesenchymal stem cells (Morikawa et al., 2009). Following Tx administration to adult *Pdgfrα-CreER^{T2}::Rosa26-YFP* transgenic mice, ~38% of PDGFRα$^+$ bone marrow stromal cells become YFP-labelled, and the recombination of cells in this region was highly specific, as all YFP$^+$ cells were PDGFRα$^+$. These data indicate, that the *Pdgfrα-CreER^{T2}* transgenic mouse induces a significant level of gene recombination in PDGFRα$^+$ bone marrow stromal cells *in vivo*, and could be useful for lineage tracing studies of this population. Furthermore, if researchers plan to use *Pdgfrα-CreER^{T2}* transgenic mice to achieve conditional gene deletion from OPCs in the CNS, they should also consider that the gene will also be deleted from cells in this population.

4.3.5 Few PDGFRα$^+$ fibroblasts become YFP-labelled in *Pdgfrα-CreER^{T2}::Rosa26YFP* transgenic mice

We identified PDGFRα$^+$ cell populations in all of the tissues and quantified the level of recombination (YFP-labelling) achieved using *Pdgfrα-CreER^{T2}* transgenic mice. The majority of PDGFRα$^+$ cell populations identified were fibroblasts (Horikawa et al., 2015). PDGFRα is an established marker for some fibroblast cell populations. For example, *in situ* hybridisation previously indicated the presence of *Pdgfrα* mRNA in the lung (Boström et al., 1996), and a GFP reporter line was then used to visualize these cells (Ntokou et al., 2015),

and determine that PDGFRα expression identifies alveolar fibroblasts (Chen et al., 2012). Hepatic stellate cells, a fibrotic cell type in the liver, have also been shown to express PDGFRα (Hayes et al., 2014; Liu et al., 2014). Furthermore, the overexpression of PDGFRα has been linked to fibrosis in many of the organs examined in this study, such as the lung, kidney and liver (Bonner, 2004; Hayes et al., 2014). In each of the tissues that contained PDGFRα^{+} fibroblasts, very few of these cells became YFP-labelled in P57+7 *Pdgfrα-CreER^{T2}::Rosa26-YFP* transgenic mice. The low level of recombination in these populations and poor specificity for recombination in these areas, suggests that these mice will have limited application for studying these cell types. Furthermore, if researchers plan to use the *Pdgfrα-CreER^{T2}* transgenic mouse to achieve conditional gene deletion from OPCs in the CNS, they are unlikely to experience unexpected effects in the lungs, liver, kidney or spleen.

4.4 Conclusions

Pdgfrα-CreER^{T2} transgenic mice are an effective tool for selectively achieving highly specific recombination in PDGFRα^{+} OPCs of the CNS. However, outside of the CNS, these mice fail to induce significant recombination in any PDGFRα^{+} cell population, with the exception PDGFRα^{+} stromal cells in the bone marrow. These data indicate that *Pdgfrα-CreER^{T2}* transgenic mice could be used to conditionally delete *Kif3a* from OPCs, to prevent cilia assembly *in vivo*, without producing significant adverse phenotypes outside of the CNS.

Chapter 5: *Kif3a* impairs OPC proliferation and oligodendrogenesis *in vivo*

5.1 Introduction

Having demonstrated that primary cilia assembly is dramatically reduced when *Kif3a* is deleted from OPCs *in vitro* (Chapter 3), and that *Pdgfrα-CreER*^{T2} transgenic mice preferentially achieve DNA recombination in PDGFRα^{+} OPCs (O'Rourke et al., 2016), I now aim to use *Pdgfrα-CreER*^{T2} transgenic mice to conditionally delete *Kif3a* and prevent primary cilium assembly by OPCs *in vivo*. The experiments presented in this Chapter will determine whether the primary cilium is necessary for OPC proliferation and oligodendrogenesis in the adult mouse brain.

The targeted deletion of *Kif3a*, a vital component of the primary cilium cytoskeleton, from specific cell types *in vivo*, has been achieved previously, by intercrossing *Kif3a*$^{fl/fl}$ transgenic mice (Marszalek et al., 2000) with transgenic mice that express Cre recombinase in the target cell population. For example, deletion of *Kif3a* from proliferative cell types, including kidney epithelial cells (Ma et al., 2013), osteoblasts (Temiyasathit et al., 2012) and cardiac myocytes (Slough et al., 2008), consistently led to decreased proliferation. In the CNS, the deletion of *Kif3a* from cerebellar granule cell precursors resulted in reduced proliferation and retarded cerebellar development (Spassky et al., 2008). Furthermore, the loss of primary cilia assembly by neural progenitors, in the developing dentate gyrus, achieved by the deletion of *Kif3a*, resulted in reduced precursor proliferation and an underdeveloped dentate gyrus (Han et al., 2008). In adulthood, deletion of the *Kif3a* gene from B1 neural stem cells, reduced neurogenesis in the ventral SVZ (Tong et al., 2014). These data indicate that deleting *Kif3a* can selectively disrupt primary cilia function on proliferating cell populations *in vivo*.

As OPCs continue to proliferate and generate new oligodendrocytes throughout life (Rivers et al., 2008; reviewed by Wang and Young, 2014), it follows that these cells will be highly reliant on signalling at the primary cilia to perform their function. Therefore, I hypothesize that the deletion of *Kif3a* from OPCs *in vivo* will result in a reduction in proliferation, as seen *in vitro* (see Chapter 3). I also hypothesise, that by preventing cilium assembly, I will halt adult oligodendrogenesis, and this will allow me to determine whether ongoing oligodendrogenesis is essential for the maintenance of motor or cognitive performance, as well as mood regulation.

5.2 Results

5.2.1 OPCs but not oligodendrocytes assemble primary cilia in the adult mouse brain

In order to determine whether cells of the oligodendrocyte lineage assemble primary cilia *in vivo,* 30µm cryosections were generated from the brains of P60 *Sox10-GFP* mice, in which GFP is under the control of the *Sox10* promoter, and all cells of the oligodendrocyte lineage are GFP-labelled (Kessaris et al., 2005). Immunohistochemistry was performed to detect cells of the oligodendrocyte lineage (GFP; blue) and determine the proportion that expressed the primary cilia markers Arl13b (red) and γ-tubulin (green) within the CC (**Fig. 5.1 a-c**). ~7% of GFP^+ cells had assembled primary cilia at P60 (**Fig. 5.1 a-c, g**) - a proportion strikingly similar to the fraction of $SOX10^+$ cells that are OPCs in the CC at that age (Rivers et al., 2008).

To determine whether the GFP^+ ciliated cells were OPCs or oligodendrocytes, cryosections were collected from P60 C57Bl6 mice and immunohistochemistry performed to detect OPCs (PDGFRα, blue) and primary cilia (Arl13b, red; γ-tubulin, green). ~72% of $PDGFR\alpha^+$ OPCs were ciliated (**Fig. 5.1 d, g**), suggesting that they made up the majority of the Sox10-GFP^+ ciliated cells, and implying that, like mature Schwann cells (Yoshimura and Takeda, 2012), mature oligodendrocytes do not have assembled primary cilia. To confirm this, I performed immunohistochemistry on cryosections from *Plp-CreER^{T2}::Rosa26-YFP* transgenic mice (P57 + 7), in which immature and mature oligodendrocytes, but not OPCs, are YFP-labelled, and found that the vast majority (~98%) of YFP^+ callosal oligodendrocytes did not have $Arl13b^+$ γ-$tubulin^+$ primary cilia assembled on their surface (**Fig. 5.1 e, g**). As OPCs can directly differentiate into OLs (Hughes et al., 2013), this process must require disassembly of the primary cilium during or at the conclusion of differentiation. Considering this, it is possible that the ~2% of YFP^+ cells that were ciliated, are differentiating oligodendrocytes, or correspond to the relatively stable population of immature (ENPP6+) oligodendrocytes (Xiao et al., 2016).

5.2.2 *In vivo*, adult OPCs disassemble their primary cilia to re-enter the cell cycle.

Having determined that OPCs, but not oligodendrocytes, have assembled primary cilia, I next aimed to determine whether OPCs disassemble their primary cilia as they progress through the cell cycle *in vivo*, as they do *in vitro* (see Chapter 3). *In vivo*, OPCs proliferate asynchronously, such that a fraction of the population is transitioning through the S and M phases of the cell cycle, at any given time (Young et al., 2013), and I hypothesise that

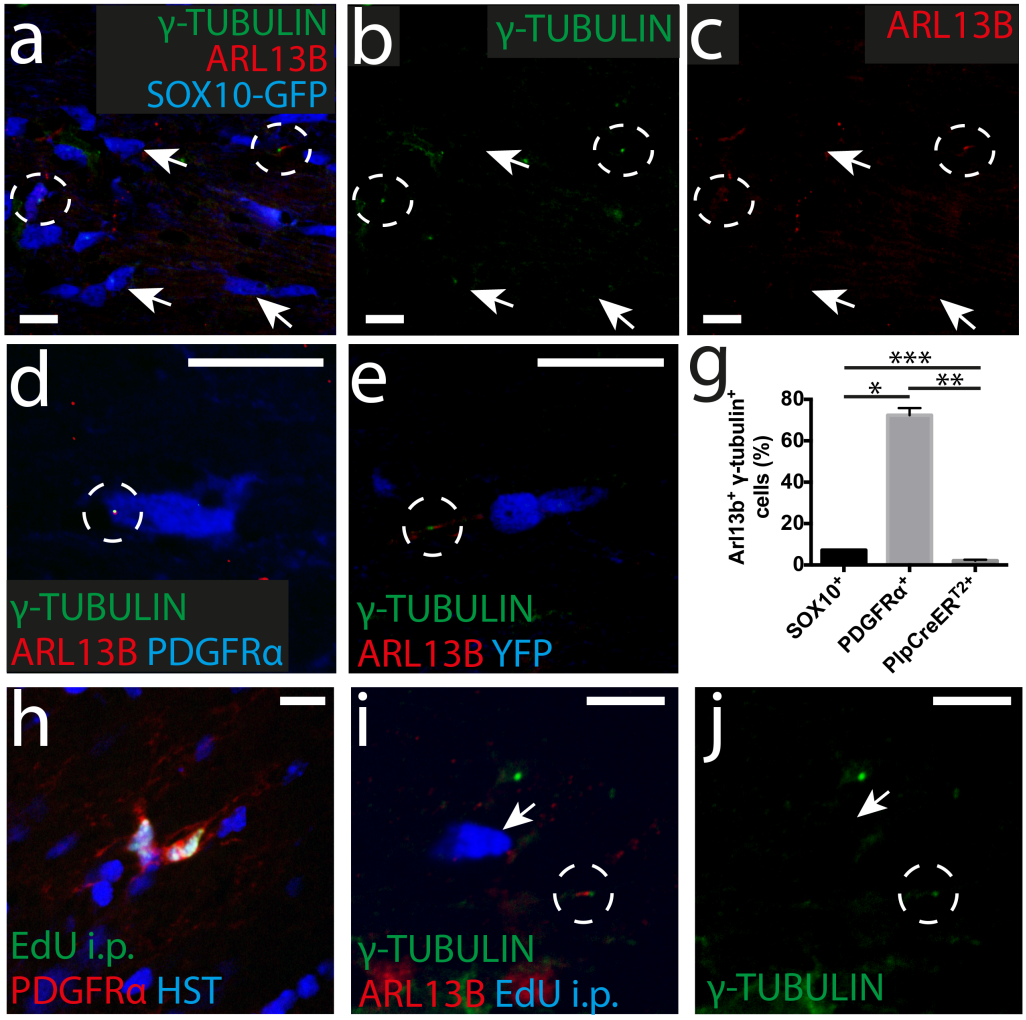

Figure 5.1: Primary cilia are disassembled as OPCs enter the cell cycle, and are not assembled on oligodendrocytes

*(**a-c**) Confocal image (single z-plane) of the CC of a P60 Sox10-GFP mouse immuno-stained to detect GFP (blue), Arl13b (red) and γ-tubulin (green). (**d**) Confocal image of the CC of a P60 C57Bl6 mouse immuno-stained to detect GFP (blue), Arl13b (red) and γ-tubulin (green). (**e**) Confocal image (single z-plane) of the corpus callosum of a P57+7 Plp-CreER^{T} :: Rosa26-YFP mouse immunostained to detect GFP (blue), Arl13b (red) and γ-tubulin (green). (**g**) Quantification of the proportion of Sox10^{+}, PDGFα^{+} and Plp^{+} cells in the CC with assembled primary cilia (avg ± stdev, n=3 per group; p<0.0001, one-way ANOVA with Bonferroni.correction). (**h**) Confocal image (single z-plane) of the CC of a P60 C57Bl6 mouse, given EdU for 6 hours and immuno-stained to detect GFP (green), PDGFRα (red) and HST (blue). (**i**) Confocal image (single z-plane) of the CC of a P60 C57Bl6 mouse given EdU given EdU for 6 hours and immuno-stained to detect EdU (blue), Arl13b (red) and γ-tubulin (green). Arrows indicate cells without cilia. Circles indicate assembled primary cilia. Scale bars represent 20μm.*

actively dividing OPCs account for the OPCs that lack an assembled primary cilia *in vivo.* To examine this possibility, EdU was administered to P60 C57Bl6 mice (as per (Wang et al., 2016)), to identify all cells entering S phase of the cell cycle over a 6-hour period. OPCs in the CC divide approximately once a week, and have an S phase of 19 ± 7 hours (Young et al., 2013) and an m phase of 1.2 ± 0.2 hours (Psachoulia et al., 2009). Therefore, very few OPCs that are entering or exiting S phase, will successfully complete their cell cycle within the 6-hour labelling period. While a large number of EdU^+ PDGFRα-negative cells could be identified within the lateral extension of the SVZ (presumably neural progenitor cells and neuroblasts), the small number of EdU^+ cells identified within the CC proper, were $PDGFR\alpha^+$ OPCs (94 of 95 EdU^+ cells) (**Fig. 5.1 h**). Furthermore, EdU^+ cells within the CC lacked $Arl13b^+$ γ-$tubulin^+$ primary cilia (80 of the 81 EdU^+ cells examined across n=3 mice) (**Fig. 5.1 i, j**), indicating that OPCs disassemble their primary cilia to enter the cell cycle *in vitro* and *in vivo*.

5.2.3 OPCs lacking *Kif3a* do not assemble primary cilia

To determine whether primary cilia assembly was not only associated with, but essential to cell cycle transition, delete *Kif3a* from OPCs *in vivo*, I administered Tx to P57 $Kif3a^{fl/fl}$ (control) and $Pdgfr\alpha\text{-}CreER^{T2}::Kif3a^{fl/fl}$ (*Kif3a*-deleted) mice (**Fig. 5.2 a**). After 14 days (P57+14), the mice were perfusion fixed and genomic DNA extracted from the hindbrain, and used to confirm *Kif3a* deletion by PCR analysis of the *Kif3a* gene. The successful amplification of a ~480bp product from the gDNA of $Kif3a^{fl/fl}$ and $Pdgfr\alpha\text{-}CreER^{T2}::Kif3a^{fl/fl}$ and, confirmed the presence of brain cells containing the $Kif3a^{fl/fl}$ allele. However, amplification of a smaller DNA product (~100bp), solely from the gDNA of Tx-dosed $Pdgfr\alpha\text{-}CreER^{T2}::Kif3a^{fl/fl}$ mice, that was absent from naïve $Pdgfr\alpha\text{-}CreER^{T2}::Kif3a^{fl/fl}$ and Tx-dosed $Kif3a^{fl/fl}$ mice, confirmed the presence of cells, from which *Kif3a* had been deleted (**Fig. 5.2 b**).

Kif3a deletion would be predicted to impair primary cilia assembly by OPCs. To investigate this directly, P57 $Pdgfr\alpha\text{-}CreER^{T2}::Rosa26\text{-}YFP$ (control) mice and $Pdgfr\alpha\text{-}CreER^{T2}::Rosa26\text{-}YFP::Kif3a^{fl/fl}$ (*Kif3a*-deleted) transgenic mice received Tx to fluorescently label OPCs and their progeny, and compare their behaviour with and without *Kif3a*, respectively. The proportion of YFP^+ cells with assembled primary cilia (Arl13b, red and γ-tubulin, green) was quantified in the CC from P57+7 to P57+30. In control mice, the proportion of YFP^+ cells that was ciliated decreased over time, with >70% of YFP^+ cells having assembled primary cilia at P57+7 and P57+14 (**Fig. 5.3 a, b, i**), but only ~47% of YFP^+ being ciliated by P57+30

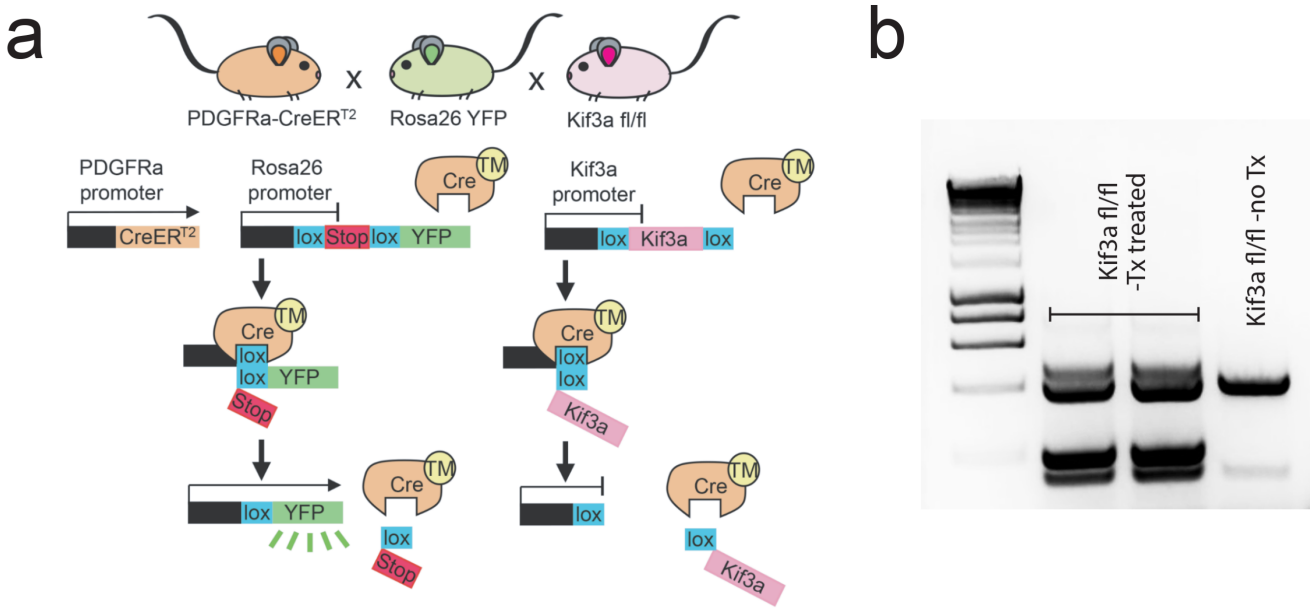

Figure 5.2: Schematic of approach to conditionally delete Kif3a from OPCs in vivo
*(**a**) Schematic of transgenic cre-lox stragegy to conditionally delete Kif3a form OPCs. (**b**) Genomic DNA was extracted from the hindbrain of adult Pdgfrα-CreER^{T2} :: Rosa26-YFP :: Kif3a$^{fl/fl}$ littermates, that received Tx (n=2) or not (n=1). Using primers to amplify a region of the Kif3a gene, it was possible to detect the presence of bands corresponding to Kif3a gene deletion in the Tx-treated mice, that was absent in the untreated mouse.*

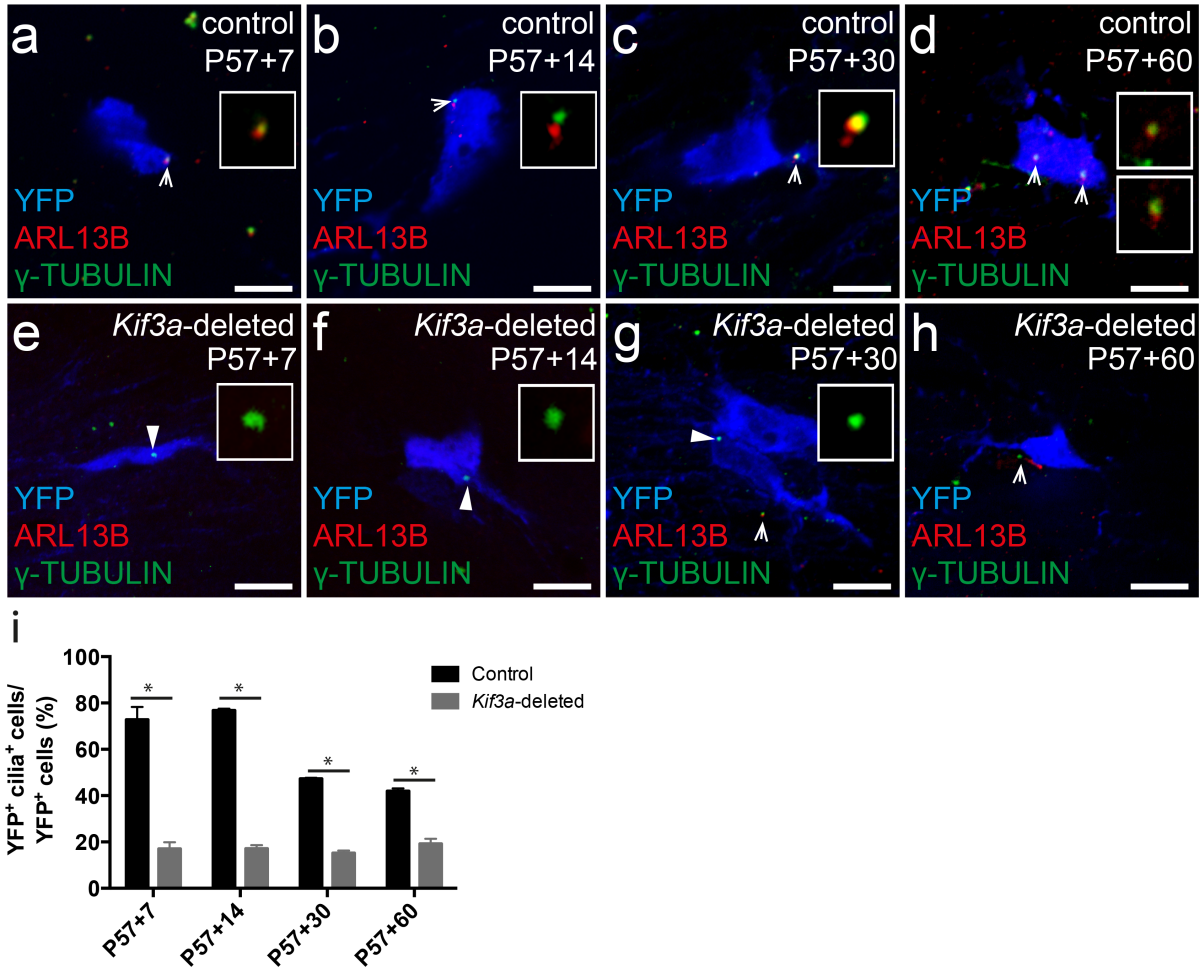

Figure 5.3: Deleting Kif3a from OPCs prevents cilium assembly in vivo
*Confocal image (single z-plane) of the CC of control (Pdgfrα-CreER^{T2} :: Rosa26-YFP) mice at P57+7 (**a**), P57+14 (**b**), P57+30 (**c**) and P57+60 (**d**), immuno-stained to detect YFP (blue), Arl13b (red) and γ-tubulin (green). Confocal image (single z-plane) of the CC of Kif3a-deleted (Pdgfrα-CreER^{T2} :: Rosa26-YFP :: Kif3a$^{fl/fl}$) mice at P57+7 (**e**), P57+14 (**f**), P57+30 (**g**) and P57+60 (**h**), immuno-stained to detect YFP (blue), Arl13b (red) and γ-tubulin (green). (**i**) Quantification of the proportion of YFP$^+$ cells in the CC with assembled primary cilia (avg ± stdev, n=3 per group; p<0.001, two-way ANOVA with Bonferroni correction). Arrows indicate assembled primary cilia. Arrowheads indicate basal bodies without assembled primary cilia. Scale bars = 10μm.*

(**Fig. 5.3 c, i**). This decline can be readily explained by the growing fraction of YFP^+ cells that became oligodendrocytes (Rivers et al., 2008).

In the CC of *Kif3a*-deleted mice, fewer YFP^+ cells were ciliated, relative to control mice, at every time point examined. At P57+7 the proportion of YFP^+ cells that was ciliated dropped from ~76% in control mice to ~17% in *Kif3a*-deleted mice (**Fig. 5.3 e, i**), and a similar reduction was observed at P57+14 (**Fig. 5.3 f, i**). Furthermore, the proportion of YFP^+ cells with cilia remained constant over time in the *Kif3a*-deleted mice, with ~15% of YFP^+ cells still having assembled cilia in P57+30 mice (**Fig. 5.3 g, i**). These data indicate that deletion of the *Kif3a* gene from OPCs successfully prevents primary cilia assembly *in vivo*, and renders the OPCs more stable, neither dividing nor differentiating over time.

5.2.4 Proliferation is impaired in *Kif3a*-deficient adult OPCs

Kif3a-deleted OPCs would still have the capacity to disassemble their primary cilia and enter the cell cycle. However, as each callosal OPC divides once every ~10 days (Rivers et al., 2008), I would predict that at P57+25 days, all OPC would have divided and subsequently failed to reassemble a primary cilia – thereby blocking their capacity to undergo subsequent cell divisions.

To determine whether OPCs lacking *Kif3a* were capable of dividing, P57+25 control and *Kif3a*-deleted mice received EdU via the drinking water for 5 days, before being perfusion fixed at P57+30. Brain cryosections were immunolabelled to detect YFP (blue), PDGFRα (green) and EdU^+ (red), and the fraction of OPCs that had undergone division (EdU^+ $PDGFR\alpha^+$/ total $PDGFR\alpha^+$), was quantified in the CC and motor cortex. Consistent with previous reports (Psachoulia et al., 2009; Young et al., 2013), the fraction of OPCs incorporating EdU, was higher in the CC (~65% of $PDGFR\alpha^+$ OPCs were EdU-labelled; **Fig. 5.4 a, e**) than the motor cortex (~11%; **Fig. 5.4 b, e**) of control mice. While this was also true for the *Kif3a*-deleted OPCs, with ~45% of callosal $PDGFR\alpha^+$ OPCs incorporating EdU (**Fig. 5.4 c, e**) relative to only ~6% in the motor cortex (**Fig. 5.4 d, e**), the rate of EdU incorporation was significantly reduced in both brain regions, relative to controls. Surprisingly, deleting *Kif3a* from OPCs, and preventing cilia assembly, did not prevent all OPCs from dividing, but significantly reduced the proportion that could.

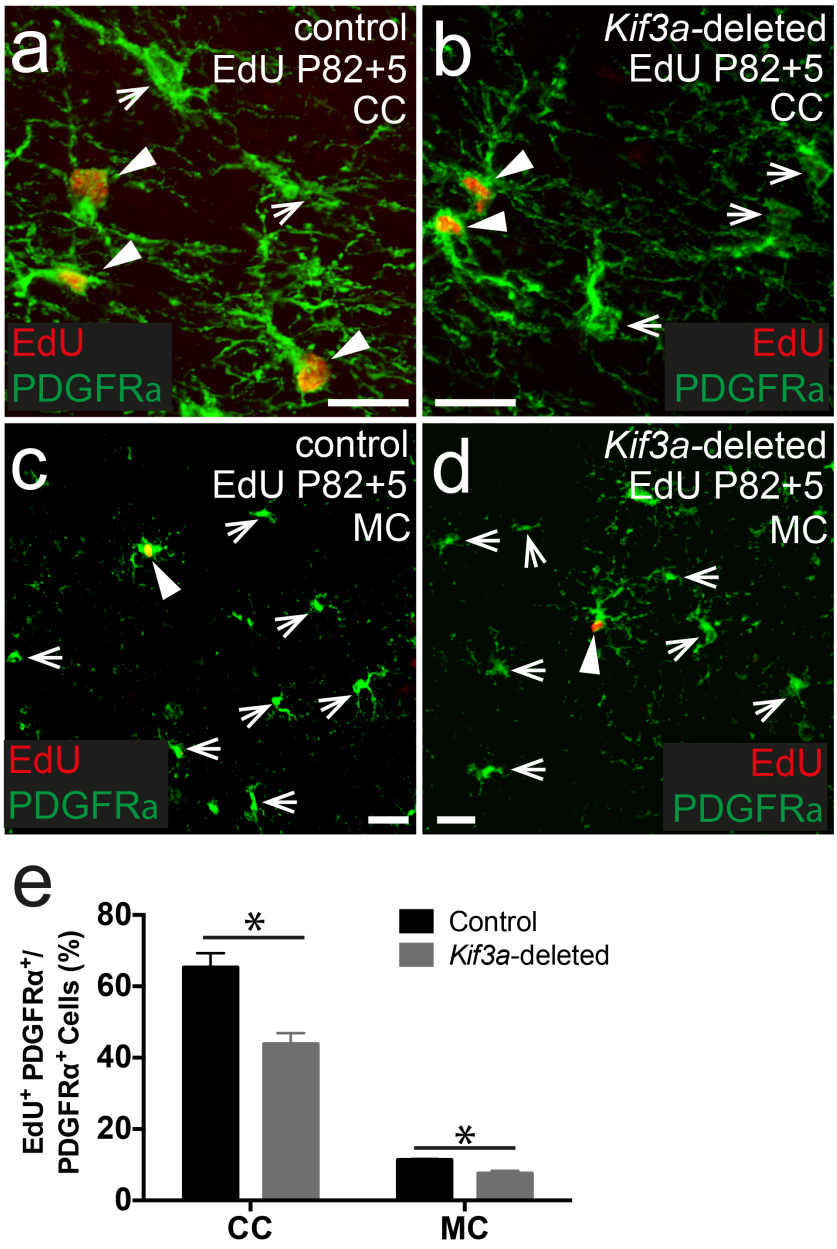

Figure 5.4: Deleting Kif3a from OPCs reduces proliferation in vivo
*Confocal image (single z-plane) of the CC of Kif3a$^{fl/fl}$ (control) (**a**) and Pdgfrα-CreER^{T2} :: Kif3a$^{fl/fl}$ (Kif3a-deleted) mice (**b**) that received EdU via their drinking water from P57+25 to P57+30, immuno-stained to detect PDGFRα (green) and EdU (red). Confocal image (single z-plane) of the primary motor cortex (MC) of control (**a**) and Kif3a-deleted (**b**) mice, that received EdU via their drinking water from P57+25 to P57+30, immuno-stained to detect PDGFRα (green) and EdU (red). (**e**) Quantification of the proportion of EdU$^+$ PDGFRα$^+$ cells in the CC and MC of control and Kif3a-deleted mice (avg ± stdev, n=3 per group; p<0.002, two-way ANOVA with Bonferroni correction). Arrows represent PDGFRα$^+$ EdU-negative cells. Arrowheads indicate PDGFRα$^+$ EdU$^+$ cells. Scale bars = 30μm.*

5.2.5 *Kif3a*-deficient adult OPCs have a reduced capacity to generate new oligodendrocytes

As OPC proliferation was reduced in *Kif3a*-deleted mice, it should follow that OPCs produce fewer new oligodendrocytes. To establish the rate at which newborn oligodendrocytes are added to the brain following the conditional deletion of *Kif3a* from OPCs, coronal brain cryosections from P57+7, 14 or 30 day control and *Kif3a*-deleted mice were processed to detect YFP (green), as well as the OPC marker, PDGFRα (red) and the nuclear stain Hoescht 33342 (blue). In control and *Kif3a*-deleted mice, >90% of OPCs in the CC and motor cortex at P57+7, P57+14 and P57+30 (n=3 per group, P=0.7, ANOVA with Bonferroni multiple comparisons test). However, the *Kif3a*-deleted OPCs generated half as many new oligodendrocytes (YFP^+, PDGFRα-negative) in the motor cortex and CC, when compared with controls, over time (**Fig. 5.5**). For example, at P57+14, ~30% of YFP^+ cells were PDGFRα-negative in the CC of control mice, compared with only ~15% in the same region of *Kif3a*-deleted mice (**Fig. 5.5 b, e, m**), suggesting that *Kif3a* deletion significantly impairs oligodendrogenesis. Similarly, in the motor cortex, where oligodendrogenesis occurs more slowly than the CC (Young et al., 2013), ~15% of the YFP^+ cells were oligodendrocytes in control mice, compared with only ~8% in *Kif3a*-deleted mice (**Fig. 5.5 h, k, n**). This relative reduction in oligodendrogenesis was also maintained at P57+30 in the CC (**Fig. 5.5 c, f, m**) and motor cortex (**Fig. 5.5 i, l, n**). The reduction in numbers of new oligodendrocytes was accompanied by a reduction in the density of newborn oligodendrocytes in both the CC and motor cortex at 7, 14 and 30 d (n=3 per group, P=0.03, two-way ANOVA with Bonferroni multiple comparisons test). These data suggest that mice in which OPCs can not assemble primary cilia, not only have a reduced rate of OPC proliferation, but ultimately have fewer new oligodendrocytes added to the brain.

5.2.6 Deleting *Kif3a* from OPCs decreases oligodendrogenesis, but has no short-term effect on gait parameters, grip strength or the optokinetic reflex of mice

Adult-born oligodendrocytes play a role in complex motor memory acquisition (McKenzie et al., 2014), but it has also been suggested that they could play an important role in maintaining CNS function (Birey et al., 2015; Schneider et al., 2016). As deleting *Kif3a* from OPCs ultimately leads to reduced oligodendrogenesis, it has the potential to impact normal CNS function. To examine the possibility, that the conditional deletion of *Kif3a* from OPCs would progressively impact motor performance, young adult control ($Kif3a^{fl/fl}$) and *Kif3a*-deleted ($Pdgfr\alpha\text{-}CreER^{T2}::Kif3a^{fl/fl}$) mice were subjected to a gait analysis (**Fig 5.6 a-h**), a grip strength assessment (**Fig 5.6 i**) and optomotor testing (**Fig 5.6 j**), prior to, and for up to 6

Figure 5.5: Deleting Kif3a from OPCs reduces oligodendrogenesis in vivo
*Confocal image of the CC of control (Pdgfrα-CreER^{T2} :: Rosa26-YFP) mice at P57+7 (**a**), P57+14 (**b**) and P57+30 (**c**), immuno-stained to detect YFP (green), PDGFRα (red) and HST (blue). Confocal image of the CC of Kif3a-deleted (Pdgfrα-CreER^{T2} :: Rosa26-YFP :: Kif3a$^{fl/fl}$) mice at P57+7 (**d**), P57+14 (**e**) and P57+30 (**f**), immuno-stained to detect YFP (green), PDGFRα (red) and HST (blue). Confocal image of the motor cortex of control P57+7 (**g**), P57+14 (**h**) and P57+30 (**i**) mice immuno-stained to detect YFP (green), PDGFRα (red) and HST (blue). Confocal image of the motor cortex of Kif3a-deleted P57+7 (**j**), P57+14 (**k**) and P57+30 (**l**) mice immuno-stained to detect YFP (green), PDGFRα (red) and HST (blue). (**m**) Quantification of the proportion of YFP$^+$ cells in the CC that have differentiated into oligodendrocytes. (**n**) Quantification of the proportion of YFP$^+$ cells in the motor cortex that have differentiated into oligodendrocytes. (avg ± stdev, n=3 per group; p<0.0014, two-way ANOVA with Bonferroni correction). Arrows indicate YFP$^+$ PDGFRα$^+$ cells. Arrowheads indicate YFP$^+$ PDGFRα-negative cells. Scale bars = 20μm (a-f) and 100 μm (g-l).*

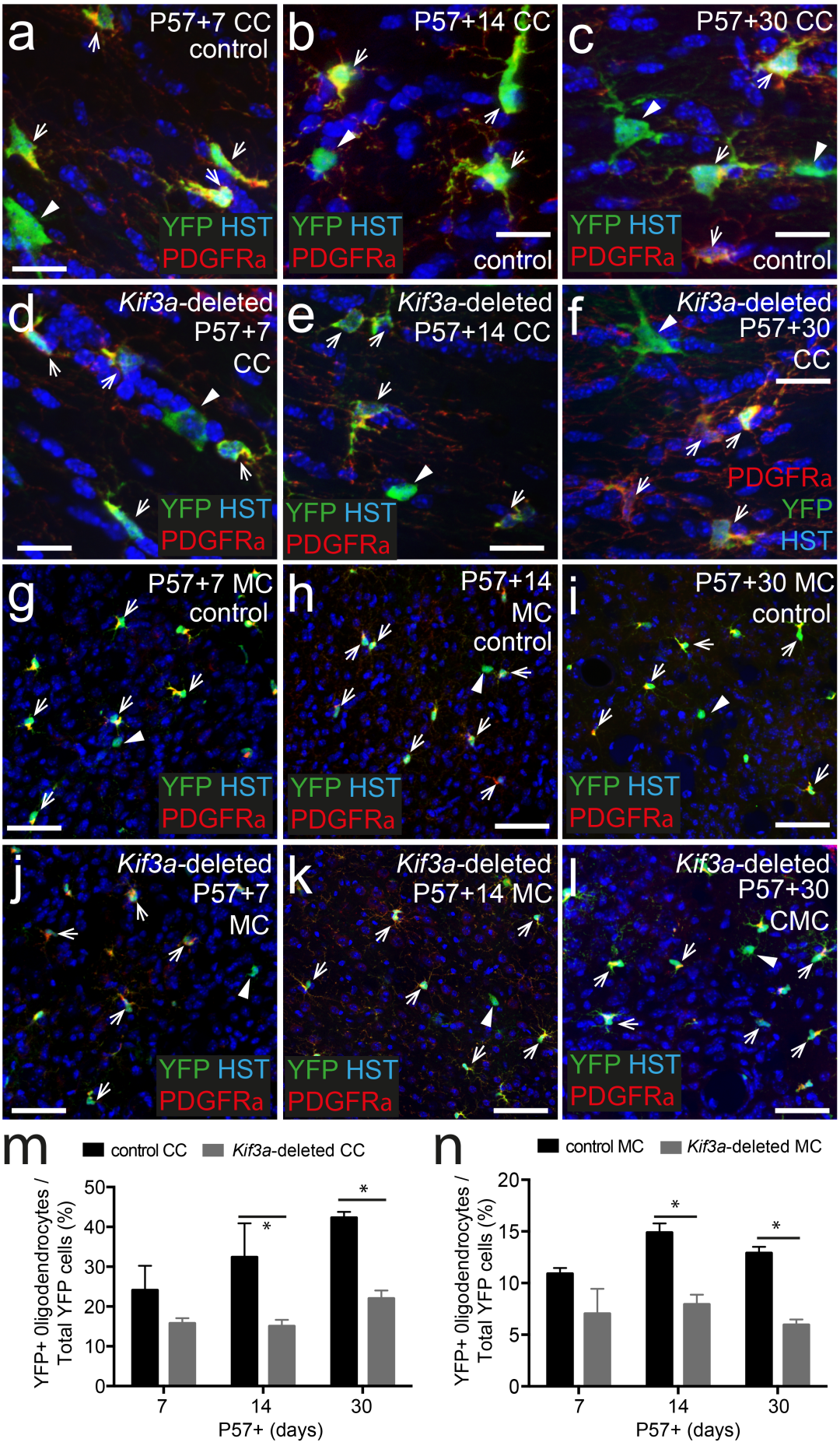
a
P57+7 CC control
YFP HST PDGFRa
b
P57+14 CC
YFP HST PDGFRa control
c
P57+30 CC
YFP HST PDGFRa control
d
Kif3a-deleted P57+7 CC
YFP HST PDGFRa
e
Kif3a-deleted P57+14 CC
YFP HST PDGFRa
f
Kif3a-deleted P57+30 CC
PDGFRa YFP HST
g
P57+7 MC control
YFP HST PDGFRa
h
P57+14 MC control
YFP HST PDGFRa
i
P57+30 MC control
YFP HST PDGFRa
j
Kif3a-deleted P57+7 MC
YFP HST PDGFRa
k
Kif3a-deleted P57+14 MC
YFP HST PDGFRa
l
Kif3a-deleted P57+30 CMC
YFP HST PDGFRa
m
control CC
Kif3a-deleted CC
YFP+ 0ligodendrocytes / Total YFP cells (%)
50
40
30
20
10
0
*
*
7
14
30
P57+ (days)
n
control MC
Kif3a-deleted MC
YFP+ 0ligodendrocytes / Total YFP cells (%)
20
15
10
5
0
*
*
7
14
30
P57+ (days)

Figure 5.6: Acutely reducing oligodendrogenesis does not affect motor or visual performance

*Control (Kif3a$^{fl/fl}$) and Kif3a-deleted (Pdgfrα-CreER^{T2} :: Kif3a$^{fl/fl}$) littermates were tested for gait, grip strength and optokinetic response prior to Tx administration (P57-2 days) and weekly from P57+7 to P57+43. (**a**) Posture plot of a mouse running at 26cm/s on a gradient of 3° showing the front right (RF), front left (LF), right hind (RH) and left hind (LH) limbs. (**b**) Quantification of the swing time of the front right (FR) limb of control and Kif3a-deleted mice over the testing period. Values recorded at 26cm/s and at a gradient of -3°. (**c**) Quantification of the stride time of the FR limb of control and Kif3a-deleted mice over the testing period. Values recorded at 26cm/s and at a gradient of -3°. (**d**) Stride frequency of the FR limb of control and Kif3a-deleted mice over the testing period. Values recorded at 26cm/s and at a gradient of -3°. (**e**) Quantification of the brake time of the FR limb of control and Kif3a-deleted mice over the testing period. Values recorded at 26cm/s and at a gradient of -3°. (**f**) Quantification of the stance time of the FR limb of control and Kif3a-deleted mice over the testing period. Values recorded at 26cm/s and at a gradient of -3°. (**g**) Quantification of the swing time of the front right (FR) limb of control and Kif3a-deleted mice over the testing period. Values recorded at 18cm/s, 22cm/s and 26cm/s and at a gradient of -3°. (**h**) Quantification of the swing time of the front right (FR) limb of control and Kif3a-deleted mice over the testing period. Values recorded at 26cm/s and at a gradient of 0°, -3° and 3°. (**i**) Quantification of the grip strength of the forelimbs and all four limbs of control and Kif3a-deleted mice over the testing period. Graph contains data pooled for both genders. (**j**) Quantification of head turns of control and Kif3a-deleted mice over the testing period during clockwise and anticlockwise drum rotation.*

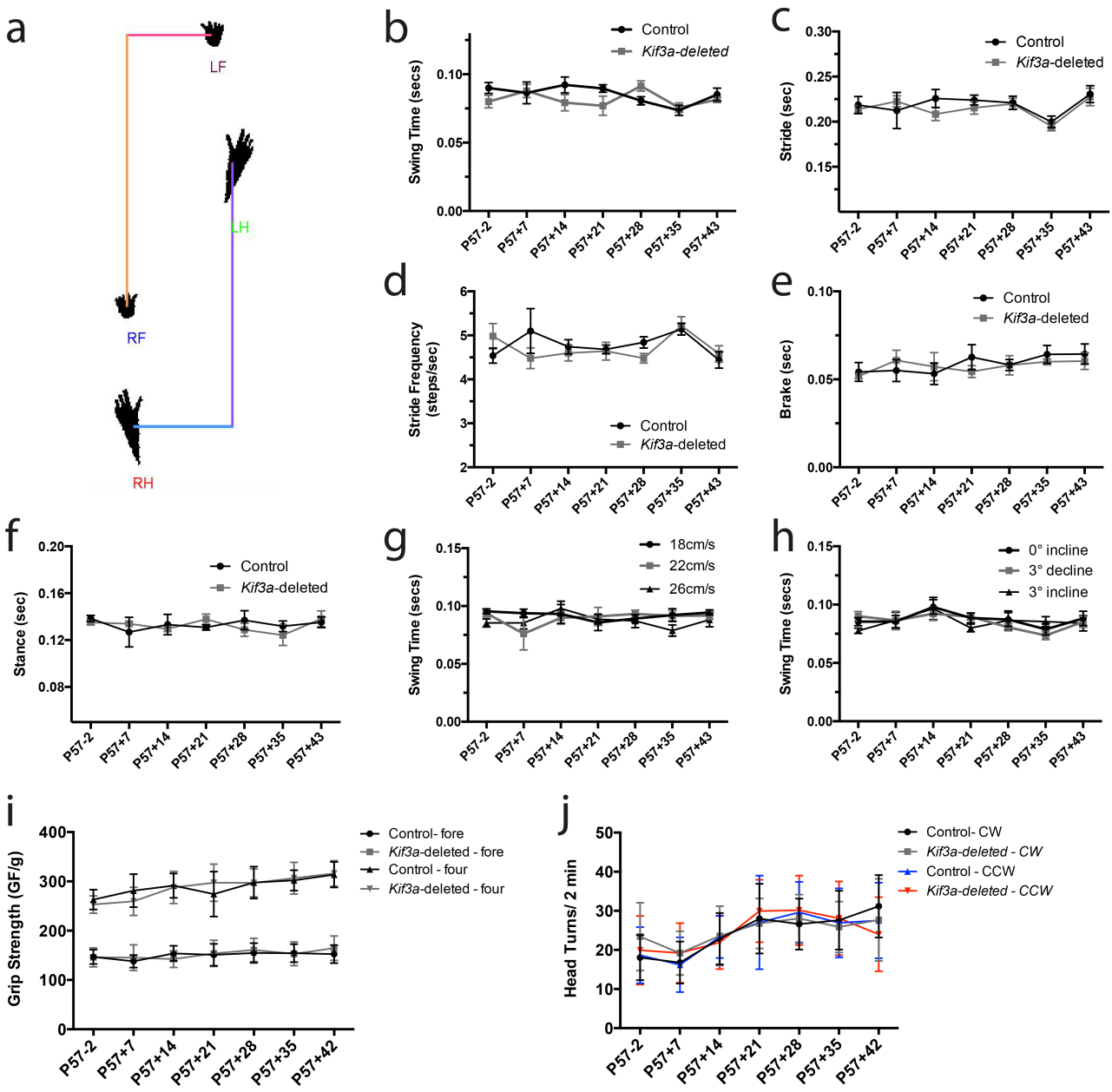
a
LF
LH
RF
RH
b
Swing Time (secs)
Control
Kif3a-deleted
c
Stride (sec)
d
Stride Frequency (steps/sec)
e
Brake (sec)
f
Stance (sec)
g
Swing Time (secs)
18cm/s
22cm/s
26cm/s
h
Swing Time (secs)
0° incline
3° decline
3° incline
i
Grip Strength (GF/g)
Control- fore
Kif3a-deleted - fore
Control - four
Kif3a-deleted - four
j
Head Turns/ 2 min
Control- CW
Kif3a-deleted - CW
Control - CCW
Kif3a-deleted - CCW
P57-2
P57+7
P57+14
P57+21
P57+28
P57+35
P57+43
P57+42

weeks after Tx administration. Prior to *Kif3a* deletion, the motor performance of each treatment group was equivalent (**Fig. 5.6**).

Many studies which have observed a decrease in myelin deposition have also observed accompanying changes in gait (Carson et al., 2015; LoPresti, 2015), additionally, increasing oligodendrocytes progenitor production has been shown to prevent gait changes which occur as a result of hypoxia-ischemia (Dizon et al., 2011). This suggests that OPC proliferation and myelination play an important role in normal CNS function and gait regulation. To examine gait, mice were placed on a Digigait^{TM} treadmill and video-recorded as they walked. 9 distinct movies were recorded per mouse, as they walked at 3 different speed settings (18, 22 and 26 cm/s), as some changes in gait are only evident at increased speeds (Crone et al., 2009). As incline has also been shown to aggravate gait changes in rodent models (Hampton et al., 2011), mice were also analyzed walking on a flat surface, on an incline and a decline (flat i.e. 0°, a 3° incline and a 3° decline), at each speed.

Each video was analyzed to quantify gait parameters, particularly stride time (the time taken to complete one stride), stride frequency (the average number of times a paw contacts the treadmill per second), swing time (the portion of the stride where the paw is moving forward but is not in contact with the treadmill), brake time (the time between initial paw contact with the belt and the maximal paw contact) and stance time (the portion of the stride in which the paw remains in contact with the belt). When control mice were running at 26cm/s, there was no significant difference identified in the stride time, stride frequency, swing time, brake time or stance time, measured at 0° +3° or -3° (n=6 per group, P=0.6, two-way ANOVA with Bonferroni multiple comparisons test). Similarly, at 26 cm/s there was no significant difference identified in the stride time, stride frequency, swing time, brake time or stance time of *Kif3a*-deleted mice walking at a 0° +3° or -3° (n=6 per group, P=0.5, two-way ANOVA with Bonferroni multiple comparisons test). These data suggest that altering the angle of running did not affect any of the parameters in either control or *Kif3a*-deleted animals.

Interestingly, when running on an incline of 0°, there was no significant difference in the stride time, swing time, brake time or stance time of control mice running at 18cm/s, 22 cm/s and 26cm/s speeds (n=6 per group, P>0.9, two-way ANOVA with Bonferroni multiple comparisons test) at any time over the testing period. However, a significant increase in stride frequency was detected with increasing running speed (n=6 per group, P=0.04, two-way ANOVA with Bonferroni multiple comparisons test), which would be expected, as a greater number of strides would be required to keep up with the accelerating treadmill. Larger changes in gait parameters in control mice would be expected with further

acceleration. Stride time, stride frequency, swing time, brake time and stance time, were not significantly different between control male and control female mice, when run at an incline of 0° at 18cm/s, 22cm/s or 26cm/s, at any testing period (n=3 per group, P=0.2, two-way ANOVA with Bonferroni multiple comparisons test). This was also the case for *Kif3a*-deleted mice (n=3 per group, P=0.1, two-way ANOVA with Bonferroni multiple comparisons test). As a result, male and female mice were pooled for Digigait^{TM} analysis, although there were equal numbers of male and female mice for each genotype.

When running at a 0° incline (i.e. flat) gait parameters including stride time, stride frequency, swing time, brake time and stance time did not differ between control and *Kif3a*-deleted mice over time, when mice were moving at 18, 22 or 26cm/s (n=6 per group, P>0.3, two-way ANOVA with Bonferroni multiple comparisons test). When running at -3° (**Fig. 5.6 b-f**) or +3°, there was similarly no effect of genotype or treatment time at 18, 22 or 26cm/s (+3°; n=6 per group, P>0.05, two-way ANOVA with Bonferroni multiple comparisons test). These data suggest that acutely reducing oligodendrogenesis, by deleting *Kif3a* from OPCs, does not result in a change in gait.

As a second measure of motor performance, the grip strength test was used to measure of both muscle strength and fine motor coordination (Deacon, 2013). Muscle strength is required to create the force necessary to pull back on the bars, but this is not possible without the fine motor coordination to grasp the bars. It would not be expected that the deletion of *Kif3a* exclusively from OPCs in the CNS would affect muscle mass, but it may affect the conduction velocity of CNS neurons which innervate the muscles responsible for grasping. Grip strength is affected in models of CNS demyelination such as EAE (Jones et al., 2008) suggesting that proper myelination is important for maintenance.

Grip strength was tested using a Chatillon grip strength meter. Mice were gently but firmly pulled along a metal grid allowing contact with either all four limbs or just the forelimbs. At each timepoint, grip strength was measured five times per mouse, and the maximum force measured was recorded and normalised to body weight [grams-force / gram body weight (GF/g)]. Grip strength differed significantly between male and female control mice, with males having a lower normalised forelimb grip strength (n=7 per group, p 0.0024, two-way ANOVA with Bonferroni multiple comparisons test) and overall normalised grip strength (n=7 per group, p 0.0002, two-way ANOVA with Bonferroni multiple comparisons test). Grip strength was consistent over time in the control group, with female mice maintaining a forelimb strength of ~6.5 GF/g and an overall grip strength of ~12 GF/g, and males maintaining a forelimb strength of ~6.0 GF/g and an overall grip strength of ~10 GF/g. This

pattern was also observed in the *Kif3a*-deleted group, with female and male measures of grip strength being equivalent to controls at each time-point (**Fig. 5.6 i,** n=7 per group, P>0.05, two-way ANOVA with Bonferroni multiple comparisons test). These data indicate that reducing oligodendrogenesis by deleting *Kif3a* does not impair fine motor performance or strength by P57+43 suggesting that acutely reducing adult oligodendrogenesis, is not sufficient to impair grip strength.

Demyelinating diseases which affect the optic nerve have been shown to result in visual impairment, including impairment in the optokinetic response in both rodents (Matsunaga et al., 2012) and humans (Raz et al., 2011). The optic nerve is a CNS region that is almost fully myelinated in adulthood, but continues to gain new myelinating oligodendrocytes throughout life (Young et al., 2013). This suggests that preventing oligodendrogenesis may affect myelin maintenance in the optic nerve, resulting in visual defects.

To test visual acuity, I measured the optomotor response of control and *Kif3a*-deleted mice. Each mouse was placed on a podium inside a rotating drum, that is patterned with black and white vertical stripes. If the mouse can see the drum rotate in a CW or CCW direction, it will move its head to follow the rotation, and then quickly return its head to the centre, before following the motion again (Abdeljalil et al., 2005). The number of optomotor head turns was counted over a 2 min period. Both control and *Kif3a*-deleted mice showed a gradual improvement in performance over time, with the number of head turns increasing in both the CW and CCW directions, between P57+7 and P57+21 (**Fig. 5.6 j**). However, there was no significant difference in performance, between control and *Kif3a*-deleted mice at any time-point examined (**Fig. 5.6**). There was also no difference in the performance of male and female mice (n=7 per group, P>0.05, two-way ANOVA with Bonferroni multiple comparisons test). These data suggest that deleting *Kif3a* from OPCs, and reducing oligodendrogenesis for 5 weeks, is insufficient to perturb CNS regulated motor and visual system function.

5.2.8 Deleting *Kif3a* from OPCs decreases oligodendrogenesis, but has no effect on short-term memory, anxiety or depression

Studies have shown that CNS myelination is important for the regulation of short-term memory, particularly working memory (Zhang et al., 2012; Kim et al., 2015). In a cuprizone model of demyelination, working memory is impaired, however, this can be reversed by treatment with Quetiapine, which stimulates oligodendrocyte production (Zhang et al., 2012). This suggests that oligodendrogenesis is important for repairing demyelination-induced deficits in short-term memory, and loss of oligodendrocyte production may affect short-term memory acquisition.

Short-term memory performance was assessed using the T-maze. The T-maze tests working memory, and was chosen due to the fact working memory has often shown to be affected in models of demyelination (Zhang et al., 2012; Kim et al., 2015). Individual control and *Kif3a*-deleted mice were placed in the start arm of the T-maze and allowed to move into the left or right arm, before being blocked in the chosen arm. When the mouse is returned to the start arm of the T-maze, in which all arms are open to it, its novelty-seeking nature, naturally inclines the mouse to choose and enter the unexplored or opposite arm of the maze (Deacon and Rawlins, 2006). This process is called spontaneous alternation. Each mouse was returned to the start arm and allowed to choose 10 times, and the number of errors in alternation was equivalent between the control and *Kif3a*-deleted mice. However, the error rate recorded for the control mice was unexpectedly high, with mice only alternating correctly ~50% of the time, which does not reflect any discrimination. Control mice would be expected to correctly spontaneously alternate >80% of the time (Deacon and Rawlins, 2006). Therefore, short-term memory was additionally examined using the novel object recognition test.

The novel object recognition test, is a two-day test that examines the ability of mice to recognise the difference between novel and familiar objects. On day 1, mice are placed in an arena containing two identical objects, and they are free to interact with those objects over a 10 min period. On day 2, they are returned to the arena, but one of the objects has been replaced with a new 'novel' object. A mouse with intact short-term memory will spend more time exploring the novel object (Taglialatela et al., 2009). Both control and *Kif3a*-deleted mice were able to recognise the novel object, and spent more time exploring the novel object relative to the familiar object (**Fig. 5.7 i, j, k**). Furthermore, the amount of time spent interacting with the novel object was equivalent between the control and *Kif3a*-deleted mice (**Fig. 5.7 i, j, k**), indicating that by P57+43, the conditional deletion of *Kif3a* from OPCs, had not affected short-term memory formation and retrieval.

Changes in myelin deposition are associated with an increased anxiety in humans and anxiety-like behaviour in rodents. Adolescent humans, with generalized anxiety, have white matter abnormalities that can be detected by DTI (Liao et al., 2014). Similarly, mice with reduced oligodendrogenesis, as a result of OPC ablation, show an increase in anxiety-like behaviour, when tested using the open-field test and elevated plus maze (Birey et al., 2015). By contrast, preventing oligodendrogenesis by deleting *Esco1* and preventing OPC proliferation, does not alter anxiety-like behaviour in the open field test (Schneider et al., 2016). In order to determine whether reducing oligodendrogenesis by deleting *Kif3a* affects anxiety-like behaviour, the performance of control and *Kif3a*-deleted mice was evaluated in

Figure 5.7: Reducing oligodendrogenesis by conditionally deleting Kif3a from OPCs does not alter short-term memory, anxiety or depressive behaviours

*Control (Kif3a$^{fl/fl}$) and Kif3a-deleted (Pdgfrα-CreER^{T2} :: Kif3a$^{fl/fl}$) littermates received Tx at P57, and underwent cognitive testing from P57+36 to P57+43. Representative elevated plus maze (EPM) tracks from control (**a**) and Kif3a-deleted (**b**) mice. (**c**) Quantification of the proportion of time spent in the open arms of the EPM by control and Kif3a-deleted mice (avg ± stdev, n=15 per group; p>0.05, t-test). Representative open field (OF) tracks from control (**d**) and Kif3a-deleted (**e**) mice. (**f**) Quantification of the proportion of time spent in the centre zone of the OF arena by control and Kif3a-deleted mice (avg ± stdev, n=15 per group; p>0.05, t-test). (**g**) Quantification of the proportion of marbles buried by control and Kif3a-deleted mice in the marble bury test (avg ± stdev, n=15 per group; p>0.05, t-test). (**h**) Quantification of the proportion of time spent actively swimming, passively swimming and floating by control and Kif3a-deleted^{l} mice in the forces swim test (avg ± stdev, n=15 per group; p>0.05, t-test). Representative novel object recognition (NOR) heat maps from control (**i**) and Kif3a-deleted (**j**) mice. (**k**) Percentage of time spent interacting with the novel object on day 2 of the NOR test by control and Kifa-deleted mice (avg ± stdev, n=15 per group; p>0.05, t-test).*

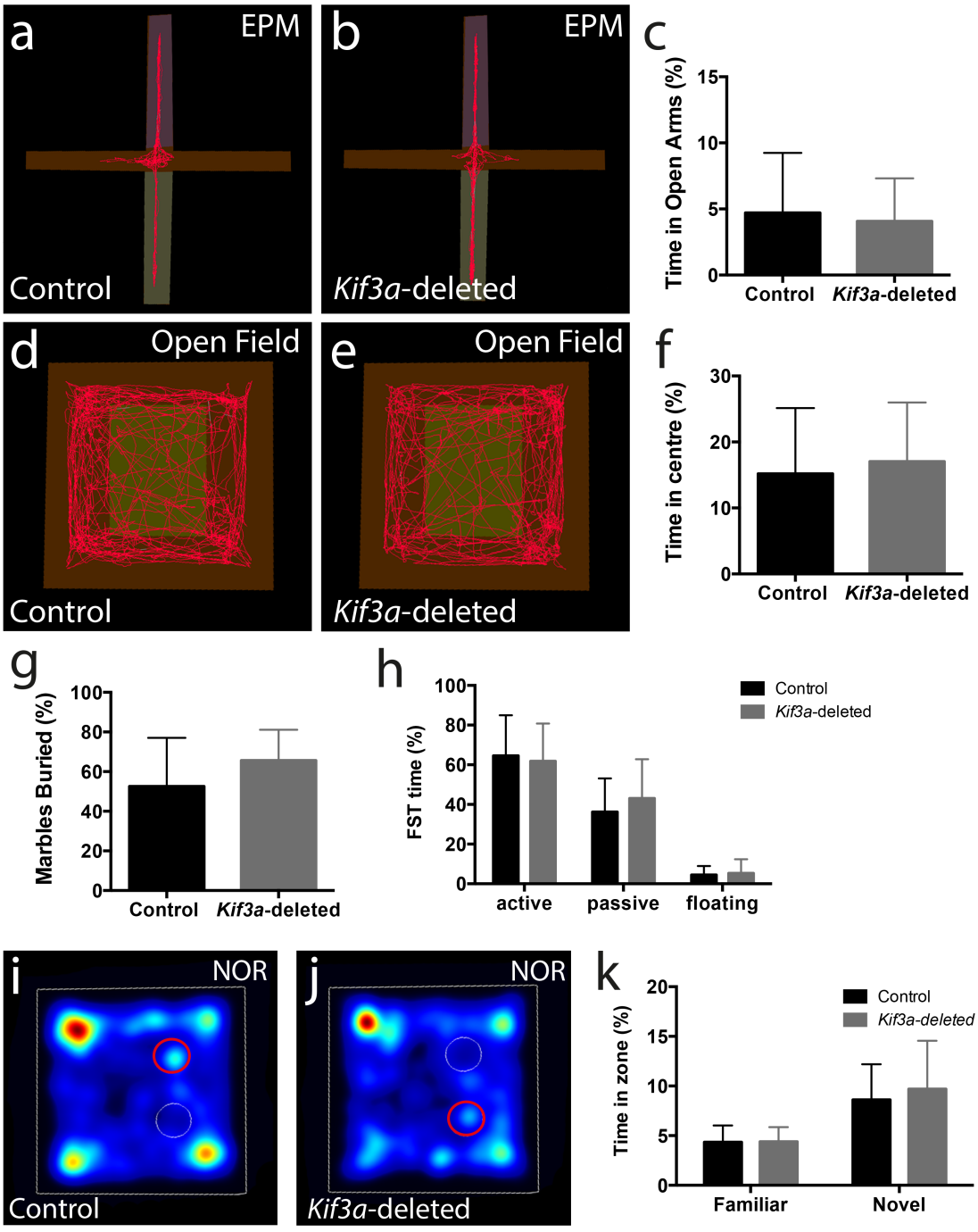
a
EPM
Control
b
EPM
Kif3a-deleted
c
Time in Open Arms (%)
15
10
5
0
Control
Kif3a-deleted
d
Open Field
Control
e
Open Field
Kif3a-deleted
f
Time in centre (%)
30
20
10
0
Control
Kif3a-deleted
g
Marbles Buried (%)
100
80
60
40
20
0
Control
Kif3a-deleted
h
FST time (%)
100
80
60
40
20
0
active
passive
floating
Control
Kif3a-deleted
i
NOR
Control
j
NOR
Kif3a-deleted
k
Time in zone (%)
20
15
10
5
0
Familiar
Novel
Control
Kif3a-deleted

the elevated plus maze, open field and marble bury tests. The elevated plus maze comprises two enclosed and two open arms raised off the ground. Each mouse is placed in the centre, and allowed to explore for five mins, and the proportion of time spent in the open and closed arms calculated. An uninhibited, less anxious mouse (increased risk-taking behaviour) will spend more time in the open arms (Walf and Frye, 2005). Mice in the control and *Kif3a*-deleted groups spent the majority of their time in the closed arms, only spending ~5% of their time in the open arms of the maze (**Fig. 5.7 a-c**). Very few mice (2 of 30, one each of *Kif3a*-deleted and control) ventured to the end of the open arm suggesting that inhibiting oligodendrogenesis by deleting *Kif3a* does not result in altered risk taking behaviour.

During the open field test, mice were placed in a 30cm x 30cm box with a brightly lit centre and shadowed edges, and allowed to explore for 5 min. Mice with heightened anxiety-like behaviour spend less time in the centre and more time at the perimeter, while mice with reduced anxiety-like behaviour explore the centre more often. Across the 5 min period, control and *Kif3a*-deleted mice behaved similarly (**Fig. 5.7 d-f**), with mice in both groups favouring the perimeter but spending ~15% of the time exploring the central zone of the box. This suggests that the conditional deletion of *Kif3a* from OPCs does not produce an anxiety-like phenotype.

Next, each control and *Kif3a*-deleted mouse was placed in a box containing 5cm deep substrate and ten marbles. The more marbles they bury over a 30 min period, the greater their anxiety-like phenotype (Deacon and Rawlins, 2005; Angoa-Pérez et al., 2013). All control and *Kif3a*-deleted mice tested buried some of the marbles, and when the number buried was quantified, there was no significant difference between genotypes (**Fig. 5.7 g**), supporting our conclusions from the previous two tests, that deleting *Kif3a* from OPCs has no effect on anxiety-like behaviour.

Preventing oligodendrogenesis during neonatal development has previously been shown to result in an increase in anxiety-like behaviour in mice (Chen et al., 2015). Additionally, mood-associated disorders, such as anxiety (Liao et al., 2014) and depression (Regenold et al., 2007; Williams et al., 2015) have been linked with abnormal myelin deposition in humans. This suggests that oligodendrogenesis, and its role in adult myelination, may be important for mood regulation in anxiety-like and depressive behaviours. To examine the possibility that *Kif3a* deletion from OPCs and the resulting reduction in oligodendrogenesis, leads to a change in depressive behaviour, control and *Kif3a*-deleted mice undertook a forced swim test. Each mouse was placed in a beaker, containing 15cm deep water, and

they were forced to swim for 5 min. The amount of time spent in active swimming and passive floating was recorded, as mice in a state of elevated depression will commit the minimal effort required to stay afloat (Can et al., 2012). The amount of time that mice in the control and *Kif3a*-deleted groups spent passively swimming or floating was equivalent, at ~5% (**Fig. 5.7 h**). These data indicate that preventing OPC proliferation and effectively halving oligodendrogenesis over a 6 week period, does not influence depressive behaviour in mice.

The data in this chapter indicate that OPCs in the adult mouse brain assemble primary cilia, but mature oligodendrocytes do not, indicating a regulatory role of the primary cilium on OPCs, which is not necessary in mature, myelinating oligodendrocytes. Additionally, the primary cilium is not assembled on OPCs that are actively dividing, suggesting that it is disassembled as they enter the cell cycle and assembled again after cell-cycle exit. Preventing primary cilium assembly in OPCs, by deleting *Kif3a*, results in reduced OPC proliferation in addition to reduced oligodendrogenesis. This acute reduction in oligodendrogenesis is not sufficient to affect gait, grip strength or optokinetic response and does not affect short-term memory, anxiety or depressive behaviours by P57+43. This suggests the reduction in oligodendrogenesis does not affect CNS function in the short-term.

5.3 Discussion

5.3.1 Primary cilia regulate OPC proliferation *in vivo*

Essentially all OPCs have assembled primary cilia on their surface, with the exception of OPCs that are transitioning through the cell cycle. This conclusion is supported by a number of observations: (i) that ~7% of Sox10-GFP$^+$ cells in the CC of adult mice have an assembled Arl13b$^+$ primary cilia extending from a γ–tubulin$^+$ basal body, a proportion similar to the fraction of Sox10-GFP$^+$ cells that would be PDGFRα$^+$ OPCs (Rivers et al., 2008); (ii) that ~75% of PDGFRα$^+$ OPCs in the CC of adult mice have assembled primary cilia at any one time, and (iii) that OPCs acutely labelled with EdU *in vivo*, identifying them as cells that have entered or have very recently exited s-phase of the cell cycle, do not have assembled primary cilia. These data are further supported by the time-lapse imaging data, presented in Chapter 3, that demonstrate the disassembly of primary cilia by OPCs *in vitro*, as they enter the cell cycle.

As the primary cilium is associated with a number of signalling pathways that influence cell proliferation (reviewed in Michaud and Yoder, 2006), it is perhaps unsurprising that a primary cilium is assembled on the surface of immature OPCs. In many cell types, including

proliferative HEK cells, the primary cilium is maintained on the surface of the cell and disassembled before a cell division occurs (Paridaen et al., 2013). Once the cilium has been disassembled the centrosomes migrate away from the cell surface and organise the mitotic spindle during division, before being trafficked back to the cell surface for primary cilium assembly once division is complete. As the primary cilium plays two major roles in the regulation of cell division: (i) it receives proliferative signals that tell the cell to divide, and (ii) it stops uncontrolled cell division by preventing mitosis when assembled, preventing cilium assembly can either reduce proliferation, due to the loss of proliferative signals such as Shh (Han et al., 2008; Spassky et al., 2008; Temiyasathit et al., 2012; Tong et al., 2014), or it can increase proliferation as cell-cycle re-entry is no longer regulated by the cilium (Lin et al., 2003; Hoang-Minh et al., 2016).

The *Kif3a*$^{fl/fl}$ mouse model has previously been used *in vivo* to knock down cilia assembly in cells in the embryonic mouse heart (Slough et al., 2008) and the developing and adult kidney (Ma et al., 2013). Progenitor cell types in the CNS, have also previously been targeted, including cerebellar granule cells (Spassky et al., 2008), neural progenitors in the developing dentate gyrus (Han et al., 2008) and B1 neural progenitors in the adult ventral SVZ (Tong et al., 2014). The conditional deletion of *Kif3a* from the DNA of OPCs in adult mice, resulted in fewer OPCs having assembled primary cilia in the CC from as early as P57+7 and this phenotype was still evident at P57+30. By P57+25, the loss of primary cilia assembly in *Kif3a*-deleted mice was clearly accompanied by a decrease in the number of OPCs that incorporated EdU, relative to control mice. This could be the result of OPCs dividing more slowly in the CC and motor cortex of *Kif3a*-deleted mice, or could be the result of OPCs failing to enter the cell cycle. Therefore, the predominant effect of preventing primary cilium assembly by OPCs *in vitro* and *in vivo*, is impaired proliferation, suggesting that the primary cilium plays a critical role in driving cell division by OPCs.

A number of signalling pathways localize to the primary cilium (reviewed in Michaud and Yoder, 2006) that are known to regulate OPC proliferation. For example, *in vitro*, OPCs express genes associated with Shh signalling (Chapter 3), which has been shown to be important for OPC generation during embryonic development (Tekki-Kessaris et al., 2001), and to regulate OPC proliferation *in vivo* (Ferent et al., 2013) and *in vitro* (Ortega et al., 2013). Shh signalling is also reliant on the primary cilium in vertebrates (reviewed in Goetz and Anderson, 2010). Alternative signalling pathways that could influence OPC proliferation via the primary cilium, include Wnt and PDGFRα. Wnt signalling can occur at the primary cilium of other cell types (Gerdes and Katsanis, 2008) and has been shown to promote OPC migration, have no effect on proliferation, and discourage oligodendrogenesis (Fancy et al.,

2009; 2011; 2014; Tsai et al., 2016). As my data suggest that signaling at the primary cilium increases OPC proliferation and promotes oligodendrogenesis, it is unlikely that disrupted Wnt signaling can account for the phenotype. PDGF-AA binding to PDGFRα is critical for OPC survival and an important regulator of OPC proliferation (Espinosa-Jeffrey et al., 2009) (reviewed in Grade et al., 2013). PDGFRα has also been shown to accumulate at the primary cilium in NIH3T3 fibroblasts in response to serum starvation, increasing the receptor density and suggesting that the primary cilium can be utilized to make PDGFRα signalling more efficient (Schneider et al., 2005). It is unlikely, however, that PDGFRα signalling in OPCs would be affected by the loss of the primary cilium due to the fact the extensive expression of PDGFRα on the cell surface of the OPC would likely compensate for its loss – unless the signal mediated at the cilium is distinct from that transduced elsewhere on the cell surface.

5.3.2 Primary cilia are not associated with differentiated oligodendrocytes

Unlike OPCs, mature oligodendrocytes do not have assembled primary cilia on their surface. The vast majority of Sox10-GFP$^+$ cells are mature oligodendrocytes, yet only 7% had assembled primary cilia. The idea that oligodendrocytes do not have assembled primary cilia is also supported by the fraction of YFP$^+$ cells with assembled primary cilia decreasing with increasing time from Tx administration, in *Pdgfrα-CreER^{T2}::Rosa26YFP* transgenic mice. At P57+7, when the majority of YFP$^+$ cells are OPCs (O'Rourke et al., 2016), ~75% of YFP$^+$ cells had assembled primary cilia, but this fraction reduced over time to only ~50% of YFP$^+$ cells by P57+30. The number of YFP$^+$ cells with assembled primary cilia decreases as the number of YFP$^+$ oligodendrocytes increases. Furthermore, ~98% of YFP$^+$ oligodendrocytes labelled in the CC of *Plp-CreER^{T2}::Rosa26-YFP* transgenic mice are not ciliated. Why a small fraction of YFP$^+$ oligodendrocytes might have primary cilia is unclear, but it is possible that the YFP$^+$ ciliated cells are newly differentiated oligodendrocytes, that had upregulated *plp* mRNA expression at the time of Tx administration, and are in the process of disassembling their primary cilia for differentiation, and correspond to the small population of premyelinating, immature oligodendrocytes (sometimes called ENPP6 cells; (Xiao et al., 2016) that can be found throughout the CNS at any given time (Trapp et al., 1997).

Cells of the oligodendrocyte lineage are not the only neural cells that appear to have cilia assembled on the surface of the immature cells, but disassembled during differentiation. Schwann cells are the myelinating cells of the peripheral nervous system. In mouse dorsal root ganglion neuron and Schwann cell co-cultures, a high proportion of the proliferative pre-myelinating Schwann cells have assembled primary cilia, but primary cilia are rarely

detected on the mature myelinating Schwann cells (Yoshimura and Takeda, 2012). As myelinating Schwann cells and oligodendrocytes are postmitotic cells, the primary cilium may be disassembled as this type of signalling is no longer required. It is certainly not uncommon for cells to lose their capacity to assemble primary cilia as they differentiate from a proliferative progenitor cell type to a post-mitotic cell type, and many post mitotic cells lose their basal bodies after differentiation (Cunha-Ferreira et al., 2009; Debec et al., 2010). This is not always the case, as some differentiated cell types, including neurons and astrocytes, have assembled primary cilia (Arellano et al., 2012; Kasahara et al., 2014). However, my data indicate this is a feature common to both post-mitotic, myelinating cell types.

5.3.3 Deleting *Kif3a* from OPCs reduces oligodendrogenesis, but does not affect motor function, anxiety or depressive behaviour

OPCs continually proliferate and differentiate into oligodendrocytes throughout life (Rivers et al., 2008). A reduction in oligodendrogenesis was observed in *Kif3a*-deleted mice from P57+14, in both the CC and motor cortex. In the CC and motor cortex, the percentage of OPCs that had differentiated was halved from control to *Kif3a*-deleted mice at P57+14 and P57+30. Furthermore, *Kif3a* is not involved in primary cilia disassembly, its absence from OPCs is unlikely to affect the capacity of an OPC to directly differentiate into an oligodendrocyte, or the capacity of an OPC exiting the cell cycle from initiating differentiation. As the overall density of OPCs was also unaffected by *Kif3a*-deletion, depletion of the progenitor pool was not a factor contributing to reduced oligodendrogenesis. However, a loss of signaling at the primary cilium may play a direct role, as blocking Shh signalling *in vitro*, by treating differentiating rat primary OPC cultures with the Smo inhibitor cyclopamine, impairs their differentiation and decreases branching complexity (Falcón-Urrutia et al., 2015), indicating that Shh signalling at the primary cilium could also drive oligodendrocyte differentiation.

The specificity of the transgenic mouse line used has been extensively characterised by the experiments performed in chapter 4 (O'Rourke et al., 2016) and has been found to be highly effective and specific, targeting >95% of OPCs in all CNS tissues. The deletion of Kif3a was targeted OPCs throughout the whole CNS, it can therefore be expected that the deletion of Kif3a would result in a system wide reduction in OPC proliferation and oligodendrogenesis, affecting brain regions responsible for motor performance and vision, but also those involved in cognition, anxiety, and depression. OPCs throughout the CNS proliferate and differentiate. The rate of OPC proliferation differs between different CNS regions, at P60 complete turnover of the OPC population in both the CC and the spinal white matter taking less than 10 days, around 20 days in the optic nerve and around 30 days in the spinal grey

matter and motor cortex (Young et al., 2013). The rate of oligodendrogenesis is also variable throughout the CNS, but new oligodendrocytes are continuously being born and myelinating, even in regions that already have high levels of myelination such as the optic nerve (Young et al., 2013). While not all brain regions have been specifically quantified it would be expected that OPCs in these regions would behave in the same manner as the rest of the CNS, undergoing continuous proliferation and differentiation. It would also be expected that they would rely on the same proliferative signals, and would respond to deletion of Kif3a in the same manner.

An area of significant interest in the myelin biology field at present, is understanding the purpose of adult oligodendrogenesis (Waly et al., 2014; Wang and Young, 2014). Herein, I demonstrate that acutely reducing OPC proliferation and oligodendrogenesis, by conditionally deleting *Kif3a* from adult OPCs in mice, did not affect motor function, as assessed by grip strength and gait analysis. By contrast, reducing oligodendrogenesis by selectively deleting the cell cycle regulator, *Esco2*, from all cells of the oligodendrocyte lineage in adult mice, induced cell death in proliferating OPCs (Schneider et al., 2016). Oligodendrogenesis was also affected, being reduced to ~30% over an 8 week period (Schneider et al., 2016). Within just 4 weeks, the performance of *Esco2*-deleted mice was impaired in the balance beam test, and by 6 weeks, in the grid walk test (Schneider et al., 2016). By contrast, preventing oligodendrogenesis, by deleting *Myrf,* a transcription factor necessary for the initiation and regulation of new myelin production, had no effect on rotarod performance by 1 month post gene-deletion (McKenzie et al., 2014). The rotarod and balance beam / grid walk tests all measure balance and motor coordination. While some motor-impaired mouse strains have been shown to perform better on static balance tests, like the balance beam, while others have been shown to perform better on moving substrates, such as the rotorod (reviewed in Deacon, 2013), it is more likely that this discrepancy can be explained by having a greater understanding of the contribution of OPCs versus newborn oligodendrocytes to motor performance maintenance. Schneider et al. (2016) demonstrated ~2/3 reduction in oligodendrogenesis when deleting *Esco2,* deletion of *Kif3a* reduced oligodendrogenesis by ~1/2. Although the reduction in oligodendrogenesis observed in my study was smaller, the difference is too small to explain such a large discrepancy in motor phenotypes. It would be valuable to extend the period of analysis to determine whether sustained Kif3a-deletion could produce a motor deficit.

In addition to examining motor performance, I examined the importance of oligodendrogenesis in mood regulation, particularly anxiety and depression. I determined that conditionally deleting *Kif3a* from OPCs did not influence anxiety over a 6 week period,

when assessed by the elevated-plus maze, the open field test and the marble bury test. These data are consistent with the phenotype produced by conditionally deleting *Esco2* from OPCs in adult mice, which did not affect their performance in the open field test over a 14 week period (Schneider et al., 2016). By contrast, reducing oligodendrogenesis by selectively expressing *iDTR*, the diphtheria toxin receptor, in adult $NG2^+$ cells, and ablating them by administering the diphtheria toxin A-chain, reduced the amount of time mice spent exploring the centre of the open field arena and reduced the amount of time mice spent in the open arms of the elevated plus maze, after only 7 days – suggesting that the ablation of OPCs can dramatically and rapidly produce an anxiety phenotype (Birey et al., 2015). This may not be the result of compromised oligodendrogenesis, but perhaps mediated by the loss of an alternative OPC function, or, for example, microglial activation in response to OPC death.

Similarly, 6 weeks after *Kif3a* deletion, control and *Kif3a*-deleted mice performed similarly in the forced swim test, indicating that they did not display depressive behaviour. However, just 7 days of NG2-cell ablation was sufficient to impair performance in the sucrose preference test, which is an alternative measure of depressive state, and 9 days was sufficient to detect a decrease in social interaction (Birey et al., 2015). In comparison to the *iDTR* approach, *Esco2* and *Kif3a* gene deletion remove fewer OPCs from the CNS, suggesting that OPCs may play an important role in mood regulation, which is distinct from their role in oligodendrogenesis.

Chapter 6: Discussion and future directions

Data presented in this thesis indicate that a subpopulation of OPCs have primary cilia assembled on their surface at any one time. This is because primary cilia disassemble just prior to cell cycle entry, and reassemble upon cell cycle exit. Furthermore, primary cilia play a critical role in regulating OPC proliferation and oligodendrogenesis, such that preventing primary cilia assembly provides a means to further probe OPC biology, and gain critical insight into the biological functions enabled by adult oligodendrogenesis.

In Chapter 3, I was able to visualize primary cilia assembly and disassembly by cultured OPCs. It would be interesting to extend this study, not only to collect additional movies and perform a more detailed analysis of this phenomenon, but also to extend the imaging period. It would be informative to show that the second daughter cell does assemble a basal body and primary cilium given more time, and to visualize asymmetric and symmetric divisions, to confirm that OPCs destined to differentiate upon cell cycle entry, never reassemble a primary cilium. Furthermore, while I was able to demonstrate that primary cilia are critical for OPC proliferation *in vitro*, it would be interesting to determine how influential Shh signaling is at the primary cilium at different stages of the cell cycle, and at different stages of differentiation. OPCs produce Shh (Ferent et al., 2013; Zhang et al., 2014), and Shh signaling regulates oligodendrogenesis (Wang and Almazan, 2016; Sanchez and Armstrong, 2018) - now *Kif3a*-deletion and primary cilia ablation provides a means to further interrogate the importance of the primary cilia for Shh regulation of cells in this lineage.

While it is well established that OPCs reside throughout the adult CNS, and continuously divide and differentiate to produce new oligodendrocytes (reviewed in Richardson et al., 2011). The potential function of adult oligodendrogenesis has been much debated. In humans, learning complex motor tasks, such as juggling (Scholz et al., 2009) or playing a musical instrument (Lee et al., 2003), is associated with changes in imaging parameters, that suggest myelin deposition is increased in the brain regions activated by the task. While this may be the result of increased oligodendrogenesis, the scale of continued oligodendrocyte generation in the human brain (Yeung et al., 2014) seems too small to account for a role in life-long learning.

In Chapter 4, I determined that *Pdgfrα-CreER*^{T2} transgenic mice efficiently target DNA recombination to OPCs in the CNS. However, these mice also induce a low level of specific and non-specific DNA recombination in cells in other tissues and organs (O'Rourke et al., 2016). While many of these cells would also have primary cilia, and similarly experience

Kif3a-deletion in *Pdgfrα-CreER*^{T2}*::Kif3a*$^{fl/fl}$ transgenic mice, I would not expect *Kif3a* deletion, in a very small subset of any single peripheral cell population, to affect motor, cognitive or mood measures, making these mice largely suitable to assess the behavioral consequences of Kif3a deletion in OPCs. However, *Pdgfrα-CreER*^{T2} transgenic mice did achieve highly specific DNA recombination in a subset of PDGFRα^{+} stromal cells in the bone marrow, and it would be interesting to carry out a histological examination of these cells to determine whether they have assemble primary cilia that are also lost in *Pdgfrα-CreER*^{T2}*::Kif3a*$^{fl/fl}$ transgenic mice.

In Chapter 5, I determined that the deletion of *Kif3a* from OPCs in vivo impaired OPC proliferation and approximately halved adult oligodendrogenesis. There have been a number of studies in recent years, which have taken different genetic approaches to either remove OPCs from the mature CNS or decrease oligodendrogenesis, in order to understand its function. Consequently, we now know that oligodendrogenesis is an important regulator of complex motor learning in mice (McKenzie et al., 2014). In the short-term, preventing oligodendrogenesis, by deleting *Myrf* from OPCs does not affect motor performance as assessed by the rotor rod test, but does delay motor skill acquisition, with both their maximum and average speeds being significantly decreased on the complex running wheel (McKenzie et al., 2014). However, *Myrf*-deletion after learning did not affect memory retrieval (McKenzie et al., 2014). In this study, oligodendrogenesis in *Myrf*-deleted animals was ~10% that of controls, which is significantly greater reduction than then ~50% reduction in the *Kif3a*-deleted mice. While the phenotype may not be as robust, it would be interesting to determine whether a 50% reduction in oligodendrogenesis is sufficient to produce complex learning deficits.

While the role of oligodendrogenesis had already been examined for complex learning, a role in short-term formation or working memory had not been, despite the fact that demyelination has been shown to be associated with reductions in short-term memory, particularly working memory (Zhang et al., 2012; Kim et al., 2015). I assessed the short-term and working memory performance of control and *Kif3a*-deleted mice in the T-maze, and the novel object recognition test and found no significant difference in the performance of control and *Kif3a*-deleted animals within 6 weeks of gene deletion. While these data suggest that oligodendrogenesis is not important for short-term and working memory, these experiments are far from conclusive. Perhaps a 50% decrease in oligodendrogenesis is not sufficient to produce a phenotype, or perhaps oligodendrogenesis would need to be blocked for a longer period of time, to ensure the depletion of the pool of immature oligodendrocytes,

that can be rapidly mobilized during learning (Sampaio-Baptista et al., 2013; McKenzie et al., 2014).

Recent studies have shown that the addition of new oligodendrocytes is important for normal motor function (Birey et al., 2015; Schneider et al., 2016). If adult-born oligodendrocytes play a role in replacing damaged or dying oligodendrocytes (Wang and Young, 2014). While I detected no change in motor and optomotor performance by P57+43 in *Kif3a*-deleted mice, this is a phenotype that would be predicted to develop slowly and over an extended period of time. Therefore, this study is still ongoing to determine whether sustained blockade of oligodendrogenesis can eventually lead to a motor degenerative phenotype.

Preventing oligodendrogenesis has also been shown to alter anxiety-like behaviour (Birey et al., 2015). In addition to motor and cognitive phenotypes, people with MS often have comorbid depression and unstable moods (Seyed Saadat et al., 2014). Recent studies have also shown an association between changes in white matter and an alteration in anxiety or depressive state. Transcriptional profiling of patients diagnosed with major depressive disorder indicated dysregulation of a number of oligodendroglial-associated genes (Aston et al., 2005). Additionally an increase in deep white matter lesions are detected in people with unipolar and bipolar depression (Regenold et al., 2007). Adolescents with generalized anxiety have also been shown to have white matter abnormalities by DTI (Liao et al., 2014). While I observed no change in anxiety or depressive state in my acute study, the strong evidence linking myelin loss with changes in anxiety and depressive state, suggests this may develop with sustained *Kif3a*-deletion.

By demonstrating that primary cilia are present on the surface of OPCs but absent from mature, myelinating oligodendrocytes and preventing cilium assembly reduces both OPC proliferation and oligodendrogenesis, this thesis improves our understanding of the relationship between the primary cilium and the oligodendrocyte lineage. I also determined that preventing cilium assembly and reducing oligodendrogenesis did not affect normal CNS function by 7 weeks post gene-deletion. However, further studies are required to elucidate the exact signalling pathways that rely upon the primary cilium in OPCs, and to observe the effect of *Kif3a*-deletion and reduced oligodendrogenesis over the longer term.

Appendix 1: Solutions

Common Laboratory Reagents

0.01M Phosphate Buffered Saline (PBS)

MilliQ water	850ml
90.0g/L Sodium chloride	100ml
28.0g/L Di-sodium hydrogen orthophosphate	40ml
31.2g/L Sodium di-hydrogen orthophosphate	10ml

Blocking Solution for Immunohistochemistry and Immunocytochemistry

FCS	1ml
Triton-x100	10µl
PBS	top up to 10ml

Solutions for DNA Extraction

DNA Extraction Buffer

1M Tris-HCL (pH8.5)	12ml
0.5M EDTA (pH8.0)	1.2ml
5M NaCl	4.8ml
10% SDS	0.2%

Note: Autoclave before adding SDS

Culture media

OPC complete cell culture media (50mL)

	Add	Final Conc.
DMEM	42ml	-
PDGFR-AA	20µl	20ng/ml
bFGF	5µl	10ng/ml
CNTF	25µl	10ng/ml
NAC	50µl	5µg/ml
NT3	5µl	1ng/ml
Biotin	10µl	1ng/ml
Forskolin	25µl	10µM

Penicillin/Streptomycin (100x)	500µl	10X
B27	1ml	2%
10X SATO stock	5ml	1X

Top up to 50 ml with DMEM and filter sterilise. Store at 4°C for up to one week.

10X SATO stock (100mL)

	Add	Final Conc.
Insulin (10mg/ml in glacial acetic acid)	100mg	50µg/ml
Progesterone (1mg/ml in EtOH)	60µg	600ng/ml
Transferrin	100mg	1mg/ml
BSA	100mg	1mg/ml
Sodium Selenite (1mg/ml in 0.1N NaOH)	40µg	400ng/ml
Putrescine	16mg	160µg/ml

Top up to 100ml with DMEM and filter sterilise. Store in 5ml aliquots at -80°C.

Live imaging media (10ml)

	Add	Final Conc.
PDGFR-AA	2µl	20ng/ml
bFGF	0.5µl	10ng/ml
CNTF	2.5µl	10ng/ml
NAC	5µl	5µg/ml
NT3	0.5µl	1ng/ml
Biotin	1µl	1ng/ml
Forskolin	2.5µl	10µM
Penicillin/Streptomycin (100x)	50µl	10x
B27	100µl	2%
10X SATO stock	500µl	1x
Glutamax	100 µl	4mM

Top up to 5ml with flurobrite DMEM and filter sterilise.

Western blot solutions

RIPA buffer (10ml)

	Add	Final Conc.
MQ water	8190µl	-
1M Tris-HCl (pH 7.4)	500µl	50mM

5M NaCl	300µl	150mM
10% NP-40	1mL	1%
Sodium deoxycholate	100mg	1%
10% SDS	10µl	0.1%
Protease inhibitor tablets	1 per 10ml	-

Aliquot and store at -20°C

Transfer buffer

	Add	Final Conc.
20X Bolt MES transfer buffer	50ml	1x
methanol (or ethanol)	100ml	10%
Bolt Antioxidant	1ml	1%
MQ water	Top up to 1L	-

LB and LB agar

	Add	Final Conc.
Tryptone	5g	1%
Yeast extract	2.5g	0.5%
NaCl	5g	1%

Make up to 500ml with MQ water and autoclave on the liquid cycle.

* To make LB agar add 5g bacteriological agar before autoclaving (1% agar)

In situ solutions

10x 'salts' solution

NaCl	2M
EDTA	50mM
Tris-HCL pH7.5	100mM
Sodium dihydrogen phosphate (NaH_2PO_4)	50mM
Sodium phosphate, dibasic (Na_2HPO_4)	50mM

DEPC-treated, autoclaved and stored at room temperature.

Hybridisation solution

'Salts'	1x
Formamide	50%
Yeast tRNA (phenol/chloroform precipitated)	0.1mg/ml
Dextran sulphate	10% (w/v)

Denhardt's	1x

Aliquot and store at -20°C

20x SSC

NaCl	175.3g
Sodium Citrate (Tribasic: Dihydrate)	88.2g
MilliQ	to 1L

***In Situ* wash solution (500ml)**

	Add	Final Conc.
Formamide	250ml	50%
20x SSC	25ml	1x
Tween 20	500µl	0.1%

5x MABT

Maleic Acid	116.1g
NaCl	87.7g
NaOH Pellets	≈77g
Tween 20 (20%)	50ml
MilliQ	to 2L

***In Situ* blocking solution**

5x MABT	100ml
Blocking reagent	50g
MQ water	top up to 500ml. Aliquot and store at -20°C.

2x Pre-staining buffer

5M NaCl	4ml
1M $MgCl_2$	10ml
1M Tris pH 9.5	20ml
Tween20	0.2ml
MilliQ	Top up to 100ml

Staining buffer

	Add	Final Conc.
2x Pre-staining buffer	15ml	1x
NBT	30µl	0.1%

BCIP	30µl	0.1%
10% PVA (w/v in MQ)	Make up to 30ml	5%

Appendix 2

Table 1. Primary antibodies (immunofluorescence)

Antibody	Concentration	Supplier
Goat anti-Pdgfrα	1:100	R & D systems
Rat anti-GFP	1:2000	Nacalai Tesque
Rabbit anti-GFP	1:200	Synaptic Systems
Mouse anti-γ-tubulin	1:500	Sigma
Rabbit anti-Arl13b	1:200	Protein Tech
Rabbit anti-S100β	1:500	Dako
Rabbit anti-GFAP	1:500	Dako
Mouse anti-NeuN	1:600	Millipore

Table 2. Secondary antibodies (Immunofluorescence)

Antibody	Wavelength	Supplier	Cat #
Donkey anti-Goat	568	Invitrogen	A-11057
Donkey anti-Goat	594	Invitrogen	A-11058
Donkey anti-Rat	488	Invitrogen	A-21208
Donkey anti-Mouse	647	Invitrogen	A-21208
Donkey anti-Rabbit	488	Invitrogen	A-21206
Donkey anti-Rabbit	568	Invitrogen	A-10042
Donkey anti-Rabbit	647	Invitrogen	A-31573

Donkey anti-Guinea Pig	568	Invitrogen	A-11075

Table 3. Antibodies (western blot)

Primary	Conc.	Cat #	Secondary	Conc.	Cat #
Rb anti-Kif3a	1:2000	Abcam ab11259	Anti-Rb HRP	1:5000	Dako P0448
Ms anti-β actin	1:15000	Sigma A2228	Anti-Ms HRP	1:5000	Dako P0447

Appendix 3

Table 4. Transgenic mice

Mouse Model	Use
Pdgfrα-histGFP and *Pdgfrα-histGFP::Kif3a$^{fl/fl}$*	The *Pdgfrα-histGFP* mice are used to generate mixed glial and OPC primary cultures. All OPCs express histone-targeted, nuclear GFP. Cells generated from mice carrying the *Kif3a$^{fl/fl}$* transgene, allow *Kif3a* to be deleted from the cultured cells.
Sox10-DTA-GFP (referred to as Sox10-GFP)	All OPCs and oligodendrocytes have cytoplasmic GFP in these mice. These mice were used to determine whether cells of the oligodendrocyte lineage had primary cilia *in vivo*.
Rosa26-YFP	This cre-sensitive reporter line was used to generate primary glial cultures and determine whether tat-cre addition to the culture medium was sufficient to activate YFP expression.
Plp-CreER^{T2}::Rosa26-YFP	The addition of Tx to these mice results in the YFP-labelling of all oligodendrocytes. These mice

	were used to determine whether primary cilia were assembled by oligodendrocytes *in vivo*.
Pdgfrα-CreER^{T2}::Rosa26YFP and *Pdgfrα-CreER^{T2} :: Rosa26-YFP :: Kif3a$^{fl/fl}$*	The administration of Tx to *Pdgfrα-CreER^{T2} :: Rosa26YFP* transgenic mice fluorescently tags PDGFRα^{+} cells, including OPCs. Furthermore, the tag is retained by all new cells they produce – allowing the quantification of oligodendrogenesis *in vivo*. When these mice also carry the *Kif3a$^{fl/fl}$* transgene, they also allow the deletion of Kif3a from OPCs and all of the cells they produce. These mice were used to determine the effect of Kif3a-deletion on oligodendrogenesis *in vivo*.
Pdgfrα-CreER^{T2}::Kif3a$^{fl/fl}$ and *Kif3a$^{fl/fl}$*	The addition of Tx to *Pdgfrα-CreER^{T2}::Kif3a$^{fl/fl}$* transgenic mice causes the deletion of *Kif3a* from OPCs and all cells they subsequently produce. Mice only containing the *Kif3a$^{fl/fl}$* transgene do not experience gene deletion and act as controls. These mice were examined to determine the behavioural consequence of conditional *Kif3a* deletion.

References

Abdeljalil J, Hamid M, Abdel-Mouttalib O, Stéphane R, Raymond R, Johan A, José S, Pierre C, Serge P (2005) The optomotor response: a robust first-line visual screening method for mice. Vision Res 45:1439–1446.

Allegretta M, Nicklas JA, Sriram S, Albertini RJ (1990) T cells responsive to myelin basic protein in patients with multiple sclerosis. Science 247:718–721.

Angoa-Pérez M, Kane MJ, Briggs DI, Francescutti DM, Kuhn DM (2013) Marble burying and nestlet shredding as tests of repetitive, compulsive-like behaviors in mice. J Vis Exp:50978.

Anthony BA, Link DC (2014) Regulation of hematopoietic stem cells by bone marrow stromal cells. Trends Immunol 35:32–37.

Arellano JI, Guadiana SM, Breunig JJ, Rakic P, Sarkisian MR (2012) Development and distribution of neuronal cilia in mouse neocortex. J Comp Neurol 520:848–873.

Aston C, Jiang L, Sokolov BP (2005) Transcriptional profiling reveals evidence for signaling and oligodendroglial abnormalities in the temporal cortex from patients with major depressive disorder. Mol Psychiatry 10:309–322.

Auderset L, Cullen CL, Young KM (2016) Low Density Lipoprotein-Receptor Related Protein 1 Is Differentially Expressed by Neuronal and Glial Populations in the Developing and Mature Mouse Central Nervous System. Coulson EJ, ed. PLoS ONE 11:e0155878.

Bambakidis NC, Wang X, Lukas RJ, Spetzler RF, Sonntag VKH, Preul MC (2010) Intravenous hedgehog agonist induces proliferation of neural and oligodendrocyte precursors in rodent spinal cord injury. Neurosurgery 67:1709–15–discussion1715.

Bansal R (2002) Fibroblast growth factors and their receptors in oligodendrocyte development: implications for demyelination and remyelination. Dev Neurosci 24:35–46.

Bansal R, Kumar M, Murray K, Morrison RS, Pfeiffer SE (1996) Regulation of FGF receptors in the oligodendrocyte lineage. Mol Cell Neurosci 7:263–275.

Barkovich AJ (2000) Concepts of myelin and myelination in neuroradiology. AJNR Am J Neuroradiol 21:1099–1109.

Barkovich AJ, Raybaud C (2012) Pediatric Neuroimaging. Lippincott Williams & Wilkins.

Baroti T, Zimmermann Y, Schillinger A, Liu L, Lommes P, Wegner M, Stolt CC (2016) Transcription factors Sox5 and Sox6 exert direct and indirect influences on oligodendroglial migration in spinal cord and forebrain. Glia 64:122–138.

Barres BA, Hart IK, Coles HS, Burne JF, Voyvodic JT, Richardson WD, Raff MC (1992) Cell death in the oligodendrocyte lineage. J Neurobiol 23:1221–1230.

Barres BA, Lazar MA, Raff MC (1994) A novel role for thyroid hormone, glucocorticoids and retinoic acid in timing oligodendrocyte development. Development 120:1097–1108.

Baumann N, Pham-Dinh D (2001) Biology of oligodendrocyte and myelin in the mammalian central nervous system. Physiol Rev 81:871–927.

Bechler ME, ffrench-Constant C (2014) Neuroscience. A new wrap for neuronal activity? Science 344:480–481.

Behrendt G, Baer K, Buffo A, Curtis MA, Faull RL, Rees MI, Götz M, Dimou L (2013) Dynamic changes in myelin aberrations and oligodendrocyte generation in chronic amyloidosis in mice and men. Glia 61:273–286.

Bengtsson SL, Nagy Z, Skare S, Forsman L, Forssberg H, Ullén F (2005) Extensive piano practicing has regionally specific effects on white matter development. Nat Neurosci 8:1148–1150.

Berbari NF, O'Connor AK, Haycraft CJ, Yoder BK (2009) The primary cilium as a complex signaling center. Curr Biol 19:R526–R535.

Bian J, Zheng J, Li S, Luo L, Ding F (2016) Sequential Differentiation of Embryonic Stem Cells into Neural Epithelial-Like Stem Cells and Oligodendrocyte Progenitor Cells. de Castro F, ed. PLoS ONE 11:e0155227.

Bielas SL et al. (2009) Mutations in INPP5E, encoding inositol polyphosphate-5-phosphatase E, link phosphatidyl inositol signaling to the ciliopathies. Nat Genet 41:1032–1036.

Birey F, Kloc M, Chavali M, Hussein I, Wilson M, Christoffel DJ, Chen T, Frohman MA, Robinson JK, Russo SJ, Maffei A, Aguirre A (2015) Genetic and Stress-Induced Loss of NG2 Glia Triggers Emergence of Depressive-like Behaviors through Reduced Secretion of FGF2. Neuron 88:941–956.

Bloodgood RA (2009) From central to rudimentary to primary: the history of an underappreciated organelle whose time has come. The primary cilium. Methods Cell Biol 94:3–52.

Bonner JC (2004) Regulation of PDGF and its receptors in fibrotic diseases. Cytokine Growth Factor Rev 15:255–273.

Boström H, Willetts K, Pekny M, Levéen P, Lindahl P, Hedstrand H, Pekna M, Hellström M, Gebre-Medhin S, Schalling M, Nilsson M, Kurland S, Törnell J, Heath JK, Betsholtz C (1996) PDGF-A signaling is a critical event in lung alveolar myofibroblast development and alveogenesis. Cell 85:863–873.

Bowen-Pope DF, Ross R (1982) Platelet-derived growth factor. II. Specific binding to cultured cells. J Biol Chem 257:5161–5171.

Bowley MP, Cabral H, Rosene DL, Peters A (2010) Age changes in myelinated nerve fibers of the cingulate bundle and corpus callosum in the rhesus monkey. J Comp Neurol 518:3046–3064.

Boyd A, Zhang H, Williams A (2013) Insufficient OPC migration into demyelinated lesions is a cause of poor remyelination in MS and mouse models. Acta Neuropathol 125:841–859.

Bradl M, Lassmann H (2010) Oligodendrocytes: biology and pathology. Acta Neuropathol 119:37–53.

Cahoy JD, Emery B, Kaushal A, Foo LC, Zamanian JL, Christopherson KS, Xing Y, Lubischer JL, Krieg PA, Krupenko SA, Thompson WJ, Barres BA (2008) A transcriptome

database for astrocytes, neurons, and oligodendrocytes: a new resource for understanding brain development and function. J Neurosci 28:264–278.

Cai J, Qi Y, Hu X, Tan M, Liu Z, Zhang J, Li Q, Sander M, Qiu M (2005) Generation of oligodendrocyte precursor cells from mouse dorsal spinal cord independent of Nkx6 regulation and Shh signaling. Neuron 45:41–53.

Cajal SRY, Swanson N, Swanson LW (1995) Histology of the Nervous System of Man and Vertebrates.

Calver AR, Hall AC, Yu WP, Walsh FS, Heath JK, Betsholtz C, Richardson WD (1998) Oligodendrocyte population dynamics and the role of PDGF in vivo. Neuron 20:869–882.

Can A, Dao DT, Arad M, Terrillion CE, Piantadosi SC, Gould TD (2012) The mouse forced swim test. J Vis Exp:e3638–e3638.

Cao Y, Cao R, Hedlund E-M (2008) R Regulation of tumor angiogenesis and metastasis by FGF and PDGF signaling pathways. J Mol Med 86:785–789.

Carson RP, Kelm ND, West KL, Does MD, Fu C, Weaver G, McBrier E, Parker B, Grier MD, Ess KC (2015) Hypomyelination following deletion of Tsc2 in oligodendrocyte precursors. Ann Clin Transl Neurol 2:1041–1054.

Carter CS, Vogel TW, Zhang Q, Seo S, Swiderski RE, Moninger TO, Cassell MD, Thedens DR, Keppler-Noreuil KM, Nopoulos P, Nishimura DY, Searby CC, Bugge K, Sheffield VC (2012) Abnormal development of NG2+PDGFR-α+ neural progenitor cells leads to neonatal hydrocephalus in a ciliopathy mouse model. Nat Med 18:1797–1804.

Catala M, Kubis N (2013) Gross anatomy and development of the peripheral nervous system. Handb Clin Neurol 115:29–41.

Chang M, Parker EA, Muller TJM, Haenen C, Mistry M, Finkielstain GP, Murphy-Ryan M, Barnes KM, Sundaram R, Baron J (2008) Changes in cell-cycle kinetics responsible for limiting somatic growth in mice. Pediatr Res 64:240–245.

Chen L, Acciani T, Le Cras T, Lutzko C, Perl A-KT (2012) Dynamic regulation of platelet-derived growth factor receptor α expression in alveolar fibroblasts during realveolarization. Am J Respir Cell Mol Biol 47:517–527.

Chen X, Zhang W, Li T, Guo Y, Tian Y, Wang F, Liu S, Shen H-Y, Feng Y, Xiao L (2015) Impairment of Oligodendroglia Maturation Leads to Aberrantly Increased Cortical Glutamate and Anxiety-Like Behaviors in Juvenile Mice. Front Cell Neurosci 9:467.

Chew L-J, Shen W, Ming X, Senatorov VV, Chen H-L, Cheng Y, Hong E, Knoblach S, Gallo V (2011) SRY-box containing gene 17 regulates the Wnt/β-catenin signaling pathway in oligodendrocyte progenitor cells. J Neurosci 31:13921–13935.

Chong JJH, Reinecke H, Iwata M, Torok-Storb B, Stempien-Otero A, Murry CE (2013) Progenitor cells identified by PDGFR-alpha expression in the developing and diseased human heart. Stem Cells Dev 22:1932–1943.

Christensen ST, Pedersen SF, Satir P, Veland IR, Schneider L (2008) The primary cilium coordinates signaling pathways in cell cycle control and migration during development and tissue repair. Curr Top Dev Biol 85:261–301.

Chung A-Y, Kim S, Kim E, Kim D, Jeong I, Cha YR, Bae Y-K, Park SW, Lee J, Park H-C (2013) Indian hedgehog B function is required for the specification of oligodendrocyte progenitor cells in the zebrafish CNS. J Neurosci 33:1728–1733.

Clark JA, Blizzard CA, Breslin MC, Yeaman EJ, Lee KM, Chuckowree JA, Dickson TC (2018) Epothilone D accelerates disease progression in the SOD1G93Amouse model of Amyotrophic Lateral Sclerosis. Neuropathol Appl Neurobiol.

Clarke LE, Young KM, Hamilton NB, Li H, Richardson WD, Attwell D (2012) Properties and fate of oligodendrocyte progenitor cells in the corpus callosum, motor cortex, and piriform cortex of the mouse. J Neurosci 32:8173–8185.

Clevers H (2006) Wnt/beta-catenin signaling in development and disease. Cell 127:469–480.

Contreras O, Rebolledo DL, Oyarzún JE, Olguín HC, Brandan E (2016) Connective tissue cells expressing fibro/adipogenic progenitor markers increase under chronic damage: relevance in fibroblast-myofibroblast differentiation and skeletal muscle fibrosis. Cell Tissue Res 364:647–660.

Corbit KC, Shyer AE, Dowdle WE, Gaulden J, Singla V, Chen M-H, Chuang P-T, Reiter JF (2008) Kif3a constrains beta-catenin-dependent Wnt signalling through dual ciliary and non-ciliary mechanisms. Nat Cell Biol 10:70–76.

Crone SA, Zhong G, Harris-Warrick R, Sharma K (2009) In mice lacking V2a interneurons, gait depends on speed of locomotion. J Neurosci 29:7098–7109.

Cunha-Ferreira I, Bento I, Bettencourt-Dias M (2009) From zero to many: control of centriole number in development and disease. Traffic 10:482–498.

Dai Z-M, Sun S, Wang C, Huang H, Hu X, Zhang Z, Lu QR, Qiu M (2014) Stage-specific regulation of oligodendrocyte development by Wnt/β-catenin signaling. J Neurosci 34:8467–8473.

Dawson MR, Levine JM, Reynolds R (2000) NG2-expressing cells in the central nervous system: are they oligodendroglial progenitors? J Neurosci Res 61:471–479.

Dawson MRL, Polito A, Levine JM, Reynolds R (2003) NG2-expressing glial progenitor cells: an abundant and widespread population of cycling cells in the adult rat CNS. Mol Cell Neurosci 24:476–488.

De Biase LM, Kang SH, Baxi EG, Fukaya M, Pucak ML, Mishina M, Calabresi PA, Bergles DE (2011) NMDA receptor signaling in oligodendrocyte progenitors is not required for oligodendrogenesis and myelination. J Neurosci 31:12650–12662.

Deacon RMJ (2013) Measuring motor coordination in mice. J Vis Exp:e2609–e2609.

Deacon RMJ, Rawlins JNP (2005) Hippocampal lesions, species-typical behaviours and anxiety in mice. Behav Brain Res 156:241–249.

Deacon RMJ, Rawlins JNP (2006) T-maze alternation in the rodent. Nat Protoc 1:7–12.

Debec A, Sullivan W, Bettencourt-Dias M (2010) Centrioles: active players or passengers during mitosis? Cell Mol Life Sci 67:2173–2194.

Dessaud E, McMahon AP, Briscoe J (2008) Pattern formation in the vertebrate neural tube:

a sonic hedgehog morphogen-regulated transcriptional network. Development 135:2489–2503.

Dimou L, Simon C, Kirchhoff F, Takebayashi H, Götz M (2008) Progeny of Olig2-expressing progenitors in the gray and white matter of the adult mouse cerebral cortex. J Neurosci 28:10434–10442.

Ding L, Saunders TL, Enikolopov G, Morrison SJ (2012) Endothelial and perivascular cells maintain haematopoietic stem cells. Nature 481:457–462.

Dizon MLV, Maa T, Kessler JA (2011) The bone morphogenetic protein antagonist noggin protects white matter after perinatal hypoxia-ischemia. Neurobiol Dis 42:318–326.

Doerflinger NH, Macklin WB, Popko B (2003) Inducible site-specific recombination in myelinating cells. Genesis 35:63–72.

Dougherty KD, Dreyfus CF, Black IB (2000) Brain-derived neurotrophic factor in astrocytes, oligodendrocytes, and microglia/macrophages after spinal cord injury. Neurobiol Dis 7:574–585.

Du Y, Dreyfus CF (2002) Oligodendrocytes as providers of growth factors. J Neurosci Res 68:647–654.

Dua T, World Health Organization, Federation MSI (2008) Atlas.

Dubois-Dalcq M, Behar T, Hudson L, Lazzarini RA (1986) Emergence of three myelin proteins in oligodendrocytes cultured without neurons. J Cell Biol 102:384–392.

Eccleston PA, Funa K, Heldin CH (1993) Expression of platelet-derived growth factor (PDGF) and PDGF alpha- and beta-receptors in the peripheral nervous system: an analysis of sciatic nerve and dorsal root ganglia. Dev Biol 155:459–470.

Ennaceur A (2014) Tests of unconditioned anxiety - pitfalls and disappointments. Physiol Behav 135:55–71.

Enuka Y, Hanukoglu I, Edelheit O, Vaknine H, Hanukoglu A (2012) Epithelial sodium channels (ENaC) are uniformly distributed on motile cilia in the oviduct and the respiratory airways. Histochem Cell Biol 137:339–353.

Espinosa L, Inglés-Esteve J, Aguilera C, Bigas A (2003) Phosphorylation by glycogen synthase kinase-3 beta down-regulates Notch activity, a link for Notch and Wnt pathways. J Biol Chem 278:32227–32235.

Espinosa-Jeffrey A, Wakeman DR, Kim SU, Snyder EY, de Vellis J (2009) Culture system for rodent and human oligodendrocyte specification, lineage progression, and maturation. Curr Protoc Stem Cell Biol Chapter 2:Unit2D.4–2D.4.26.

Falcón-Urrutia P, Carrasco CM, Lois P, Palma V, Roth AD (2015) Shh Signaling through the Primary Cilium Modulates Rat Oligodendrocyte Differentiation. Eugenin EA, ed. PLoS ONE 10:e0133567.

Fancy SPJ, Baranzini SE, Zhao C, Yuk D-I, Irvine K-A, Kaing S, Sanai N, Franklin RJM, Rowitch DH (2009) Dysregulation of the Wnt pathway inhibits timely myelination and remyelination in the mammalian CNS. Genes Dev 23:1571–1585.

Fancy SPJ, Harrington EP, Baranzini SE, Silbereis JC, Shiow LR, Yuen TJ, Huang EJ, Lomvardas S, Rowitch DH (2014) Parallel states of pathological Wnt signaling in neonatal brain injury and colon cancer. Nat Neurosci 17:506–512.

Fancy SPJ, Harrington EP, Yuen TJ, Silbereis JC, Zhao C, Baranzini SE, Bruce CC, Otero JJ, Huang EJ, Nusse R, Franklin RJM, Rowitch DH (2011) Axin2 as regulatory and therapeutic target in newborn brain injury and remyelination. Nat Neurosci 14:1009–1016.

Feigenson K, Reid M, See J, Crenshaw EB, Grinspan JB (2009) Wnt signaling is sufficient to perturb oligodendrocyte maturation. Mol Cell Neurosci 42:255–265.

Ferent J, Zimmer C, Durbec P, Ruat M, Traiffort E (2013) Sonic Hedgehog signaling is a positive oligodendrocyte regulator during demyelination. J Neurosci 33:1759–1772.

Fields RD (2008) White matter in learning, cognition and psychiatric disorders. Trends Neurosci 31:361–370.

Fogarty M, Richardson WD, Kessaris N (2005) A subset of oligodendrocytes generated from radial glia in the dorsal spinal cord. Development 132:1951–1959.

Foran DR, Peterson AC (1992) Myelin acquisition in the central nervous system of the mouse revealed by an MBP-Lac Z transgene. J Neurosci 12:4890–4897.

Ford-Perriss M, Abud H, Murphy M (2001) Fibroblast growth factors in the developing central nervous system. Clin Exp Pharmacol Physiol 28:493–503.

Fortin D, Rom E, Sun H, Yayon A, Bansal R (2005) Distinct fibroblast growth factor (FGF)/FGF receptor signaling pairs initiate diverse cellular responses in the oligodendrocyte lineage. J Neurosci 25:7470–7479.

Frantz DJ (2012) Neurologic complications of bariatric surgery: involvement of central, peripheral, and enteric nervous systems. Curr Gastroenterol Rep 14:367–372.

Fruttiger M, Karlsson L, Hall AC, Abramsson A, Calver AR, Boström H, Willetts K, Bertold CH, Heath JK, Betsholtz C, Richardson WD (1999) Defective oligodendrocyte development and severe hypomyelination in PDGF-A knockout mice. Development 126:457–467.

Furusho M, Dupree JL, Nave K-A, Bansal R (2012) Fibroblast growth factor receptor signaling in oligodendrocytes regulates myelin sheath thickness. J Neurosci 32:6631–6641.

Furusho M, Kaga Y, Ishii A, Hébert JM, Bansal R (2011) Fibroblast growth factor signaling is required for the generation of oligodendrocyte progenitors from the embryonic forebrain. J Neurosci 31:5055–5066.

Gaesser JM, Fyffe-Maricich SL (2016) Intracellular signaling pathway regulation of myelination and remyelination in the CNS. Exp Neurol 283:501–511.

Gan Q, Lee A, Suzuki R, Yamagami T, Stokes A, Nguyen BC, Pleasure D, Wang J, Chen H-W, Zhou CJ (2014) Pax6 mediates ß-catenin signaling for self-renewal and neurogenesis by neocortical radial glial stem cells. Stem Cells 32:45–58.

Garbay B, Heape AM, Sargueil F, Cassagne C (2000) Myelin synthesis in the peripheral

nervous system. Prog Neurobiol 61:267–304.

Garcia-Gonzalo FR, Reiter JF (2012) Scoring a backstage pass: mechanisms of ciliogenesis and ciliary access. J Cell Biol 197:697–709.

Gerdes JM, Katsanis N (2008) Ciliary function and Wnt signal modulation. Curr Top Dev Biol 85:175–195.

Gerdes JM, Liu Y, Zaghloul NA, Leitch CC, Lawson SS, Kato M, Beachy PA, Beales PL, DeMartino GN, Fisher S, Badano JL, Katsanis N (2007) Disruption of the basal body compromises proteasomal function and perturbs intracellular Wnt response. Nat Genet 39:1350–1360.

Gibson DA, Ma L (2011) Developmental regulation of axon branching in the vertebrate nervous system. Development 138:183–195.

Glenn K, Bowen-Pope DF, Ross R (1982) Platelet-derived growth factor. III. Identification of a platelet-derived growth factor receptor by affinity labeling. J Biol Chem 257:5172–5176.

Gnessi L, Basciani S, Mariani S, Arizzi M, Spera G, Wang C, Bondjers C, Karlsson L, Betsholtz C (2000) Leydig cell loss and spermatogenic arrest in platelet-derived growth factor (PDGF)-A-deficient mice. J Cell Biol 149:1019–1026.

Goetz SC, Anderson KV (2010) The primary cilium: a signalling centre during vertebrate development. Nat Rev Genet 11:331–344.

Gorivodsky M, Mukhopadhyay M, Wilsch-Braeuninger M, Phillips M, Teufel A, Kim C, Malik N, Huttner W, Westphal H (2009) Intraflagellar transport protein 172 is essential for primary cilia formation and plays a vital role in patterning the mammalian brain. Dev Biol 325:24–32.

Goto H, Inaba H, Inagaki M (2017) Mechanisms of ciliogenesis suppression in dividing cells. Cell Mol Life Sci 74:881–890.

Grade S, Bernardino L, Malva JO (2013) Oligodendrogenesis from neural stem cells: perspectives for remyelinating strategies. Int J Dev Neurosci 31:692–700.

Grinspan J, Wrabetz L, Kamholz J (1993) Oligodendrocyte maturation and myelin gene expression in PDGF-treated cultures from rat cerebral white matter. J Neurocytol 22:322–333.

Guleria S, Kelly TG (2014) Myelin, myelination, and corresponding magnetic resonance imaging changes. Radiol Clin North Am 52:227–239.

Guo F, Lang J, Sohn J, Hammond E, Chang M, Pleasure D (2015) Canonical Wnt signaling in the oligodendroglial lineage--puzzles remain. Glia 63:1671–1693.

Hall CN, Reynell C, Gesslein B, Hamilton NB, Mishra A, Sutherland BA, O'Farrell FM, Buchan AM, Lauritzen M, Attwell D (2014) Capillary pericytes regulate cerebral blood flow in health and disease. Nature 508:55–60.

Hamilton TG, Klinghoffer RA, Corrin PD, Soriano P (2003) Evolutionary divergence of platelet-derived growth factor alpha receptor signaling mechanisms. Mol Cell Biol 23:4013–4025.

Hampton TG, Kale A, Amende I, Tang W, McCue S, Bhagavan HN, VanDongen CG (2011) Gait disturbances in dystrophic hamsters. J Biomed Biotechnol 2011:235354–235358.

Han Y-G, Spassky N, Romaguera-Ros M, Garcia-Verdugo J-M, Aguilar A, Schneider-Maunoury S, Alvarez-Buylla A (2008) Hedgehog signaling and primary cilia are required for the formation of adult neural stem cells. Nat Neurosci 11:277–284.

Hanafy KA, Sloane JA (2011) Regulation of remyelination in multiple sclerosis. FEBS Lett 585:3821–3828.

Hart CE, Forstrom JW, Kelly JD, Seifert RA, Smith RA, Ross R, Murray MJ, Bowen-Pope DF (1988) Two classes of PDGF receptor recognize different isoforms of PDGF. Science 240:1529–1531.

Hart IK, Richardson WD, Heldin CH, Westermark B, Raff MC (1989) PDGF receptors on cells of the oligodendrocyte-type-2 astrocyte (O-2A) cell lineage. Development 105:595–603.

Hayes BJ, Riehle KJ, Shimizu-Albergine M, Bauer RL, Hudkins KL, Johansson F, Yeh MM, Mahoney WM, Yeung RS, Campbell JS (2014) Activation of platelet-derived growth factor receptor alpha contributes to liver fibrosis. Haybaeck J, ed. PLoS ONE 9:e92925.

He X, Semenov M, Tamai K, Zeng X (2004) LDL receptor-related proteins 5 and 6 in Wnt/beta-catenin signaling: arrows point the way. Development 131:1663–1677.

Hermanson M, Funa K, Hartman M, Claesson-Welsh L, Heldin CH, Westermark B, Nistér M (1992) Platelet-derived growth factor and its receptors in human glioma tissue: expression of messenger RNA and protein suggests the presence of autocrine and paracrine loops. Cancer Res 52:3213–3219.

Hermanson M, Funa K, Koopmann J, Maintz D, Waha A, Westermark B, Heldin CH, Wiestler OD, Louis DN, Deimling von A, Nistér M (1996) Association of loss of heterozygosity on chromosome 17p with high platelet-derived growth factor alpha receptor expression in human malignant gliomas. Cancer Res 56:164–171.

Hill RA, Patel KD, Goncalves CM, Grutzendler J, Nishiyama A (2014) Modulation of oligodendrocyte generation during a critical temporal window after NG2 cell division. Nat Neurosci 17:1518–1527.

Hoang-Minh LB, Deleyrolle LP, Siebzehnrubl D, Ugartemendia G, Futch H, Griffith B, Breunig JJ, De Leon G, Mitchell DA, Semple-Rowland S, Reynolds BA, Sarkisian MR (2016) Disruption of KIF3A in patient-derived glioblastoma cells: effects on ciliogenesis, hedgehog sensitivity, and tumorigenesis. Oncotarget 7:7029–7043.

Hong S-K, Dawid IB (2009) FGF-dependent left-right asymmetry patterning in zebrafish is mediated by Ier2 and Fibp1. Proc Natl Acad Sci USA 106:2230–2235.

Horikawa S, Ishii Y, Hamashima T, Yamamoto S, Mori H, Fujimori T, Shen J, Inoue R, Nishizono H, Itoh H, Majima M, Abraham D, Miyawaki T, Sasahara M (2015) PDGFRα plays a crucial role in connective tissue remodeling. Sci Rep 5:17948.

Horner PJ, Power AE, Kempermann G, Kuhn HG, Palmer TD, Winkler J, Thal LJ, Gage FH (2000) Proliferation and differentiation of progenitor cells throughout the intact adult rat spinal cord. J Neurosci 20:2218–2228.

Huang P, Schier AF (2009) Dampened Hedgehog signaling but normal Wnt signaling in zebrafish without cilia. Development 136:3089–3098.

Huangfu D, Anderson KV (2005) Cilia and Hedgehog responsiveness in the mouse. Proc Natl Acad Sci USA 102:11325–11330.

Huangfu D, Liu A, Rakeman AS, Murcia NS, Niswander L, Anderson KV (2003) Hedgehog signalling in the mouse requires intraflagellar transport proteins. Nature 426:83–87.

Hudish LI, Galati DF, Ravanelli AM, Pearson CG, Huang P, Appel B (2016) miR-219 regulates neural progenitors by dampening apical Par protein-dependent Hedgehog signaling. Development 143:2292–2304.

Hughes EG, Appel B (2016) The cell biology of CNS myelination. Curr Opin Neurobiol 39:93–100.

Hughes EG, Kang SH, Fukaya M, Bergles DE (2013) Oligodendrocyte progenitors balance growth with self-repulsion to achieve homeostasis in the adult brain. Nat Neurosci 16:668–676.

Ishikawa H, Marshall WF (2011) Ciliogenesis: building the cell's antenna. Nat Rev Mol Cell Biol 12:222–234.

Jones MV, Nguyen TT, Deboy CA, Griffin JW, Whartenby KA, Kerr DA, Calabresi PA (2008) Behavioral and pathological outcomes in MOG 35-55 experimental autoimmune encephalomyelitis. J Neuroimmunol 199:83–93.

Kang SH, Fukaya M, Yang JK, Rothstein JD, Bergles DE (2010) NG2+ CNS glial progenitors remain committed to the oligodendrocyte lineage in postnatal life and following neurodegeneration. Neuron 68:668–681.

Kang SH, Li Y, Fukaya M, Lorenzini I, Cleveland DW, Ostrow LW, Rothstein JD, Bergles DE (2013) Degeneration and impaired regeneration of gray matter oligodendrocytes in amyotrophic lateral sclerosis. Nat Neurosci 16:571–579.

Karlsson L, Bondjers C, Betsholtz C (1999) Roles for PDGF-A and sonic hedgehog in development of mesenchymal components of the hair follicle. Development 126:2611–2621.

Karlsson L, Lindahl P, Heath JK, Betsholtz C (2000) Abnormal gastrointestinal development in PDGF-A and PDGFR-(alpha) deficient mice implicates a novel mesenchymal structure with putative instructive properties in villus morphogenesis. Development 127:3457–3466.

Karussis D (2014) The diagnosis of multiple sclerosis and the various related demyelinating syndromes: a critical review. J Autoimmun 48-49:134–142.

Kasahara K, Miyoshi K, Murakami S, Miyazaki I, Asanuma M (2014) Visualization of astrocytic primary cilia in the mouse brain by immunofluorescent analysis using the cilia marker Arl13b. Acta Med Okayama 68:317–322.

Kedia S, Chattarji S (2014) Marble burying as a test of the delayed anxiogenic effects of acute immobilisation stress in mice. J Neurosci Methods 233:150–154.

Kenney AM, Rowitch DH (2000) Sonic hedgehog promotes G(1) cyclin expression and

sustained cell cycle progression in mammalian neuronal precursors. Mol Cell Biol 20:9055–9067.

Kessaris N, Fogarty M, Iannarelli P, Grist M, Wegner M, Richardson WD (2006) Competing waves of oligodendrocytes in the forebrain and postnatal elimination of an embryonic lineage. Nat Neurosci 9:173–179.

Kim LJ, Martinez D, Fiori CZ, Baronio D, Kretzmann NA, Barros HMT (2015) Hypomyelination, memory impairment, and blood-brain barrier permeability in a model of sleep apnea. Brain Res 1597:28–36.

Kim S, Dynlacht BD (2013) Assembling a primary cilium. Curr Opin Cell Biol 25:506–511.

Kobayashi T, Dynlacht BD (2011) Regulating the transition from centriole to basal body. J Cell Biol 193:435–444.

Kukley M, Nishiyama A, Dietrich D (2010) The fate of synaptic input to NG2 glial cells: neurons specifically downregulate transmitter release onto differentiating oligodendroglial cells. J Neurosci 30:8320–8331.

Kulesskaya N, Voikar V (2014) Assessment of mouse anxiety-like behavior in the light-dark box and open-field arena: role of equipment and procedure. Physiol Behav 133:30–38.

Kumamoto N, Gu Y, Wang J, Janoschka S, Takemaru K-I, Levine J, Ge S (2012) A role for primary cilia in glutamatergic synaptic integration of adult-born neurons. Nat Neurosci 15:399–405–S1.

Kurahashi M, Mutafova-Yambolieva V, Koh SD, Sanders KM (2014) Platelet-derived growth factor receptor-α-positive cells and not smooth muscle cells mediate purinergic hyperpolarization in murine colonic muscles. Am J Physiol, Cell Physiol 307:C561–C570.

Kurahashi M, Nakano Y, Peri LE, Townsend JB, Ward SM, Sanders KM (2013) A novel population of subepithelial platelet-derived growth factor receptor α-positive cells in the mouse and human colon. Am J Physiol Gastrointest Liver Physiol 304:G823–G834.

Kurahashi M, Zheng H, Dwyer L, Ward SM, Koh SD, Sanders KM (2011) A functional role for the “fibroblast-like cells” in gastrointestinal smooth muscles. J Physiol (Lond) 589:697–710.

Lancaster MA, Schroth J, Gleeson JG (2011) Subcellular spatial regulation of canonical Wnt signalling at the primary cilium. Nat Cell Biol 13:700–707.

Lang J, Maeda Y, Bannerman P, Xu J, Horiuchi M, Pleasure D, Guo F (2013) Adenomatous polyposis coli regulates oligodendroglial development. J Neurosci 33:3113–3130.

Lasiene J, Matsui A, Sawa Y, Wong F, Horner PJ (2009) Age-related myelin dynamics revealed by increased oligodendrogenesis and short internodes. Aging Cell 8:201–213.

Lassmann H (1983) Comparative neuropathology of chronic experimental allergic encephalomyelitis and multiple sclerosis. Schriftenr Neurol 25:1–135.

Lee DJ, Chen Y, Schlaug G (2003) Corpus callosum: musician and gender effects. Neuroreport 14:205–209.

Lepanto P, Davison C, Casanova G, Badano JL, Zolessi FR (2016) Characterization of primary cilia during the differentiation of retinal ganglion cells in the zebrafish. Neural Dev 11:10.

Levine JM (1994) Increased expression of the NG2 chondroitin-sulfate proteoglycan after brain injury. J Neurosci 14:4716–4730.

Levine JM, Beasley L, Stallcup WB (1986) Localization of a neurectoderm-associated cell surface antigen in the developing and adult rat. Brain Res 392:211–222.

Levison SW, Young GM, Goldman JE (1999) Cycling cells in the adult rat neocortex preferentially generate oligodendroglia. J Neurosci Res 57:435–446.

Lewin B (2007) Cells. Jones & Bartlett Learning.

Liao M, Yang F, Zhang Y, He Z, Su L, Li L (2014) White matter abnormalities in adolescents with generalized anxiety disorder: a diffusion tensor imaging study. BMC Psychiatry 14:41.

Lin F, Hiesberger T, Cordes K, Sinclair AM, Goldstein LSB, Somlo S, Igarashi P (2003) Kidney-specific inactivation of the KIF3A subunit of kinesin-II inhibits renal ciliogenesis and produces polycystic kidney disease. Proc Natl Acad Sci USA 100:5286–5291.

Liu C, Li J, Xiang X, Guo L, Tu K, Liu Q, Shah VH, Kang N (2014) PDGF receptor-α promotes TGF-β signaling in hepatic stellate cells via transcriptional and posttranscriptional regulation of TGF-β receptors. Am J Physiol Gastrointest Liver Physiol 307:G749–G759.

Liu Y, Rao MS (2004) Olig genes are expressed in a heterogeneous population of precursor cells in the developing spinal cord. Glia 45:67–74.

LoPresti P (2015) Inducible Expression of a Truncated Form of Tau in Oligodendrocytes Elicits Gait Abnormalities and a Decrease in Myelin: Implications for Selective CNS Degenerative Diseases. Neurochem Res 40:2188–2199.

Love S (2006) Demyelinating diseases. J Clin Pathol 59:1151–1159.

Lucchinetti C, Brück W, Parisi J, Scheithauer B, Rodriguez M, Lassmann H (1999) A quantitative analysis of oligodendrocytes in multiple sclerosis lesions. A study of 113 cases. Brain 122 (Pt 12):2279–2295.

Lucker BF, Behal RH, Qin H, Siron LC, Taggart WD, Rosenbaum JL, Cole DG (2005) Characterization of the intraflagellar transport complex B core: direct interaction of the IFT81 and IFT74/72 subunits. J Biol Chem 280:27688–27696.

Ma M, Tian X, Igarashi P, Pazour GJ, Somlo S (2013) Loss of cilia suppresses cyst growth in genetic models of autosomal dominant polycystic kidney disease. Nat Genet 45:1004–1012.

Maki T, Liang AC, Miyamoto N, Lo EH, Arai K (2013) Mechanisms of oligodendrocyte regeneration from ventricular-subventricular zone-derived progenitor cells in white matter diseases. Front Cell Neurosci 7:275.

Makinodan M, Rosen KM, Ito S, Corfas G (2012) A critical period for social experience-dependent oligodendrocyte maturation and myelination. Science 337:1357–1360.

Makwana M, Raivich G (2005) Molecular mechanisms in successful peripheral regeneration. FEBS J 272:2628–2638.

Marshall WF, Rosenbaum JL (2001) Intraflagellar transport balances continuous turnover of outer doublet microtubules: implications for flagellar length control. J Cell Biol 155:405–414.

Marszalek JR, Liu X, Roberts EA, Chui D, Marth JD, Williams DS, Goldstein LS (2000) Genetic evidence for selective transport of opsin and arrestin by kinesin-II in mammalian photoreceptors. Cell 102:175–187.

Marszalek JR, Ruiz-Lozano P, Roberts E, Chien KR, Goldstein LS (1999) Situs inversus and embryonic ciliary morphogenesis defects in mouse mutants lacking the KIF3A subunit of kinesin-II. Proc Natl Acad Sci USA 96:5043–5048.

Matsunaga Y, Kezuka T, An X, Fujita K, Matsuyama N, Matsuda R, Usui Y, Yamakawa N, Kuroda M, Goto H (2012) Visual functional and histopathological correlation in experimental autoimmune optic neuritis. Invest Ophthalmol Vis Sci 53:6964–6971.

McIntyre JC et al. (2012) Gene therapy rescues cilia defects and restores olfactory function in a mammalian ciliopathy model. Nat Med 18:1423–1428.

McKenzie IA, Ohayon D, Li H, de Faria JP, Emery B, Tohyama K, Richardson WD (2014) Motor skill learning requires active central myelination. Science 346:318–322.

McKinnon RD, Matsui T, Dubois-Dalcq M, Aaronson SA (1990) FGF modulates the PDGF-driven pathway of oligodendrocyte development. Neuron 5:603–614.

Merchán P, Bribián A, Sánchez-Camacho C, Lezameta M, Bovolenta P, de Castro F (2007) Sonic hedgehog promotes the migration and proliferation of optic nerve oligodendrocyte precursors. Mol Cell Neurosci 36:355–368.

Michaud EJ, Yoder BK (2006) The primary cilium in cell signaling and cancer. Cancer Res 66:6463–6467.

Mierzwa AJ, Sullivan GM, Beer LA, Ahn S, Armstrong RC (2014) Comparison of cortical and white matter traumatic brain injury models reveals differential effects in the subventricular zone and divergent Sonic hedgehog signaling pathways in neuroblasts and oligodendrocyte progenitors. ASN Neuro 6:175909141455178.

Mierzwa AJ, Zhou Y-X, Hibbits N, Vana AC, Armstrong RC (2013) FGF2 and FGFR1 signaling regulate functional recovery following cuprizone demyelination. Neurosci Lett 548:280–285.

Mietto BS, Mostacada K, Martinez AMB (2015) Neurotrauma and inflammation: CNS and PNS responses. Mediators Inflamm 2015:251204–251214.

Milner R, Anderson HJ, Rippon RF, McKay JS, Franklin RJ, Marchionni MA, Reynolds R, Ffrench-Constant C (1997) Contrasting effects of mitogenic growth factors on oligodendrocyte precursor cell migration. Glia 19:85–90.

Miron VE, Jung CG, Kim HJ, Kennedy TE, Soliven B, Antel JP (2008) FTY720 modulates human oligodendrocyte progenitor process extension and survival. Ann Neurol 63:61–71.

Miron VE, Ludwin SK, Darlington PJ, Jarjour AA, Soliven B, Kennedy TE, Antel JP (2010) Fingolimod (FTY720) enhances remyelination following demyelination of organotypic cerebellar slices. Am J Pathol 176:2682–2694.

Mishra A, O'Farrell FM, Reynell C, Hamilton NB, Hall CN, Attwell D (2014) Imaging pericytes and capillary diameter in brain slices and isolated retinae. Nat Protoc 9:323–336.

Morikawa S, Mabuchi Y, Kubota Y, Nagai Y, Niibe K, Hiratsu E, Suzuki S, Miyauchi-Hara C, Nagoshi N, Sunabori T, Shimmura S, Miyawaki A, Nakagawa T, Suda T, Okano H, Matsuzaki Y (2009) Prospective identification, isolation, and systemic transplantation of multipotent mesenchymal stem cells in murine bone marrow. J Exp Med 206:2483–2496.

Müller MS, Fox R, Schousboe A, Waagepetersen HS, Bak LK (2014) Astrocyte glycogenolysis is triggered by store-operated calcium entry and provides metabolic energy for cellular calcium homeostasis. Glia 62:526–534.

Nakamura M, Katano M, Fujimoto K, Morisaki T (1997) A new prognostic strategy for gastric carcinoma: mRNA expression of tumor growth-related factors in endoscopic biopsy specimens. Ann Surg 226:35–42.

Neugebauer JM, Amack JD, Peterson AG, Bisgrove BW, Yost HJ (2009) FGF signalling during embryo development regulates cilia length in diverse epithelia. Nature 458:651–654.

Nishiyama A, Komitova M, Suzuki R, Zhu X (2009) Polydendrocytes (NG2 cells): multifunctional cells with lineage plasticity. Nat Rev Neurosci 10:9–22.

Noseda M, Harada M, McSweeney S, Leja T, Belian E, Stuckey DJ, Abreu Paiva MS, Habib J, Macaulay I, de Smith AJ, al-Beidh F, Sampson R, Lumbers RT, Rao P, Harding SE, Blakemore AIF, Jacobsen SE, Barahona M, Schneider MD (2015) PDGFRα demarcates the cardiogenic clonogenic Sca1+ stem/progenitor cell in adult murine myocardium. Nat Commun 6:6930.

Ntokou A, Klein F, Dontireddy D, Becker S, Bellusci S, Richardson WD, Szibor M, Braun T, Morty RE, Seeger W, Voswinckel R, Ahlbrecht K (2015) Characterization of the platelet-derived growth factor receptor-α-positive cell lineage during murine late lung development. Am J Physiol Lung Cell Mol Physiol 309:L942–L958.

Ocbina PJR, Tuson M, Anderson KV (2009) Primary Cilia Are Not Required for Normal Canonical Wnt Signaling in the Mouse Embryo Heisenberg C-P, ed. PLoS ONE 4:e6839.

Oishi T, Uezumi A, Kanaji A, Yamamoto N, Yamaguchi A, Yamada H, Tsuchida K (2013) Osteogenic differentiation capacity of human skeletal muscle-derived progenitor cells. Asakura A, ed. PLoS ONE 8:e56641.

Olsen JA, Akirav EM (2015) Remyelination in multiple sclerosis: cellular mechanisms and novel therapeutic approaches. J Neurosci Res 93:687–696.

Omatsu Y, Sugiyama T, Kohara H, Kondoh G, Fujii N, Kohno K, Nagasawa T (2010) The essential functions of adipo-osteogenic progenitors as the hematopoietic stem and progenitor cell niche. Immunity 33:387–399.

Ornitz DM, Itoh N (2015) The Fibroblast Growth Factor signaling pathway. Wiley Interdiscip

Rev Dev Biol 4:215–266.

O'Rourke M, Gasperini, R., & Young, K. M. (2014). Adult myelination: wrapping up neuronal plasticity. *Neural Regeneration Research*, *9*(13), 1261–1264. http://doi.org/10.4103/1673-5374.137571

O'Rourke M, Cullen CL, Auderset L, Pitman KA, Achatz D, Gasperini R, Young KM (2016) Evaluating Tissue-Specific Recombination in a Pdgfrα-CreERT2 Transgenic Mouse Line. Arai K, ed. PLoS ONE 11:e0162858.

Ortega JA, Radonjić NV, Zecevic N (2013) Sonic hedgehog promotes generation and maintenance of human forebrain Olig2 progenitors. Front Cell Neurosci 7:254.

Ortega MC, Cases O, Merchán P, Kozyraki R, Clemente D, de Castro F (2012) Megalin mediates the influence of sonic hedgehog on oligodendrocyte precursor cell migration and proliferation during development. Glia 60:851–866.

Palazzo A, Ackerman B, Gundersen GG (2003) Cell biology: Tubulin acetylation and cell motility. Nature 421:230–230.

Palma V, Lim DA, Dahmane N, Sánchez P, Brionne TC, Herzberg CD, Gitton Y, Carleton A, Alvarez-Buylla A, Ruiz i Altaba A (2005) Sonic hedgehog controls stem cell behavior in the postnatal and adult brain. Development 132:335–344.

Pan J, Snell WJ (2005) Chlamydomonas shortens its flagella by activating axonemal disassembly, stimulating IFT particle trafficking, and blocking anterograde cargo loading. Dev Cell 9:431–438.

Pannérec A, Formicola L, Besson V, Marazzi G, Sassoon DA (2013) Defining skeletal muscle resident progenitors and their cell fate potentials. Development 140:2879–2891.

Paolicelli RC, Bolasco G, Pagani F, Maggi L, Scianni M, Panzanelli P, Giustetto M, Ferreira TA, Guiducci E, Dumas L, Ragozzino D, Gross CT (2011) Synaptic pruning by microglia is necessary for normal brain development. Science 333:1456–1458.

Paridaen JTML, Wilsch-Bräuninger M, Huttner WB (2013) Asymmetric inheritance of centrosome-associated primary cilium membrane directs ciliogenesis after cell division. Cell 155:333–344.

Park H-C, Shin J, Appel B (2004) Spatial and temporal regulation of ventral spinal cord precursor specification by Hedgehog signaling. Development 131:5959–5969.

Parretta E, Cassese G, Santoni A, Guardiola J, Vecchio A, Di Rosa F (2008) Kinetics of in vivo proliferation and death of memory and naive CD8 T cells: parameter estimation based on 5-bromo-2'-deoxyuridine incorporation in spleen, lymph nodes, and bone marrow. J Immunol 180:7230–7239.

Pedersen LB, Rosenbaum JL (2008) Intraflagellar transport (IFT) role in ciliary assembly, resorption and signalling. Curr Top Dev Biol 85:23–61.

Plotnikova OV, Seo S, Cottle DL, Conduit S, Hakim S, Dyson JM, Mitchell CA, Smyth IM (2015) INPP5E interacts with AURKA, linking phosphoinositide signaling to primary cilium stability. J Cell Sci 128:364–372.

Pringle NP, Mudhar HS, Collarini EJ, Richardson WD (1992) PDGF receptors in the rat

CNS: during late neurogenesis, PDGF alpha-receptor expression appears to be restricted to glial cells of the oligodendrocyte lineage. Development 115:535–551.

Pringle NP, Yu WP, Guthrie S, Roelink H, Lumsden A, Peterson AC, Richardson WD (1996) Determination of neuroepithelial cell fate: induction of the oligodendrocyte lineage by ventral midline cells and sonic hedgehog. Dev Biol 177:30–42.

Psachoulia K, Jamen F, Young KM, Richardson WD (2009) Cell cycle dynamics of NG2 cells in the postnatal and ageing brain. Neuron Glia Biol 5:57–67.

Purves D (2012) Neuroscience. Sinauer Associates Incorporated.

Raff MC, Miller RH, Noble M (1983) A glial progenitor cell that develops in vitro into an astrocyte or an oligodendrocyte depending on culture medium. Nature 303:390–396.

Raper J, Mason C (2010) Cellular strategies of axonal pathfinding. Cold Spring Harb Perspect Biol 2:a001933–a001933.

Raz N, Dotan S, Benoliel T, Chokron S, Ben-Hur T, Levin N (2011) Sustained motion perception deficit following optic neuritis: Behavioral and cortical evidence. Neurology 76:2103–2111.

Regenold WT, Phatak P, Marano CM, Gearhart L, Viens CH, Hisley KC (2007) Myelin staining of deep white matter in the dorsolateral prefrontal cortex in schizophrenia, bipolar disorder, and unipolar major depression. Psychiatry Res 151:179–188.

Reichsman F, Smith L, Cumberledge S (1996) Glycosaminoglycans can modulate extracellular localization of the wingless protein and promote signal transduction. J Cell Biol 135:819–827.

Richardson WD, Kessaris N, Pringle N (2006) Oligodendrocyte wars. Nat Rev Neurosci 7:11–18.

Richardson WD, Young KM, Tripathi RB, McKenzie I (2011) NG2-glia as multipotent neural stem cells: fact or fantasy? Neuron 70:661–673.

Rieder CL, Jensen CG, Jensen LC (1979) The resorption of primary cilia during mitosis in a vertebrate (PtK1) cell line. J Ultrastruct Res 68:173–185.

Rivers LE, Young KM, Rizzi M, Jamen F, Psachoulia K, Wade A, Kessaris N, Richardson WD (2008) PDGFRA/NG2 glia generate myelinating oligodendrocytes and piriform projection neurons in adult mice. Nat Neurosci 11:1392–1401.

Rosenbaum JL, Child FM (1967) Flagellar regeneration in protozoan flagellates. J Cell Biol 34:345–364.

Rosenbaum JL, Witman GB (2002) Intraflagellar transport. Nat Rev Mol Cell Biol 3:813–825.

Rowitch DH, Lu QR, Kessaris N, Richardson WD (2002) An “oligarchy” rules neural development. Trends Neurosci 25:417–422.

Ruat M, Roudaut H, Ferent J, Traiffort E (2012) Hedgehog trafficking, cilia and brain functions. Differentiation 83:S97–S104.

Ruiz i Altaba A, Mas C, Stecca B (2007) The Gli code: an information nexus regulating cell fate, stemness and cancer. Trends Cell Biol 17:438–447.

Sampaio-Baptista C, Khrapitchev AA, Foxley S, Schlagheck T, Scholz J, Jbabdi S, DeLuca GC, Miller KL, Taylor A, Thomas N, Kleim J, Sibson NR, Bannerman D, Johansen-Berg H (2013) Motor skill learning induces changes in white matter microstructure and myelination. J Neurosci 33:19499–19503.

Sanchez GM, Alkhori L, Hatano E, Schultz SW, Kuzhandaivel A, Jafari S, Granseth B, Alenius M (2016) Hedgehog Signaling Regulates the Ciliary Transport of Odorant Receptors in Drosophila. Cell Rep 14:464–470.

Sanchez MA, Armstrong RC (2018) Postnatal Sonic hedgehog (Shh) responsive cells give rise to oligodendrocyte lineage cells during myelination and in adulthood contribute to remyelination. Exp Neurol 299:122–136.

Satir P, Christensen ST (2007) Overview of structure and function of mammalian cilia. Annu Rev Physiol 69:377–400.

Sánchez I, Dynlacht BD (2016) Cilium assembly and disassembly. Nat Cell Biol 18:711–717.

Schneider L, Clement CA, Teilmann SC, Pazour GJ, Hoffmann EK, Satir P, Christensen ST (2005) PDGFRalphaalpha signaling is regulated through the primary cilium in fibroblasts. Curr Biol 15:1861–1866.

Schneider S, Gruart A, Grade S, Zhang Y, Kröger S, Kirchhoff F, Eichele G, Delgado García JM, Dimou L (2016) Decrease in newly generated oligodendrocytes leads to motor dysfunctions and changed myelin structures that can be rescued by transplanted cells. Glia 64:2201–2218.

Scholz J, Klein MC, Behrens TEJ, Johansen-Berg H (2009) Training induces changes in white-matter architecture. Nat Neurosci 12:1370–1371.

Seeley ES, Nachury MV (2010) The perennial organelle: assembly and disassembly of the primary cilium. J Cell Sci 123:511–518.

Senyo SE, Steinhauser ML, Pizzimenti CL, Yang VK, Cai L, Wang M, Wu T-D, Guerquin-Kern J-L, Lechene CP, Lee RT (2013) Mammalian heart renewal by pre-existing cardiomyocytes. Nature 493:433–436.

Seyed Saadat SM, Hosseininezhad M, Bakhshayesh B, Seyed Saadat SN, Nabizadeh SP (2014) Prevalence and predictors of depression in Iranian patients with multiple sclerosis: a population-based study. Neurol Sci 35:735–740.

Seyed-Razavi Y, Williams B, Winkler DA, Bertoncello I (2013) Mesenchymal stromal cell turnover in the normal adult lung revisited. Am J Physiol Lung Cell Mol Physiol 305:L635–L641.

Shim AH-R, Liu H, Focia PJ, Chen X, Lin PC, He X (2010) Structures of a platelet-derived growth factor/propeptide complex and a platelet-derived growth factor/receptor complex. Proc Natl Acad Sci USA 107:11307–11312.

Shin S, Xue H, Mattson MP, Rao MS (2007) Stage-dependent Olig2 expression in motor neurons and oligodendrocytes differentiated from embryonic stem cells. Stem Cells Dev 16:131–141.

Simons M, Trotter J (2007) Wrapping it up: the cell biology of myelination. Curr Opin Neurobiol 17:533–540.

Skoda AM, Simovic D, Karin V, Kardum V, Vranic S, Serman L (2017) The role of the Hedgehog signaling pathway in cancer: A comprehensive review. Bosn J Basic Med Sci 0.

Skripuletz T, Hackstette D, Bauer K, Gudi V, Pul R, Voss E, Berger K, Kipp M, Baumgärtner W, Stangel M (2013) Astrocytes regulate myelin clearance through recruitment of microglia during cuprizone-induced demyelination. Brain 136:147–167.

Slough J, Cooney L, Brueckner M (2008) Monocilia in the embryonic mouse heart suggest a direct role for cilia in cardiac morphogenesis. Dev Dyn 237:2304–2314.

Snaidero N, Möbius W, Czopka T, Hekking LHP, Mathisen C, Verkleij D, Goebbels S, Edgar J, Merkler D, Lyons DA, Nave K-A, Simons M (2014) Myelin membrane wrapping of CNS axons by PI(3,4,5)P3-dependent polarized growth at the inner tongue. Cell 156:277–290.

Soriano P (1997) The PDGF alpha receptor is required for neural crest cell development and for normal patterning of the somites. Development 124:2691–2700.

Sorokin SP (1968) Centriole formation and ciliogenesis. Aspen Emphysema Conf 11:213–216.

Spassky N, Han Y-G, Aguilar A, Strehl L, Besse L, Laclef C, Ros MR, Garcia-Verdugo JM, Alvarez-Buylla A (2008) Primary cilia are required for cerebellar development and Shh-dependent expansion of progenitor pool. Dev Biol 317:246–259.

Srinivas S, Watanabe T, Lin CS, William CM, Tanabe Y, Jessell TM, Costantini F (2001) Cre reporter strains produced by targeted insertion of EYFP and ECFP into the ROSA26 locus. BMC Dev Biol 1:4.

Stamos JL, Weis WI (2013) The β-catenin destruction complex. Cold Spring Harb Perspect Biol 5:a007898–a007898.

Sugiarto S, Persson AI, Munoz EG, Waldhuber M, Lamagna C, Andor N, Hanecker P, Ayers-Ringler J, Phillips J, Siu J, Lim DA, Vandenberg S, Stallcup W, Berger MS, Bergers G, Weiss WA, Petritsch C (2011) Asymmetry-defective oligodendrocyte progenitors are glioma precursors. Cancer Cell 20:328–340.

Sugiyama T, Kohara H, Noda M, Nagasawa T (2006) Maintenance of the hematopoietic stem cell pool by CXCL12-CXCR4 chemokine signaling in bone marrow stromal cell niches. Immunity 25:977–988.

Taglialatela G, Hogan D, Zhang W-R, Dineley KT (2009) Intermediate- and long-term recognition memory deficits in Tg2576 mice are reversed with acute calcineurin inhibition. Behav Brain Res 200:95–99.

Tang F, Lane S, Korsak A, Paton JFR, Gourine AV, Kasparov S, Teschemacher AG (2014) Lactate-mediated glia-neuronal signalling in the mammalian brain. Nat Commun 5:3284.

Tekki-Kessaris N, Woodruff R, Hall AC, Gaffield W, Kimura S, Stiles CD, Rowitch DH, Richardson WD (2001) Hedgehog-dependent oligodendrocyte lineage specification in the telencephalon. Development 128:2545–2554.

Temiyasathit S, Tang WJ, Leucht P, Anderson CT, Monica SD, Castillo AB, Helms JA, Stearns T, Jacobs CR (2012) Mechanosensing by the primary cilium: deletion of Kif3A

reduces bone formation due to loading. Leipzig ND, ed. PLoS ONE 7:e33368.

Thomas AM, Seidlits SK, Goodman AG, Kukushliev TV, Hassani DM, Cummings BJ, Anderson AJ, Shea LD (2014) Sonic hedgehog and neurotrophin-3 increase oligodendrocyte numbers and myelination after spinal cord injury. Integr Biol (Camb) 6:694–705.

Tong CK, Fuentealba LC, Shah JK, Lindquist RA, Ihrie RA, Guinto CD, Rodas-Rodriguez JL, Alvarez-Buylla A (2015) A Dorsal SHH-Dependent Domain in the V-SVZ Produces Large Numbers of Oligodendroglial Lineage Cells in the Postnatal Brain. Stem Cell Reports 5:461–470.

Tong CK, Han Y-G, Shah JK, Obernier K, Guinto CD, Alvarez-Buylla A (2014) Primary cilia are required in a unique subpopulation of neural progenitors. Proc Natl Acad Sci USA 111:12438–12443.

Trapp BD, Nishiyama A, Cheng D, Macklin W (1997) Differentiation and death of premyelinating oligodendrocytes in developing rodent brain. J Cell Biol 137:459–468.

Tripathi RB, Clarke LE, Burzomato V, Kessaris N, Anderson PN, Attwell D, Richardson WD (2011) Dorsally and ventrally derived oligodendrocytes have similar electrical properties but myelinate preferred tracts. J Neurosci 31:6809–6819.

Tripathi RB, Jackiewicz M, McKenzie IA, Kougioumtzidou E, Grist M, Richardson WD (2017) Remarkable Stability of Myelinating Oligodendrocytes in Mice. Cell Rep 21:316–323.

Tripathi RB, Rivers LE, Young KM, Jamen F, Richardson WD (2010) NG2 glia generate new oligodendrocytes but few astrocytes in a murine experimental autoimmune encephalomyelitis model of demyelinating disease. J Neurosci 30:16383–16390.

Trotter J, Karram K, Nishiyama A (2010) NG2 cells: Properties, progeny and origin. Brain Res Rev 63:72–82.

Tsai H-H, Niu J, Munji R, Davalos D, Chang J, Zhang H, Tien A-C, Kuo CJ, Chan JR, Daneman R, Fancy SPJ (2016) Oligodendrocyte precursors migrate along vasculature in the developing nervous system. Science 351:379–384.

Vallstedt A, Klos JM, Ericson J (2005) Multiple dorsoventral origins of oligodendrocyte generation in the spinal cord and hindbrain. Neuron 45:55–67.

Van Duyne GD (2015) Cre Recombinase. Microbiol Spectr 3:MDNA3–0014–2014.

van Heyningen P, Calver AR, Richardson WD (2001) Control of progenitor cell number by mitogen supply and demand. Curr Biol 11:232–241.

Veeman MT, Axelrod JD, Moon RT (2003) A second canon. Functions and mechanisms of beta-catenin-independent Wnt signaling. Dev Cell 5:367–377.

Vora P, Pillai PP, Zhu W, Mustapha J, Namaka MP, Frost EE (2011) Differential effects of growth factors on oligodendrocyte progenitor migration. Eur J Cell Biol 90:649–656.

Voyvodic JT (1989) Target size regulates calibre and myelination of sympathetic axons. Nature 342:430–433.

Walf AA, Frye CA (2005) Antianxiety and antidepressive behavior produced by physiological

estradiol regimen may be modulated by hypothalamic-pituitary-adrenal axis activity. Neuropsychopharmacology 30:1288–1301.

Waly El B, Macchi M, Cayre M, Durbec P (2014) Oligodendrogenesis in the normal and pathological central nervous system. Front Neurosci 8:145.

Walz W (2000) Role of astrocytes in the clearance of excess extracellular potassium. Neurochem Int 36:291–300.

Wang L-C, Almazan G (2016) Role of Sonic Hedgehog Signaling in Oligodendrocyte Differentiation. Neurochem Res 41:3289–3299.

Wang S, Bolós M, Clark R, Cullen CL, Southam KA, Foa L, Dickson TC, Young KM (2016) Amyloid β precursor protein regulates neuron survival and maturation in the adult mouse brain. Mol Cell Neurosci 77:21–33.

Wang S, Young KM (2014) White matter plasticity in adulthood. Neuroscience 276:148–160.

Watzlawik JO, Warrington AE, Rodriguez M (2013) PDGF is required for remyelination-promoting IgM stimulation of oligodendrocyte progenitor cell proliferation. Stangel M, ed. PLoS ONE 8:e55149.

Waxman SG, Bennett MV (1972) Relative conduction velocities of small myelinated and non-myelinated fibres in the central nervous system. Nature New Biol 238:217–219.

Wechsler-Reya RJ, Scott MP (1999) Control of neuronal precursor proliferation in the cerebellum by Sonic Hedgehog. Neuron 22:103–114.

Wegner M (2001) Expression of transcription factors during oligodendroglial development. Microsc Res Tech 52:746–752.

Wilkins A, Majed H, Layfield R, Compston A, Chandran S (2003) Oligodendrocytes promote neuronal survival and axonal length by distinct intracellular mechanisms: a novel role for oligodendrocyte-derived glial cell line-derived neurotrophic factor. J Neurosci 23:4967–4974.

Williams MR, Sharma P, Fung KL, Pearce RKB, Hirsch SR, Maier M (2015) Axonal myelin increase in the callosal genu in depression but not schizophrenia. Psychol Med 45:2145–2155.

Wine-Lee L, Ahn KJ, Richardson RD, Mishina Y, Lyons KM, Crenshaw EB (2004) Signaling through BMP type 1 receptors is required for development of interneuron cell types in the dorsal spinal cord. Development 131:5393–5403.

Winey M, O'Toole E (2014) Centriole structure. Philos Trans R Soc Lond, B, Biol Sci 369:20130457–20130457.

Woodruff RH, Fruttiger M, Richardson WD, Franklin RJM (2004) Platelet-derived growth factor regulates oligodendrocyte progenitor numbers in adult CNS and their response following CNS demyelination. Mol Cell Neurosci 25:252–262.

Wu B, Guo S, Jiang T, Ren X (2011) In vitro culture and characterization of oligodendrocyte precursor cells derived from neonatal rats. Neurol Res 33:593–599.

Wu M, Hernandez M, Shen S, Sabo JK, Kelkar D, Wang J, O'Leary R, Phillips GR, Cate HS,

Casaccia P (2012) Differential modulation of the oligodendrocyte transcriptome by sonic hedgehog and bone morphogenetic protein 4 via opposing effects on histone acetylation. J Neurosci 32:6651–6664.

Xavier GM, Seppala M, Barrell W, Birjandi AA, Geoghegan F, Cobourne MT (2016) Hedgehog receptor function during craniofacial development. Dev Biol 415:198–215.

Xiao L, Ohayon D, McKenzie IA, Sinclair-Wilson A, Wright JL, Fudge AD, Emery B, Li H, Richardson WD (2016) Rapid production of new oligodendrocytes is required in the earliest stages of motor-skill learning. Nat Neurosci 19:1210–1217.

Xing YL, Röth PT, Stratton JAS, Chuang BHA, Danne J, Ellis SL, Ng SW, Kilpatrick TJ, Merson TD (2014) Adult neural precursor cells from the subventricular zone contribute significantly to oligodendrocyte regeneration and remyelination. J Neurosci 34:14128–14146.

Xu Q, Zhang Y, Wei Q, Huang Y, Hu J, Ling K (2016) Phosphatidylinositol phosphate kinase PIPKIγ and phosphatase INPP5E coordinate initiation of ciliogenesis. Nat Commun 7:10777.

Yamauchi H, Miyakawa N, Miyake A, Itoh N (2009) Fgf4 is required for left-right patterning of visceral organs in zebrafish. Dev Biol 332:177–185.

Yao PJ, Petralia RS, Ott C, Wang Y-X, Lippincott-Schwartz J, Mattson MP (2015) Dendrosomatic Sonic Hedgehog Signaling in Hippocampal Neurons Regulates Axon Elongation. J Neurosci 35:16126–16141.

Yao Z-F, Wang Y, Lin Y-H, Wu Y, Zhu A-Y, Wang R, Shen L, Xi J, Qi Q, Jiang Z-Q, Lü H-Z, Hu J-G (2017) Transplantation of PDGF-AA-Overexpressing Oligodendrocyte Precursor Cells Promotes Recovery in Rat Following Spinal Cord Injury. Front Cell Neurosci 11:79.

Ye P, Hu Q, Liu H, Yan Y, D'ercole AJ (2010) beta-catenin mediates insulin-like growth factor-I actions to promote cyclin D1 mRNA expression, cell proliferation and survival in oligodendroglial cultures. Glia 58:1031–1041.

Yeung MSY, Zdunek S, Bergmann O, Bernard S, Salehpour M, Alkass K, Perl S, Tisdale J, Possnert G, Brundin L, Druid H, Frisén J (2014) Dynamics of oligodendrocyte generation and myelination in the human brain. Cell 159:766–774.

Yoshimura K, Takeda S (2012) Hedgehog signaling regulates myelination in the peripheral nervous system through primary cilia. Differentiation 83:S78–S85.

Young KM, Mitsumori T, Pringle N, Grist M, Kessaris N, Richardson WD (2010) An Fgfr3-iCreER(T2) transgenic mouse line for studies of neural stem cells and astrocytes. Glia 58:943–953.

Young KM, Psachoulia K, Tripathi RB, Dunn S-J, Cossell L, Attwell D, Tohyama K, Richardson WD (2013) Oligodendrocyte dynamics in the healthy adult CNS: evidence for myelin remodeling. Neuron 77:873–885.

Zaghloul NA, Brugmann SA (2011) The emerging face of primary cilia. Genesis 49:231–246.

Zawadzka M, Rivers LE, Fancy SPJ, Zhao C, Tripathi R, Jamen F, Young K, Goncharevich A, Pohl H, Rizzi M, Rowitch DH, Kessaris N, Suter U, Richardson WD, Franklin RJM (2010) CNS-resident glial progenitor/stem cells produce Schwann cells as well as

oligodendrocytes during repair of CNS demyelination. Cell Stem Cell 6:578–590.

Zhang J, Markovic-Plese S, Lacet B, Raus J, Weiner HL, Hafler DA (1994) Increased frequency of interleukin 2-responsive T cells specific for myelin basic protein and proteolipid protein in peripheral blood and cerebrospinal fluid of patients with multiple sclerosis. J Exp Med 179:973–984.

Zhang J, Zhang ZG, Li Y, Ding X, Shang X, Lu M, Elias SB, Chopp M (2015) Fingolimod treatment promotes proliferation and differentiation of oligodendrocyte progenitor cells in mice with experimental autoimmune encephalomyelitis. Neurobiol Dis 76:57–66.

Zhang Y, Chen K, Sloan SA, Bennett ML, Scholze AR, O'Keeffe S, Phatnani HP, Guarnieri P, Caneda C, Ruderisch N, Deng S, Liddelow SA, Zhang C, Daneman R, Maniatis T, Barres BA, Wu JQ (2014) An RNA-sequencing transcriptome and splicing database of glia, neurons, and vascular cells of the cerebral cortex. J Neurosci 34:11929–11947.

Zhang Y, Kwon S, Yamaguchi T, Cubizolles F, Rousseaux S, Kneissel M, Cao C, Li N, Cheng H-L, Chua K, Lombard D, Mizeracki A, Matthias G, Alt FW, Khochbin S, Matthias P (2008) Mice lacking histone deacetylase 6 have hyperacetylated tubulin but are viable and develop normally. Mol Cell Biol 28:1688–1701.

Zhang Y, Zhang H, Wang L, Jiang W, Xu H, Xiao L, Bi X, Wang J, Zhu S, Zhang R, He J, Tan Q, Zhang D, Kong J, Li X-M (2012) Quetiapine enhances oligodendrocyte regeneration and myelin repair after cuprizone-induced demyelination. Schizophr Res 138:8–17.

Zhou Q, Choi G, Anderson DJ (2001) The bHLH transcription factor Olig2 promotes oligodendrocyte differentiation in collaboration with Nkx2.2. Neuron 31:791–807.

Zhu K, Sun J, Kang Z, Zou Z, Wu G, Wang J (2016) Electroacupuncture Promotes Remyelination after Cuprizone Treatment by Enhancing Myelin Debris Clearance. Front Neurosci 10:613.

Zhu X, Hill RA, Dietrich D, Komitova M, Suzuki R, Nishiyama A (2011) Age-dependent fate and lineage restriction of single NG2 cells. Development 138:745–753.

Zimmermann KW (1898) Beiträge zur Kenntnis einiger Drüsen und Epithelien.